Modeling of an Industrial Hydrocracker Reactor

by

Ümmühan CANAN

A Thesis Submitted to the
Graduate School of Engineering
in Partial Fulfillment of the Requirements for
the Degree of

Master of Science
in
Chemical and Biological Engineering

Koç University
November, 2011

Koc University

Graduate School of Sciences and Engineering

This is to certify that I have examined this copy of a master's thesis by

Ümmühan CANAN

and have found that it is complete and satisfactory in all respects,
and that any and all revisions required by the final
examining committee have been made.

Committee Members:

_____

Yaman ARKUN (Advisor)

_____

Can ERKEY

_____

Murat SÖZER

_____

_____

Date: 01/11/2011

ABSTRACT

The aim of this study is to model an industrial hydrocracker reactor. As preliminary work, the industrial hydrocracker reactor was simulated by the Aspen HYSYS Hydrocracker. Next, a first principle model was developed in which the discrete lumping approach was adopted. Since the model consists of a set of ordinary differential equations and algebraic equations which have to be solved simultaneously, a code was written by using MATLAB. Parameter estimation was performed to match model predictions with real plant data. Under constant conversion operating conditions model estimates matched the plant data closely. In order to investigate the effect of catalyst deactivation on parameters, the constant-conversion model was updated using data corresponding to operating days with different catalyst activity. While significant changes in the product distribution parameters and heat of reaction parameters were not observed, rate constant parameters correlated well with catalyst deactivation. Since the reactor inlet temperatures are the major independent and adjustable process variables, their effect on plant products and conversion was also studied. For the constant conversion training data, the model showed low sensitivity of conversion to reactor inlet temperatures. Next, a new model was developed by estimating the parameters using operating data at two different conversion levels. Simulations showed that an overall 3.1 °C increase in inlet temperatures along the reactor affected the conversion by 0.75 % which is a remarkable value for an Hydrocracker unit. Finally, the predictive ability of the model was questioned by analyzing the plant data. It was observed that increase in inlet temperatures resulted in the same conversion for some days of operation. This means that in order to keep conversion constant the reactor inlet temperatures are adjusted by the existing advanced control system to reject disturbances such as feed properties, catalyst deactivation or other operation conditions. The developed model cannot predict such changes. However its parameters can be updated on-line to match different plant data that includes disturbance effects. Alternatively, a fundamental or empirical disturbance model can be integrated into the developed model in order to predict the behavior of the process under realistic disturbances.

ÖZET

Bu çalışmanın amacı, endüstriyel bir Hidrokraker reaktörünü modellemektir. Ön çalışma olarak, endüstriyel Hidrokraker reaktörü Aspen HYSYS Hydrocracker kullanılarak simule edilmiştir. Daha sonra, kesikli gruplama yaklaşımının uygulanması ile model geliştirilmiştir. Model aynı anda çözülmesi gereken bir dizi diferansiyel ve cebirsel denklemlerden oluştuğu için, MATLAB kullanılarak bir kod yazılmıştır. Parametre tahmini gerçek veri ile model tahminlerini eşleştirmek için yapılmıştır. Sabit dönüşümlü operasyon koşulları altında, model tahminleri gerçek veriyle yakın bir şekilde örtüşmüştür. Sabit dönüşümlü model, kataliz deaktivasyonunun parametreler üzerindeki etkisini gözlemlemek için farklı kataliz aktivitesi olan operasyon günlerinin verileri kullanılarak güncellenmiştir. Ürün dağılım parametreleri ile reaksiyon ısısı parametrelerinde önemli değişiklikler gözlenmezken, reaksiyon hız sabiti parametreleri kataliz deaktivasyonu ile ilişkilidir. Rektör giriş sıcaklıkları bağımsız ve ayarlanabilir majör değişkenler oldukları için, onların ürünler ve dönüşüm üzerindeki etkileri de çalışılmıştır. Model, sabit dönüşüm verisi için, reaktör giriş sıcaklıklarına düşük dönüşüm hassasiyeti göstermiştir. Daha sonra, iki farklı dönüşüm verisi kullanılarak tahmin edilen parametrelerle yeni bir model geliştirilmiştir. Simulasyonlar reaktör boyunca giriş sıcaklıklarındaki toplam 3.1 °C lik artışın dönüşümü % 0.75 etkilediğini göstermiştir ki bu değer hidrokraker ünitesi için dikkat çekicidir. Son olarak, modelin öngörü kabiliyeti ünite verileri analiz edilerek sorgulanmıştır. Bazı operasyon günleri için giriş sıcaklıklarındaki artışların aynı dönüşümle sonuçlandığı gözlemlenmiştir. Bu, dönüşümü sabit tutabilmek için, reaktör giriş sıcaklıklarının ileri kontrol sistemi tarafından besleme özellikleri, kataliz deaktivasyonu yada diğer operasyon koşulları gibi bozan etkenleri elimine etmek için ayarlandığı anlamına gelir. Geliştirilmiş model bu değişiklikleri tahmin edemez. Bununla beraber, modelin parametreleri bozan etkenleri içeren farklı ünite verilerini eşleştirmek üzere güncellenebilir. Ya da, proses davranışını tahmin edebilmek için geliştirilmiş modele bir bozan etken modeli entegre edilebilir.

ACKNOWLEDGEMENTS

With all respect and gratitude, I would like to express my sincere thanks to my advisor, Prof. Dr. Yaman ARKUN, for his guidance, encouraging support and patience throughout my graduate study and thesis period. I will always remember him with his honesty and kindness. I would like to extend my grateful thanks to Prof. Dr. Can ERKEY and Assoc. Prof. Dr. Murat SÖZER for their participation in my thesis committee.

My deep sense gratitude to Turkish Petroleum Refineries Corporation (TÜPRAŞ) Directorship support in particular to Murat YILDIRIM, the manager of R&D Department. I owe a great many thanks to Dila GÖKÇE KUZU, as the project leader, and the project members Emre Özgen KUZU, Berna ÇAKAL, Görkem OĞUR and Fırat UZMAN for their technical collaboration and kind support.

Special thanks to Hasan ŞILDIR for his helpful suggestions.

I am extremely grateful to Clive BEAUTYMAN for his kind support in ASPEN Hydrocracker simulations. Without him, the preliminary work of this study could never be completed.

Last but not least I wish to express my gratitude to my family for their boundless love, moral support and sacrifices throughout my life.

TABLE OF CONTENTS

LIST OF FIGURES

LIST OF TABLES

Chapter 1

1. INTRODUCTION

Hydrocracking is one of the significant processes in petroleum refineries. As the name implies, hydrocracking involves cracking reactions in the presence of hydrogen. Heavy oil fractions are converted into high quality middle distillates and lighter products such as diesel, kerosene, naphtha, fuel oil, LPG etc by the hydrocracking process.

Due to environmental concerns, low-sulfur diesel demand has increased after 1990s. Similarly, worldwide jet fuel demand has increased recently as well. Therefore, the importance of hydrocracking has been growing because it is the best source for both low-sulfur diesel and high-smoke point jet fuel. Under these conditions, it is very important to operate hydrocracker unit (HCU) optimally. Thus, considerable amount of research has been conducted on this topic.

Different modeling approaches have been reported in the literature. While continuous lumping approach treats reaction mixture as a continuum, discrete lumping approach divides the reaction mixture into pseudocomponents. However, structure oriented lumping defines the mixture according to the structure of the compounds. Hence, it is more complex than the other methods and requires more experimental data and computational power.

This thesis concentrates on modeling and simulation of an industrial hydrocracker reactor. A first-principle model was developed in which discrete lumping approach was adopted. The model was validated with real plant data. In the next chapter, a review on historical development of hydrocracking, the process itself and more detailed review on modeling approaches are given. In chapter 3, the preliminary work that was performed using Aspen HYSYS Hydrocracker is presented. Chapter 4 explains the characterization of feed and products. The developed model is described in chapter 5 and the estimation and sensitivity analysis of model parameters are given in chapter 6. The final results are presented and discussed in the next chapter and the thesis is finalized with conclusions.

Chapter 2

2. LITERATURE REVIEW

2.1. BRIEF HISTORY

Hydrocracking technology was first developed in Germany as early as 1915 for coal conversion. The first plant was put on stream in Leuna Germany in 1927, applying what may be considered the first commercial hydrocracking process [2]. In the mid 1950s the automobile industry started the manufacture of high performance cars which required high-octane gasoline. Furthermore, the switch of railroads from steam to diesel engines after World War II and the introduction of commercial jet aircraft in the late 1950s increased the demand for diesel and jet fuel [2]. With these advances, hydrocracking technology became more important and by the development of new, zeolite catalysts in 1960s, grew rapidly. After 1970s, many hydrocracker plants were initiated all over the world for the production of middle distillates. In the environmentally conscious 1990s, hydrocracking is the best source of low-sulfur and low-aromatics diesel fuel as well as high-smoke point jet fuel [3]. Today, in 2000s, this technology still remains to be significant and hydrocracking continues to be one of the most attractive process alternatives to produce intermediate distillates from heavy crude oils in the presence of hydrogen gas [4].

2.2. HYDROCRACKING PROCESS

Normally, hydrocracking is carried out in a high pressure trickle bed reactor. The hydrocracking of petroleum fractions involves complex chemistry, including various reactions such as hydrogenation/dehydrogenation, isomerization, C-C bond scission, hydrogen transfer, pairing reactions, ring saturation and ring opening [5]. There are two main types of reactions that take place in hydrocracking units: treating and cracking. Hydrodesulfurization (HDS) and hydrodenitrogenation (HDN) are the primary treating reactions. Organic sulfur is transformed into H_2S by HDS and the nitrogen is transformed into NH_3 by HDN. Hydrogen is consumed in all treating reactions. The mechanisms of HDS and HDN are given in Figure 2.1 and Figure 2.2 respectively.

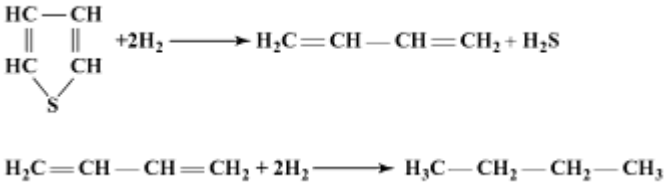

Figure 2.1 Mechanism for HDS

As seen above, sulfur is removed first and then the saturation of olefin compound occurs.

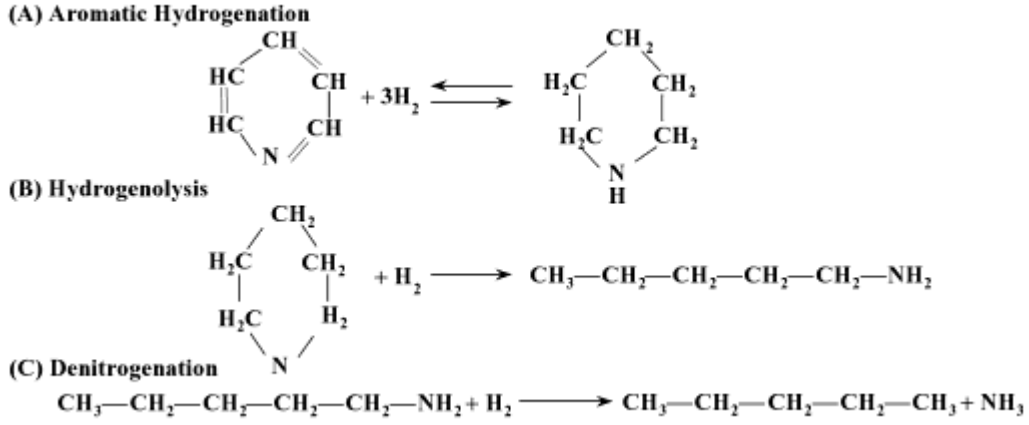

Figure 2.2 Mechanism for HDN

As can be seen in Figure 2.2, HDN has a different path: Hydrogenation occurs first, then followed by hydrogenolysis and finally denitrogenation occurs.

The cracking reaction is slightly endothermic while the hydrogenation reaction is highly exothermic. Hence, the overall hydrocracking process is highly exothermic. Cracking reactions begin with generation of an olefin by dehydrogenation on the metal sites and conversion of the olefin to a carbenium ion. Then, this carbenium ion forms a more stable tertiary carbenium ion. The cracking occurs at the β position at acidic sites to form an α olefin and a new carbenium ion. The new carbenium ion will continue to react until it collides with another carbenium ion. Finally, olefin hydrogenation completes the mechanism. Figure 2.3 illustrates the specific steps involved in the hydrocracking of paraffins.

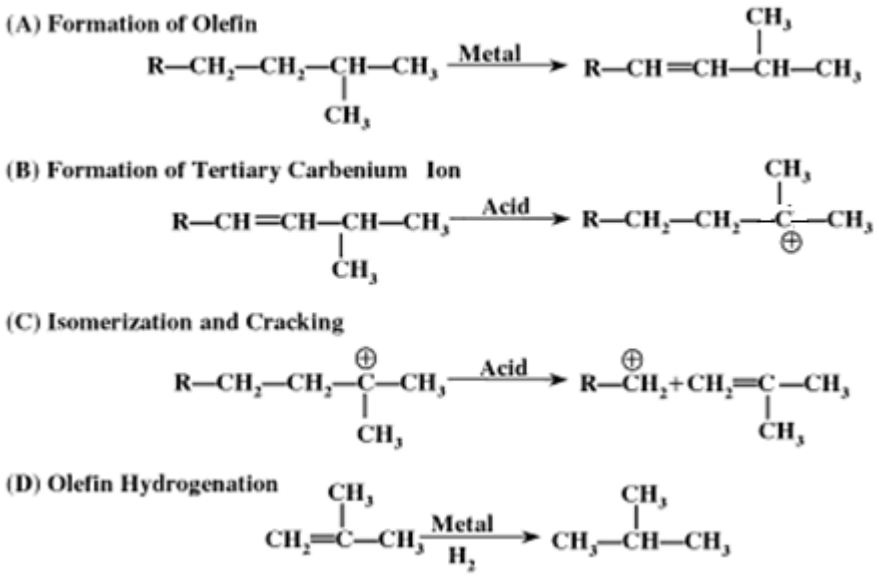

Figure 2.3 Hydrocracking mechanism of n-paraffines

2.3. CATALYSTS USED IN THE PROCESS

Hydrocracking catalysts have both cracking and hydrogenation function. While the cracking function is provided by an acidic support, the hydrogenation/dehydrogenation function is provided by metals. The acidic support consists of amorphous oxides (silica-alumina), a crystalline zeolite (mostly modified Y zeolite) plus binder (alumina) or a mixture of crystalline zeolite and amorphous oxides [2]. A metal, a metal oxide, a metal sulfide or a combination of these compounds may be the metal function of the catalyst. The most commonly used metal function is a combination of Group VIA (Mo, W) and Group VIIIA (Co, Ni) metal sulfides. Although it has moderate activity compared to Pd or Pt, the sulfur tolerant makes it preferential. The composition of the catalyst depends on the final product requirements and mode of operation [7]. A guideline of catalyst composition is given in the following table.

Table 2.1 Types of catalysts used in different hydrocracking processes [8]

Application type	Process type (# stages)	Hydrogenerating function			Acid function	
		Pd	Ni–Mo	Ni–W	Y-type zeolite	SiO_2/Al_2O_3 amorphous
Max. Naphtha	One	xxx	x	x	xxx	
Max. Naphtha	Two	xxx			xxx	
Max. Kerosene	One		xxx	x	xxx	
Max. Kerosene	Two	x	x	x	x	x
Max. Diesel oil	One		x	x	x	x
Max. Diesel oil	Two		x	x		x
Max. Lube oils	One		x	x	x	x

x represents frequency of use

2.4. PRODUCTS OF THE PROCESS

By hydrocracking of heavy vacuum gas oil, many valuable products are obtained. They are summarized as follows.

1. **Light End Components**
    - Boiling range = less than 40 °C
    - Consists of 1-4 carbon atoms
    - Often liquefied under pressure to form LPG (Liquefied Petroleum Gas)
2. **Light Naphtha**
    - Boiling range = 30-90 °C
    - Consists of 5-6 carbon atoms
    - Further processed to make gasoline
3. **Heavy Naphtha**
    - Boiling range = 90-200 °C
    - Consists of 6-12 carbon atoms
    - Further processed to make gasoline
4. **Kerosene**
    - Boiling range = 150-275 °C
    - Consists of 6-16 carbon atoms
    - Fuel for jet engines

5. **Diesel**
    - Boiling range = 200-350 °C
    - Consists of 8-21 carbon atoms
    - Diesel fuel

2.5. PROCESS CONFIGURATION

The choice of process configuration is tied to the catalyst system which affects product quality, yield and total economics of the process. The possible reactor (cracker) modes are single-stage once-through, single-stage with recycle and two stage operations.

2.5.1. Single-Stage Once-Through

As can be seen in Figure 2.4, the configuration is very simple. This type of unit is the lowest cost hydrocracking unit, and can process heavy, high boiling feed stocks and produce high value unconverted material which becomes feed stocks for FCC units, ethylene plants or lube oil units. In general, the conversion is 60-70%, but can range as high as 90 % [2].

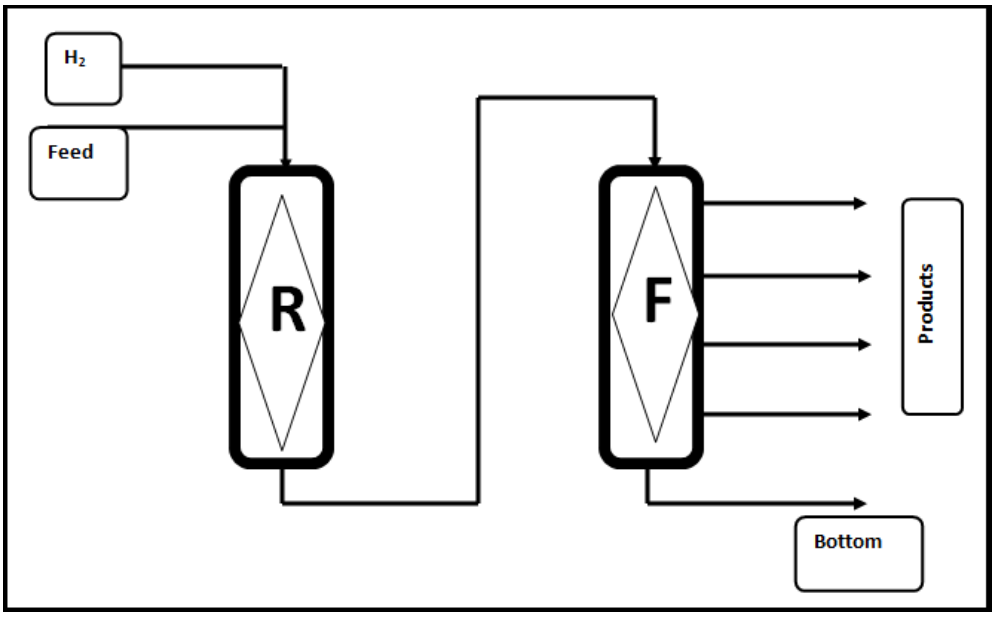

Figure 2.4 Single stage once-through operation, R: Reactor and F: Fractionator

2.5.2. Single-Stage with Recycle

Single-stage with recycle is the most widely used mode of operation in which the unconverted feed is sent back to reactor section for further conversion. (Figure 2.5) It is especially used to maximize diesel product.

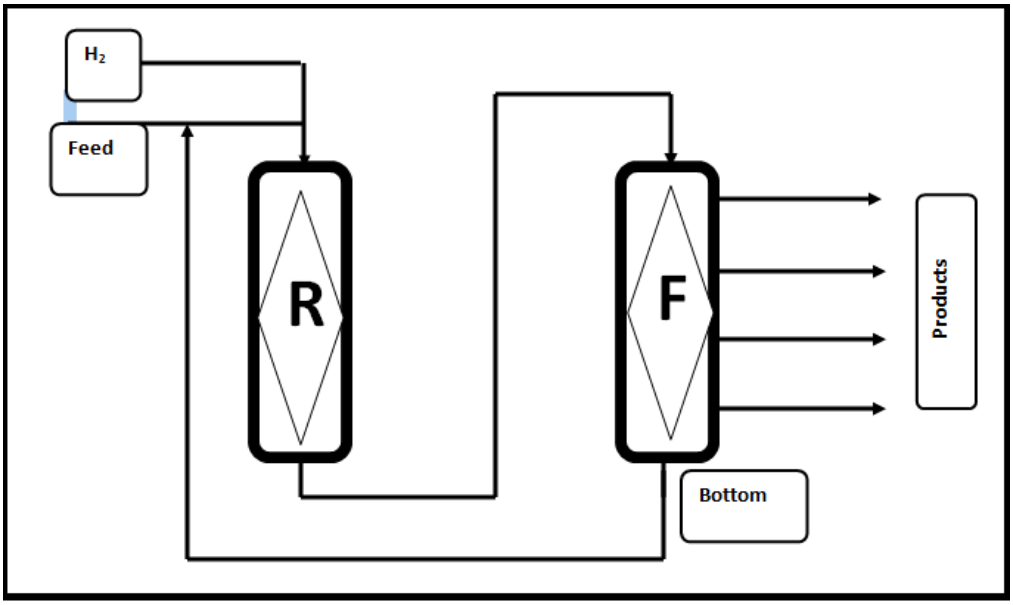

Figure 2.5 Single stage with recycle operation

2.5.3. Two Stage

This configuration is also widely used. The unconverted material from the first stage becomes the feed for the second stage. The two stage mode allows more flexible adjustment of operating conditions and the distribution between the naphtha and middle distillate is more flexible. Although it requires a higher investment, overall it is more economical [9].

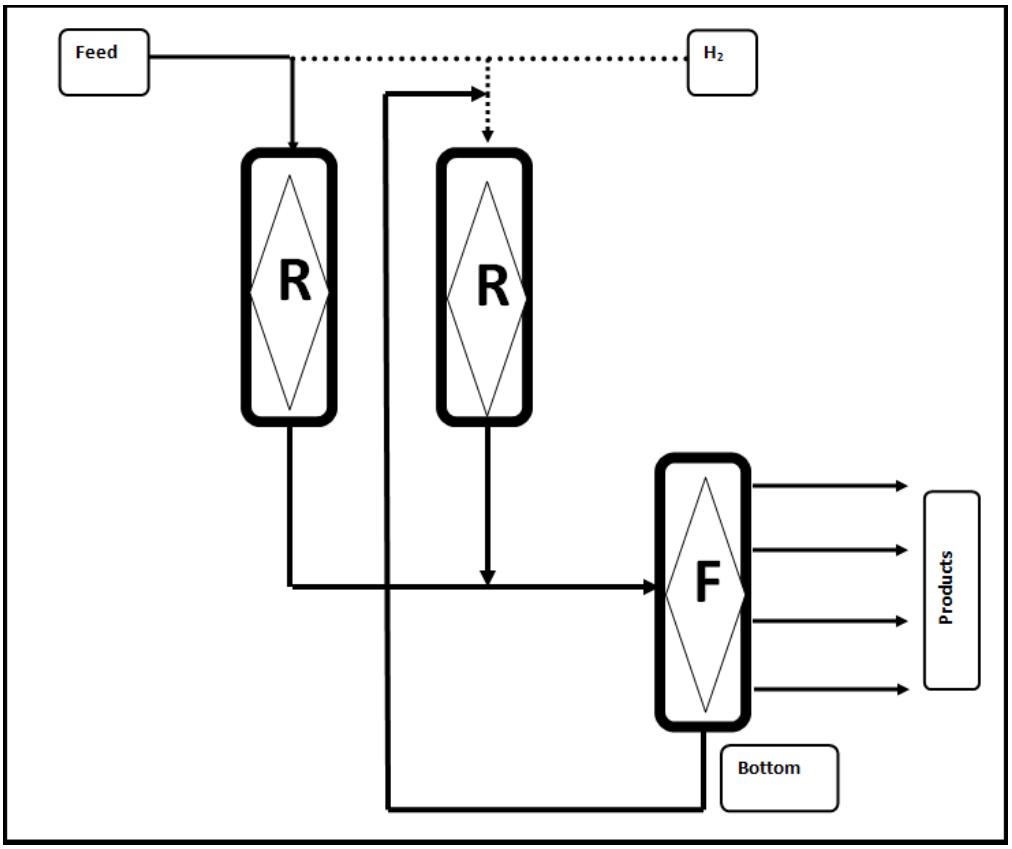

Figure 2.6 Two stage operation

2.6. A GENERAL PROCESS FLOW OF A HYDROCRACKER UNIT (HCU)

Hydrocracking is a catalytic process used in refineries for converting heavy oil fractions into high quality middle distillates and lighter products such as diesel, kerosene, naphtha and LPG. The process takes place in hydrogen-rich atmosphere at high temperatures (260-420 °C) and pressures (35-200 bar). A generalized and simplified flow sheet is given in Figure 2.7.

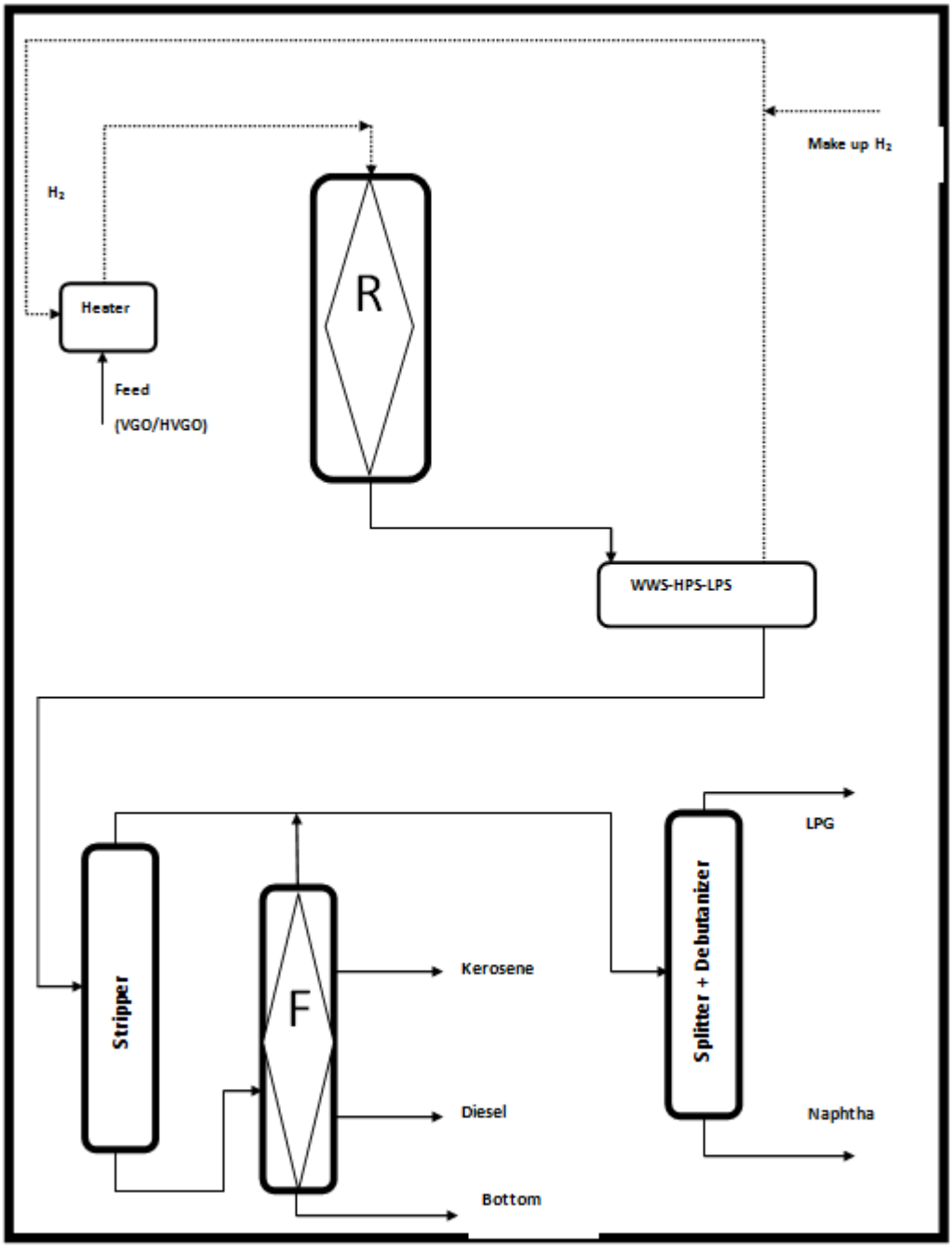

Figure 2.7 A Simplified Flow Sheet of a Hydrocracker Unit (HCU)

A hydrocracker unit (HCU) in a refinery consists of mainly two sections; the reactor section and the fractionators section. The reaction takes place in the reactor section and the products are separated in the fractionators section.

The feedstock is generally vacuum gas oil (VGO) or heavy vacuum gas oil (HVGO). The feed and high-pressure hydrogen are heated in a fuel-fired heater before entering the first reactor of the reactor section. As stated in section 2.5, different configurations of reactors are available in the refineries.

The effluent from the reactor section is sent to a wash water separator (WWS) where most of the NH_3 is removed. During this process, a negligible amount of H_2S is also lost. The stream then is routed into a high-pressure separator (HPS) for separation into three phases: hydrogen-rich gas, hydrocarbon liquid and water. The hydrogen-rich gas is mixed with hydrogen make up and recycled back to the reactor section. The hydrocarbon liquid is sent to low-pressure separator (LPS). The reduction in pressure partially vaporizes the liquid. H_2S is recovered from the resulting vapor. The liquid hydrocarbon is then fed into the fractionators section.

There are a number of distillation columns in fractionators section. The first column is a steam stripper where high volatility and low volatility products are separated. The high volatility products are fed to debutanizer. The lighter products like CH_4, C_2H_6 and LPG are recovered from top of this column. LPG is obtained by a further LPG treatment. The other products (CH_4, C_2H_6) are called fuel gas. The bottom stream of debutanizer is sent to splitter where light naphtha and heavy naphtha are separated. Low volatility products from steam stripper are routed into a series of multi-component distillation columns called fractionators. The middle distillates diesel and kerosene are obtained by the separation process in these columns. The unconverted gas oil is taken from bottom. In some refineries, it is recycled back to reactor section. The top product of fractionators is mixed with the top product of stripper and then sent to debutanizer.

2.7. MODELING APPROACHES

Different modeling approaches to hydrocracking have been reported in the literature. These approaches are classified as.

- Discrete lumping
- Continuous lumping
- Structure oriented lumping and single event models

2.7.1. Discrete Lumping

In this approach, the reaction mixture is divided into discrete pseudocompounds (lumps) based on their boiling range, molecular weight or carbon number distribution [6]. Quader and Hill [10], Weekman and Nace [11], Orochko et. Al [12], Zhorov [13], Usami [14] etc. developed models to predict yields based on the selection of small number of products and devised various parallel and series reactions to produce them. Kinetic parameters were determined to best fit experimental data. The main disadvantage of this approach is that a

change in product specifications or number of products would require reformulation of the model and refitting of the experimental data. Stangeland [15] developed a better and simple approach where the same parameters could be used to describe the yields for similar feeds even if their boiling ranges were different [16]. The model includes four parameters; one parameter gives the butane yield, another describes the type of feed (e.g. naphthenic or paraffinic) or type of catalytic process (e.g. random or selective), and the last two parameters quantify the reaction rate of each pseudocomponent. Mohanty et al [17] implemented Stangeland's model for a two-stage hydrocracking unit. The feed and products were cut into 23 pseudocomponents and pseudo-homogeneous first order reactions were assumed. The kinetic constant reported by Quader and Hill [10] was employed in the model. Although the model validated against the plant data, it should be noted that with the parameters reported by Mohanty et al, the mass balance closure in each individual hydrocracking reaction is not satisfied [18]. Dassori and Pacheco [16] modified Stangeland's model by adding two additional parameters. The kinetic parameters were regressed by Levenberg-Marquard algorithm such that the mass balance in each reaction is satisfied. They used a second order rate constant to quantify the effect of hydrogen partial pressure on the rate of cracking [18] Bhutani [1] applied a multi-objective optimization to a hydrocracker unit for the first time to provide a range of optimal operating conditions. He also adopted Mohanty's model which is originally based on Stangeland' s model.

Although Stangeland's model has been widely used in fuel processing industry, some other models have been developed as well. Krishna and Saxena [19] proposed a model based on the analogy between reactions of hydrocracking and phenomena of axial-dispersion of a tracer in a flow [18]. This model used only two parameters and was validated by experimental data. Mosby et al [20] developed a model to describe resid hydrocracking by devising the reaction path through which the resid is converted to gas oil, distillate, naphtha, and gases [18]. Both the resid and each of the hydrocracked products are considered to be a single chemical species with a single cracking rate constant.

2.7.2. Continuous Lumping

Continuous lumping considers the reactive mixture to form a continuum mixture with respect to its species type, boiling point, molecular weight, etc [6]. The idea of continuous mixture was originally proposed by DeDonder [21]. Aris and Gavalas [22] were the pioneering researchers who discussed the idea of continuous mixture in terms of chemical reactions, including of course the description of many parallel reactions as those occurring in

hydrocracking of oil fractions [4]. After Aris and Gavalas, several researches have been reported. Chou and Ho [23] have provided a procedure for continuum lumping of nonlinear reaction. McCoy and Wang [24] have formulated a general expression for the stoichiometric coefficient of binary size reduction, and showed how it can be well represented by a Gaussian form under specific conditions. Practical applications of the continuous lumping have been reported by Browarzik and Kehlen [25] and Peixoto and deMedeiros [26]. However these approaches were not extended to complex mixtures such as crude oils and residua [4].

Application of continuous lumping to hydrocracking of vacuum gas oil was described by Laxminarasimhan et al [5]. In the model, a normalized TBP as a function of an index was used instead of TBP. The reactivity was considered to be monotonic and represented by a simple power law type function. A yield distribution function in skewed Gaussian form was derived from literature and the model equations were formulated as a function of reactivity following the procedure proposed by Chou and Ho [23]. Based on this model, Khorasheh et al [27-29] have extended the application of the continuous lumping to model hydrocracking, hydrodesulfurization (HDS) and hydrodenitrogenation (HDN) in order to predict the dependence of parameters with temperature. Basak et al [6] have modeled the hydrogen consumption and the bed temperature profile in an industrial hydrocracker by employing the continuous lumping model.

2.7.3. Structure Oriented Lumping and Single Event Models

Structure oriented lumping kinetic models, which employ most of the information obtained with the modern analytical techniques for model reaction modeling at a molecular level, have been proposed for some catalytic processes [18]. The lumps are defined according to the structure of the compounds in the reacting mixture. Liguras and Allen [30-31] described a mixture with several hundred pseudocomponents where selection is based on a set of typical routine analytical data and whose reactions are based on group contribution methods [6]. The detailed concept of structure oriented lumping was developed by Quann and Jaffe [33]. In this model, molecules and reactions are described with a notation of vectors by which reaction networks can be represented with the help of computer. Due to its detailed approach, this model requires large experimental data bank and computational power.

A fundamental kinetic modeling on hydrocracking of (cyclo)-alkanes using single-event kinetics was proposed by Froment and coworkers [34-35]. In this approach, carbenium ion chemistry was considered to describe the elementary reactions at molecular level [36]. Martens [37] derived a model by partially relumping the single event kinetic equations

starting from the strategy described by Froment [34-35]. Although theoretically independent of feedstock or reactor configuration, the application of single-event models to industrial processes is still far from being achieved due to analytical complexity and modeling limitations [38].

Chapter 3

3. SIMULATIONS BY ASPEN HYSYS HYDROCRACKER

Modeling of an industrial hydrocracking reactor is a difficult task due to the complexity of the process. Therefore, a preliminary work is necessary in order to understand how hydrocracking unit operates. Since ASPEN HYSYS Refining has a strong reputation in chemical industry, the preliminary work was done by using this program. The performed work included simulations and calibration of the model. The details were presented in the following sections.

3.1. AN OVERVIEW OF ASPEN HYSYS HYDROCRACKER

The Hydrocracker model in Aspen HYSYS Refining can be used for simulating multi-stage hydrocracker units. The hydrocracker simulation module includes feed characterization, reactor section; recycle gas loop(s), product separation, and product mapper. The Hydrocracker within Aspen HYSYS Refining has its own set of component library as shown in Table 3.1. The components cover light-ends, sulfur and nitrogen compounds and different classes of hydrocarbons that include one-ring naphthenics to 4-ring aromatics.

Table 3.1. *Component List of Aspen Hydrocracker [39]*

1	Nitrogen	27	C10N	55	MAN2LO	83	HTHAN
2	H2S	28	MN2LO	56	MA2NLO	84	MTHA2
3	Hydrogen	29	MN2HI	57	HAN2	85	HTHA2
4	Ammonia	30	HN2	58	VAN2	86	VTHA2N
Light Ends		31	VN2	59	MA2NLo	87	VTHA3
5	C1	32	MN3LO	60	MA2NHi	**Nitrogen Components**	
6	C2	33	MN3HI	61	HA2N	88	LBNIT
7	C3	34	HN3	62	VA2N	89	LNNIT
8	C4	35	VN3	63	HA3	90	MBNITN
9	C5	36	HN4	64	VA3	91	MBNITA
Paraffines		37	VN4	65	MANALO	92	MNNITA
10	C6P	**Aromatics**		66	MANAHI	93	HBNITAN
11	C7P	38	C6A	67	HANA	94	MBNITA2
12	C8P	39	C7A	68	VANA	95	MNNITA2
13	C9P	40	C8A	69	HA4	96	VBNITA2N
14	C10P	41	C9A	70	VA4	97	VNNITA3
15	C14P	42	C10A	71	HAN3		
16	C18P	43	MA1Lo	72	VAN3		
17	C26P	44	MA1Hi	73	HA2N2		
18	C47P	45	HA1	74	VA2N2		
Naphthenes		46	VA1	**Sulfur Components**			
19	C6N	47	MANLO	75	LTH		
20	C7N	48	MANHI	76	LS8		
21	C8N	49	HAN	77	MS12		
22	C9N	50	VAN	78	HS28		
23	MN1Lo	51	MA2LO	79	LTHA		
24	MN1Hi	52	MA2HI	80	MTHA		
25	HN1	53	HA2	81	MTHN		
26	VN1	54	VA2	82	MTHAN		

The following list is a legend to decode the meaning of components given in the table above.

- **Components starting with C:** The number beside C indicates the carbon number of the component. The endings A-N-P indicate aromatics, paraffines and naphthenes respectively.
- **Components starting with NC:** They are normal paraffines.
- **Components starting with IC:** They are iso-paraffines.
- **Components starting with L:** They boil in the gasoline range.

- **Components starting with M:** They boil in the distillates range. An ending with LO shows 14 carbons. An ending with HI shows 18 carbons.
- **Components starting with H:** They boil in the gas-oil range and have 21 carbons.
- **Components starting with V:** They boil in the vacuum resid range and have 47 carbons.
- **Components ending with N_2:** They are two-ring naphthenic compounds. The prefix number indicates the number of carbons.
- **S** represents a sulfuric structure.
- **Th** represents thiophene ring.
- **BNit** represents a ring structure containing basic nitrogen.
- **NNit** represents a ring structure containing non-basic nitrogen.
- **ANA** represents two aromatic rings separated by a naphthenic ring.

Feed type specifies a base composition of components in the kinetic reactor model basis. This base fingerprint, along with the distillation, gravity, sulfur content, nitrogen and basic nitrogen content, and bromine number is used to calculate the composition of the feed.

The following reaction types are covered in the model:

- Hydrodesulfurization (HDS)
- Hydrodenitrogenation (HDN)
- Saturation of aromatics (Hydrogenation)
- Ring opening
- Ring dealkylation
- Paraffin hydrocracking
- Saturation of olefins

Rate equations are based on the Langmiur-Hinshelwood mechanism. H_2S inhibits HDS reactions, and both NH_3 and organic nitrogen inhibit acid-catalysed reactions. For each reaction type, an adsorption term is calculated as a multiplier for the rate expression. Each reaction type is first order with respect to the hydrocarbon and each reaction type has a unique order for hydrogen. There are also a set of activity factors that affect various reactions based on the type of reaction and the boiling point of the component.

Rate expression for component A is as follows;

$$\frac{d[A]}{dt} = ACT \times ADS \times [A] \times [H_2]^n \qquad (1)$$

Where,

ACT=Total activity for the reaction

ADS= Adsorption Term

n= unique for each type of reaction

The Hydrocracker model also includes a deactivation model which allows the model to predict the number of days remaining in a catalyst cycle. The deactivation is a function of the amount of multi-ring aromatics in the feed, and the H_2 partial pressure of the system.

3.2. SIMULATIONS

The aim was to simulate the reactor section of an industrial hydrocracker unit. As can be seen in figure 3.1, the system consists of two reactors, hydrotreater and hydrocracker respectively, in series.

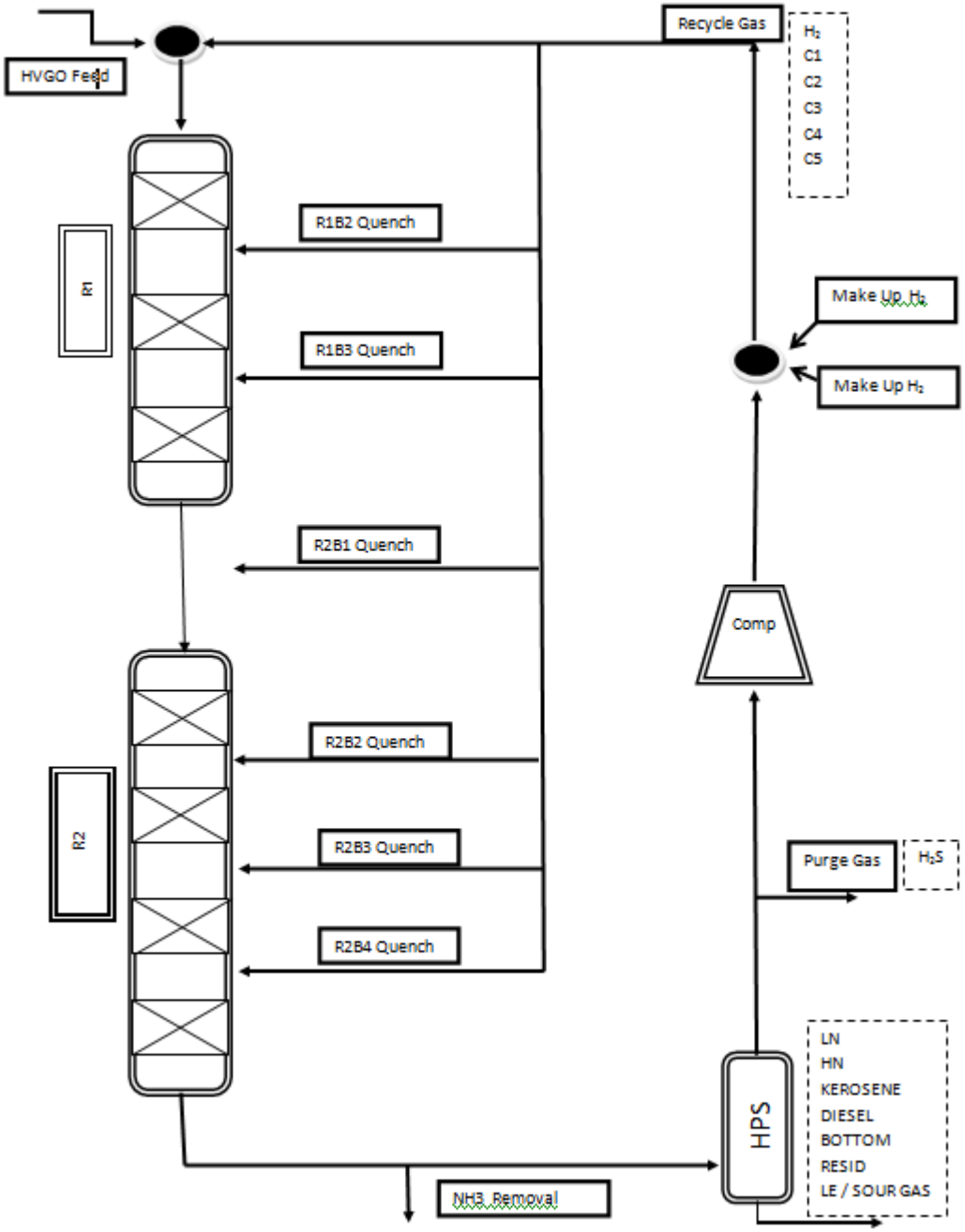

Figure 3.1Simple Flow Sheet

The configuration of the reactor section, the feed type and assay properties that are associated with the feed, the operation conditions, the number of days that the catalyst is in service and the weight-average-bed-temperature (WABT) at the end of the cycle are needed to run the simulations. The simulations were performed by using real plant data. For the first run, the conversion was too low to be accepted and the reactor temperature profile was inconsistent with real plant data as can be seen in Table 3.2 and 3.3 respectively.

Table 3.1 Comparison in terms of conversion

	PLANT	ASPEN
Conversion	46.00%	5.15%

$*Conversion = \left[\frac{(Feed - Bottom)}{Feed} \times 100\right]$

Table 3.2 Comparison in terms of temperature rise

Temperature Rise (PLANT)				**Temperature Rise (ASPEN)**			
	R1	**R2**			**R1**	**R2**	
Bed1	8.43	9.46	C	**Bed1**	7.50	4.43	C
Bed2	5.25	8.93	C	**Bed2**	3.25	3.13	C
Bed3	6.90	5.87	C	**Bed3**	3.47	2.69	C
Bed4	0.00	5.04	C	**Bed4**	0.00	2.39	C

The results showed that the default parameter set of Aspen model did not work for the industrial plant. Hence, calibration (parameter estimation) of the model was inevitable to simulate the plant.

3.3. CALIBRATION OF THE ASPEN MODEL

Since catalyst type, reactor configuration, feed properties and operating conditions vary for different plants, the calibration of the parameter set is essential. The desired values for temperature profile, pressure drop profile, quench flows, NH3 removal, H_2 consumption should be given to the program as inputs of the calibration. Before starting calibration, it should be checked if the overall mass balance is satisfied or not. That is the sum of feed and H_2 make-up flow rates must be equal to the sum of products, NH_3 removal and purge gas flow rates. Although purge gas mechanism is not used in industrial plant, to satisfy overall mass balance, purge gas flow is added to the system. Since purge gas means H_2S removal in this case, its composition was assumed to be solely H_2S. Besides the overall mass balance, component balance based on hydrogen, carbon, sulfur and nitrogen should also be satisfied. Apart from NH_3 and H_2S removal, the H-C-S-N content of products is also important to have

a satisfied material balance. The initial guesses for H-C-S-N content of products were based on the data from literature [40-41] which was summarized in Table 3.4.

Table 3.3 Data for initial values of H-C-S-N content of products

	Average Formula	H Content weight%	C content weight %	S content weight%	N content ppm
Light Naptha	C6H14	83.72	16.28	0-1	0-1
Heavy Naptha	C8H18	84.21	15.79	0-1	0-1
Kerosene	C10H22	84.51	15.49	0-1	0-1
Diesel	C12H23	86.23	13.77	0-1	0-1
Bottom	C20H40	85.71	14.29	0-1	0-1

Then they were adjusted to satisfy the material balance. Hence, the industrial data was verified for consistency before using for calibration.

Aspen HYSYS Hydrocracker has a large set of “calibration factors” and “objective function”. One should first decide the parameters that will construct the objective function, then the calibration factors that are to be tuned to achieve the objective function. Many trials had been performed to obtain a calibrated model. The set of calibration factors and objective function were given in Table 3.5 and 3.6, respectively with the default and tuned values of the parameters. The parameters labeled with a star are the ones selected to construct the objective function and the ones selected as tuning parameters for calibrating the model.

Table 3.4 The parameters that construct objective function

OBJECTIVE FUNCTION			
	Default Sigma	**Tuned Sigma**	
Temperature Rise			
RIBI Temperature Rise [C]	1	1	*
RIB2 Temperature Rise [C]	1	1	*
RIB3 Temperature Rise [C]	1	1	*
R2BI Temperature Rise [C]	1	1	*
R2B2 Temperature Rise [C]	1	1	*
R2B3 Temperature Rise [C]	1	1	*
R2B4 Temperature Rise [C]	1	1	*
Recycle Quench Flows			
Reactor 1			
Bed 1 [STD_m3/h]	720	5000	*
Bed 2 [STD_m3/h]	720	2000	*
Bed 3 [STD_m3/h]	720	3000	*
Reactor 2			
Bed 1 [STD_m3/h]	720	5000	*
Bed 2 [STD_m3/h]	720	4000	*
Bed 3 [STD_m3/h]	720	2000	*
Bed 4 [STD_m3/h]	720	2000	*
Purge Gas Flow - Loop 1 [STD_m3/h]	36	36	
H2 Makeup 1 rate - Loop 1 [STD_m3/h]	36	5000	*
H2 Consumption [STD_m3/m3]	1	25	*

OBJECTIVE FUNCTION (Continue)			
	Default Sigma	**Tuned Sigma**	
Product Flow and Properties			*
Naphtha C6-430F Vol. Flow [m3/h]	1	1	
Diesel 430F-700F Vol. Flow [m3/h]	1	1	
Bottoms 700-1000F Vol. Flow [m3/h]	1	1	
Resid 1000F + Vol. Flow [m3/h]	1	1	
C1C2 Yield [%]	1	1	*
C3 Yield [%]	1	1	*
C4 Yield [%]	1	1	*
Sulfur in Bottom 700+F [ppmwt]	10	100	
Nitrogen in Bottom 700+F [ppmwt]	10	20	
Sulfur in Diesel 430-700 F [ppmwt]	10	100	
Nitrogen in Diesel 430-700 F [ppmwt]	10	20	
Nitrogen in R1 Effluent [ppmwt]	10	10	
Naphtha C6-430F Mass Flow [kg/h]	500	700	*
Diesel 430F-700F Mass Flow [kg/h]	500	500	*
Bottoms 700-1000F Mass Flow [kg/h]	500	100	*
Resid 1000F + Mass Flow [kg/h]	500	10	*
Extended Product Flows			
Light Naphtha 260 F Mass Flow [kg/h]	500	500	
Heavy Naphtha 260-430 F Mass Flow [kg/h]	500	500	
Light Distillate 430-580 F Mass Flow [kg/h]	500	500	
Heavy Distillate 580-700 F Mass Flow [kg/h]	500	500	
Bottoms 700-1000 F Mass Flow [kg/h]	500	500	
Resid 1000 F- Mass Flow [kg/h]	500	500	
Light Naphtha 260 F Vol. Flow [m3/h]	1	1	
Heavy Naphtha 260-430 F Vol. Flow [m3/h]	1	1	
Light Distillate 430-580 F Vol. Flow [m3/h]	1	1	
Heavy Distillate 580-700 F Vol. Flow [m3/h]	1	1	
Bottoms 700-1000 F Vol. Flow [m3/h]	1	1	
Resid 1000 F- Vol. Flow [m3/h]	1	1	

**Sigma shows how close one would like to match the parameters*

Table 3.5 The parameters that construct the calibration set

CALIBRATION SET FACTORS			
	Default	**AfterTuning**	
Global Activity			*
Reactor 1- Bed 1	0.2	1.073	*
Reactor 1- Bed 2	0.2	1.464526638	*
Reactor 1- Bed 3	0.2	2.007229405	*
Reactor 2- Bed 1	0.2	1.881	*
Reactor 2- Bed 2	0.2	2.295	*
Reactor 2- Bed 3	0.2	1.289	*
Reactor 2- Bed 4	0.2	1.218	*
Overall HDS Activity			
Treating Bed	9.76E-02	2.47E-02	*
Treating Bed to Cracking Bed Ratio	0.633594	7.49E-02	*
430- HDS Activity			
Treating Bed	1	1.005117406	
Treating Bed to Cracking Bed Ratio	1	1.007391736	
430-950 HDS Activity			
Treating Bed	0.75812	5	
Treating Bed to Cracking Bed Ratio	1	0.566	
950+ HDS Activity			
Treating Bed	1	1.00E-02	
Treating Bed to Cracking Bed Ratio	1	0.515889533	
Overall HDN Activity			
Treating Bed	0.25083	0.2281	
Treating Bed to Cracking Bed Ratio	0.834171	0.1887	
430- HDN Activity			
Treating Bed	1.216553	4.354218027	
Treating Bed to Cracking Bed Ratio	1	0.252421686	

CALIBRATION SET FACTORS (Continue)			
	Default	**After tuning**	
950+ HDN Activity			
Treating Bed	1.665281	1.141	
Treating Bed to Cracking Bed Ratio	1	0.55	
Overall SAT Activity			
Treating Bed	7.00E-02	0.165964211	*
Treating Bed to Cracking Bed Ratio	1.03472	1.012	*
430- SAT Activity			
Treating Bed	1	1.1	
Treating Bed to Cracking Bed Ratio	1	0.9	
430-950 SAT Activity			
Treating Bed	0.903228	0.203334715	*
Treating Bed to Cracking Bed Ratio	1	2.048	*
950+ SAT Activity			
Treating Bed	0.918217	0.218214215	*
Treating Bed to Cracking Bed Ratio	1	2	*
Overall Cracking Activity			
Treating Bed	0.167863	1.28E-02	*
Treating Bed to Cracking Bed Ratio	1.00E-02	5.00E-02	*
430- Cracking Activity			
Treating Bed	2.200145	2.42	
Treating Bed to Cracking Bed Ratio	1	0.9	
430-950 Cracking Activity			
Treating Bed	2.49799	2.659549173	*
Treating Bed to Cracking Bed Ratio	1	0.100098612	*

CALIBRATION SET FACTORS (Continue)			
	Default	**After tuning**	
950+ Cracking Activity			
Treating Bed	0.8	1.443732665	
Treating Bed to Cracking Bed Ration	1	1.50E-02	
Overall Ring Opening Activity			
Treating Bed	5.00E-03	1.38E-03	
Treating Bed to Cracking Bed Ratio	1.00E-02	2.52E-02	
430- Ring Opening Activity			
Treating Bed	1	1.1	
Treating Bed to Cracking Bed Ratio	1	0.9	
430-950 Ring Opening Activity			
Treating Bed	1	2	
Treating Bed to Cracking Bed Ratio	1	0.2943	
950+ Ring Opening Activity			
Treating Bed	1	3.25E-02	
Treating Bed to Cracking Bed Ratio	1	1.38	
Light Gas Tuning Factors			
C1	8.899997	1.964	
C2	4.999998	10	
C3	1	0.3158	
C4	0.1	4.05E-02	
Catalyst Deactivation			
Initial Deactivation Constant	99915	99915	
Long Term Deactivation Constant	705.8265	705.8265	
Activation Energy	41868	41868	
WABT Bias	-1.01E -06	5.284666646	

CALIBRATION SET FACTORS (Continue)			
	Default	**After tuning**	
Reactor Pressure Drop Factor			
Reactor 1- Bed 1	2.15E-03	1.93E-02	
Reactor 1- Bed 2	2.15E-03	2.19E-02	
Reactor 1- Bed 3	2.15E-03	2.50E-02	
Reactor 2- Bed 1	2.15E-03	2.75E-02	
Reactor 2- Bed 2	2.15E-03	1.98E-02	
Reactor 2- Bed 3	2.15E-03	2.42E-02	
Reactor 2- Bed 4	2.15E-03	2.23E-02	

With the calibrated model, successful predictions were achieved as can be seen in the following tables.

Table 3.6 Comparison in terms of overall conversion

	PLANT	**ASPEN**
Conversion	46.00%	45.85%

Table 3.7 Comparison in terms of temperature rise

Temperature Rise (PLANT)				**Temperature Rise (ASPEN)**			
	R1	**R2**			**R1**	**R2**	
Bed1	10.20	11.45	C	**Bed1**	9.98	11.35	C
Bed2	6.35	10.80	C	**Bed2**	6.69	10.01	C
Bed3	8.35	7.10	C	**Bed3**	8.44	6.90	C
Bed4	0.00	6.10	C	**Bed4**	0.00	5.82	C

Table 3.8 Comparison in terms of H_2 Make-up and H_2 Consumption

	PLANT	**ASPEN**
H_2 Makeup 1 rate - Loop 1 [STD_m3/h]	27250.00	24880.02
H_2 Consumption [STD_m3/m3]	143.00	128.81

Table 3.9 Comparison in terms of product flows

	PLANT	**ASPEN**
C1C2 Yield [%]	0.51	0.30
C3 Yield [%]	0.31	0.66
C4 Yield [%]	1.76	2.22
Naphtha C6-430F Mass Flow [kg/h]	*	37748.80
Diesel 430F-700F Mass Flow [kg/h]	*	26502.31
Bottoms 700-1000F Mass Flow [kg/h]	*	6752.44

**Plant product ranges are different from ASPEN ranges.*

Since the fractionators were not simulated, the product flows were given by Aspen standard cuts. As can be seen in the following table, the standard cuts of Aspen differ from fractionated cuts of industrial plant.

Table 3.10 The temperature ranges of standard cuts and fractionated cuts

	Standard Cuts (defined by ASPEN)	**Fractionated Cuts (defined by PLANT)**
Naphtha	C6-430F (C6-211 °C)	35 °C- 144 °C
Diesel	430F-700F (211-371 °C)	148 °C- 365 °C
Bottom	700F-1000F (371-537 °C)	279 °C- 488 °C

A true boiling point (TBP) vs. mass fraction graph was plotted with respect to Aspen product mixture (the effluent of reactor section), industrial product mixture and individual products of industrial plant as seen in Figure 3.2. In order to convert standard cuts into fractionated cuts, that figure was used.

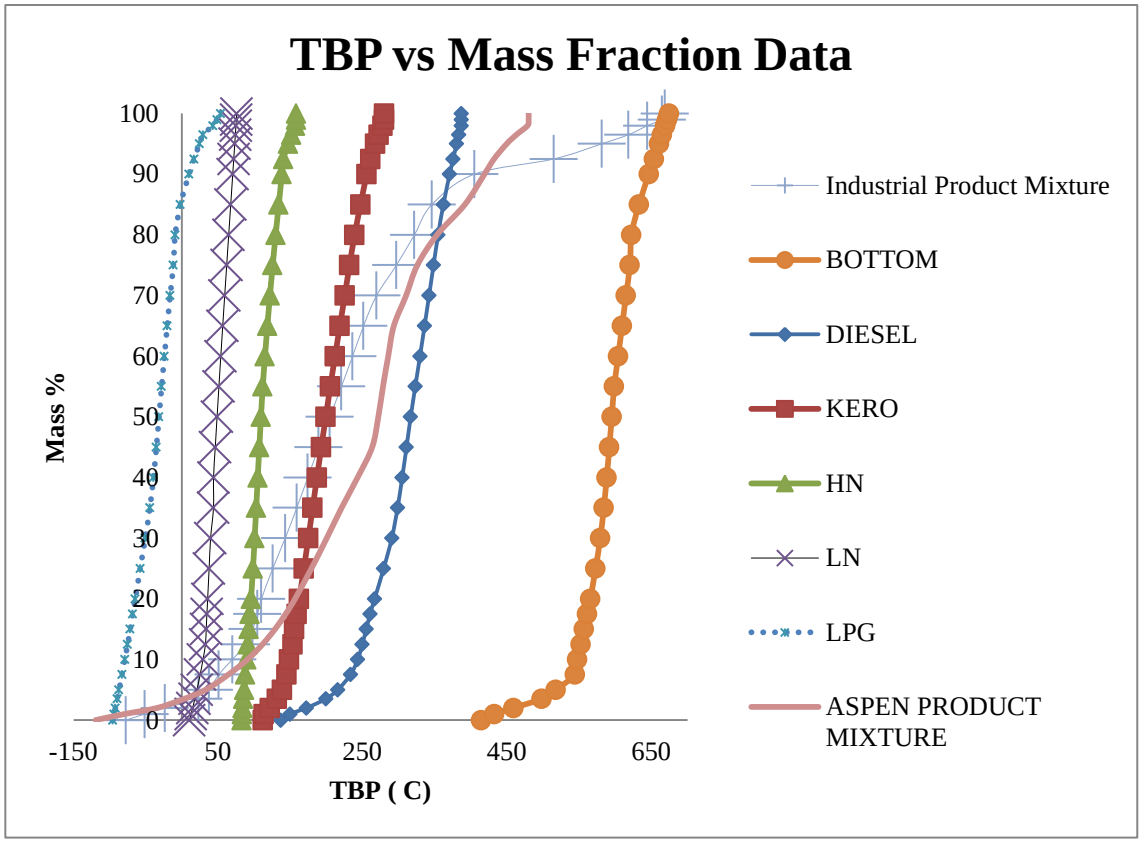

Figure 3.2 TBP vs Mass Fraction Data for individual products, industrial and ASPEN product mixture

ASPEN gives TBP data of product mixture. The industrial distillation data of individual products were converted into TBP data by ASPEN Oil Manager. The industrial product mixture was obtained by blending these individual products, again using ASPEN Oil Manager. The further details of this process are given in chapter 4.

In fact it is easily observed that there is a significant mismatch between the simulated product mixture and industrial product mixture data curves. The flows of individual products were computed by using the following equations along with Figure 3.2.

$$M_{ASPEN\,ProductMixture} \times 0.005 = M_{SourGas} \tag{2}$$

$$M_{ASPEN\,ProductMixture} \times (0.04 - 0.005) = M_{LPG} \times 0.9 \tag{3}$$

$$M_{ASPEN\,ProductMixture} \times (1 - 0.9) = M_{Bottom} \tag{4}$$

$$M_{ASPEN\,ProductMixture} \times (0.085 - 0.025) = M_{LN} \tag{5}$$

$$M_{ASPEN\,ProductMixture} \times (0.125 - 0.085) = M_{HN} \times 0.55 \tag{6}$$

$$M_{ASPEN\,ProductMixture} \times (0.83 - 0.56) = M_{Diesel} \times (1 - 0.25) \tag{7}$$

$$M_{ASPEN\,ProductMixture} = M_{SourGas} + M_{LPG} + M_{Bottom} + M_{LN} + M_{HN} + M_{Diesel} + M_{Kerosene} \quad (8)$$

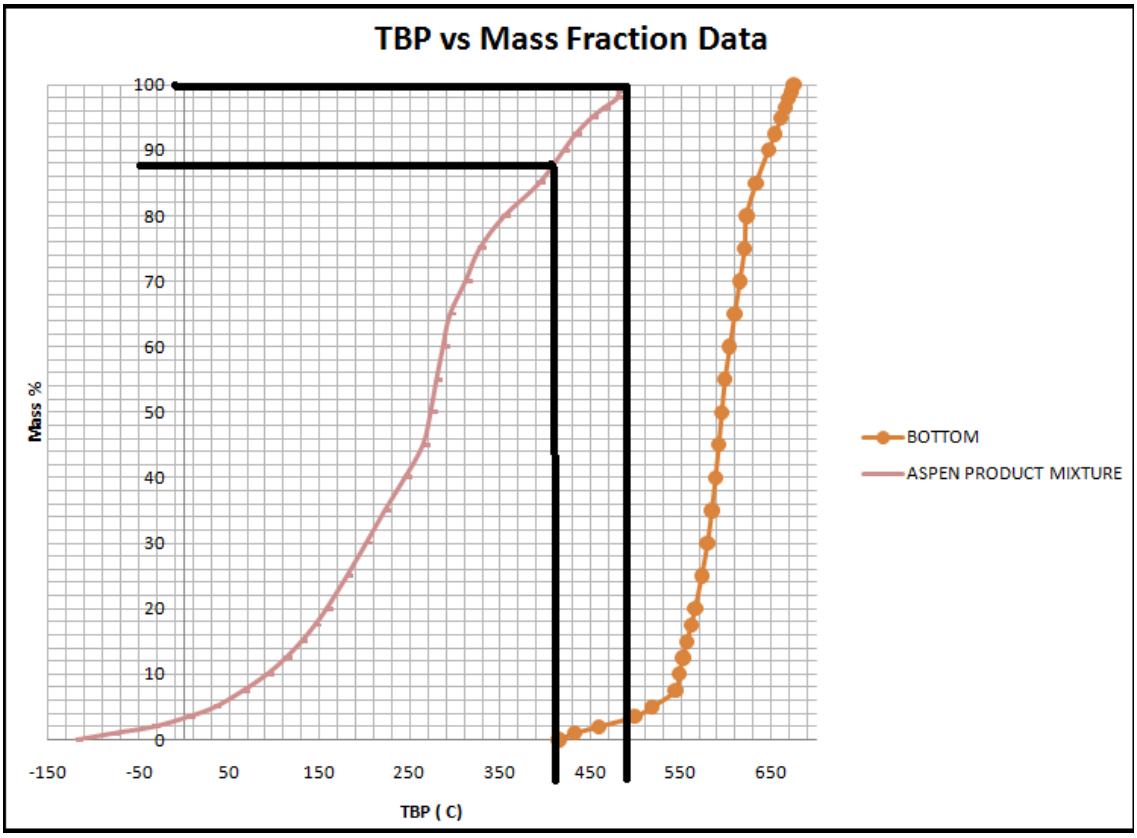

Figure 3.3 TBP vs. Mass Fraction Graph of Bottom and ASPEN product mixture

The TBP curves of bottom and ASPEN product mixture were given in Figure 3.3. The initial boiling point of bottom is around 410 °C and the corresponding mass fraction of ASPEN product mixture is 90 % for this point. Hence, the 90% to 100 % portion of ASPEN product mixture curve would represent the individual bottom product. Therefore, the mass flow of bottom can be found easily by equation 4. The other equations were constructed in the same manner.

The results were as follows.

Table 3.11 Comparison of product flows in terms of PLANT cuts

	PLANT	**ASPEN**
Sour Gas	2590.50	391.00
LPG	2434.50	3039.00
LN	6270.00	4884.50
HN	13531.50	5683.50
KERO	31446.00	28594.00
DIESEL	17703.50	28134.00
BOTTOM	5070.00	7815.00

Despite a satisfying overall conversion, the distribution of products needed to be improved as seen in Table 3.12. One suggestion to improve the yields was to re-define the composition of purge gas. As stated earlier, the purge gas phenomena generally means H_2S removal. In this industrial plant, H_2S is removed by off-gas which is called as “sour gas”. Then, the composition of sour gas would be a better assumption for purge gas composition. However, this new assumption did not make much difference on the results. At this point, the most meaningful suggestion to improve the results would to generate a new calibration set. Nevertheless, generating that new calibration set was not proceeded because the study up to here was useful enough to understand the process and unit. Hence, the preliminary work for modeling of a hydrocracker reactor was completed.

Chapter 4

4. FEED AND PRODUCT CHARACTERIZATION

Discrete lumping method requires that the feed and products are divided into pseudocomponents. This process is called characterization. For this study, characterization was performed by ASPEN HYSYS Oil Manager. However, some background information is given in the following sections to understand the results better.

4.1. DISTILLATION METHODS

Volatility characteristics are vital when petroleum fractions are to be discussed. There are two main methods; ASTM (American Society for Testing and Materials) Distillations and TBP (True Boiling Point) Distillations. The main difference between these groups is the degree of fractionation obtained during distillation.

TBP Distillations are performed in a multi-stage batch fractionation with high reflux ratios conducted at atmospheric or vacuum conditions. The high degree of fractionation gives accurate component distributions for mixtures. Therefore, TBP curves of petroleum fractions were used for this study.

In ASTM Distillations, since only one equilibrium stage is used and no reflux is returned, the degree of separation is not good. However, it is used on a routine basis in a plant due to its simplicity [2]. There are different ASTM methods. In our case, ASTM D86 and ASTM D1160 were used to characterize the fractions. ASTM D86 is carried out at atmospheric pressures and the curves are plotted with respect to volume percent [42]. It is used for the distillation of light naptha, heavy naptha, kerosene and diesel. On the other hand, ASTM D1160 is used for heavy products such as bottom and feed (HVGO) itself. It is carried out at pressures between 1 mmHg and 50 mmHg, absolute [42].

API Data Book [42] presents standard procedures for converting ASTM Distillations and TBP Distillations into each other. The ASTM D86 and ASTM D1160 Distillation data obtained from the industrial plant were converted into TBP Distillation data by ASPEN HYSYS Oil Manager which uses the standard procedures described in API Data Book as well.

4.2. DIVIDING TBP CURVE INTO PSEUDOCOMPONENTS

Typically, the crude TBP between 100 F and resid end point is divided into narrow cuts, each spanning 20 F. These cuts are defined as *standard TBP boiling ranges* and components boiling in these ranges are called pseudocomponents. Since the ranges are small enough, pseudocomponents act like pure components. Providing narrower cuts, any other range can be used as shown as shown in Figure 4.1. As seen in this figure, once the cut points of the pseudocomponents are defined, the volume percent of each cut can easily be computed from TBP curve of crude.

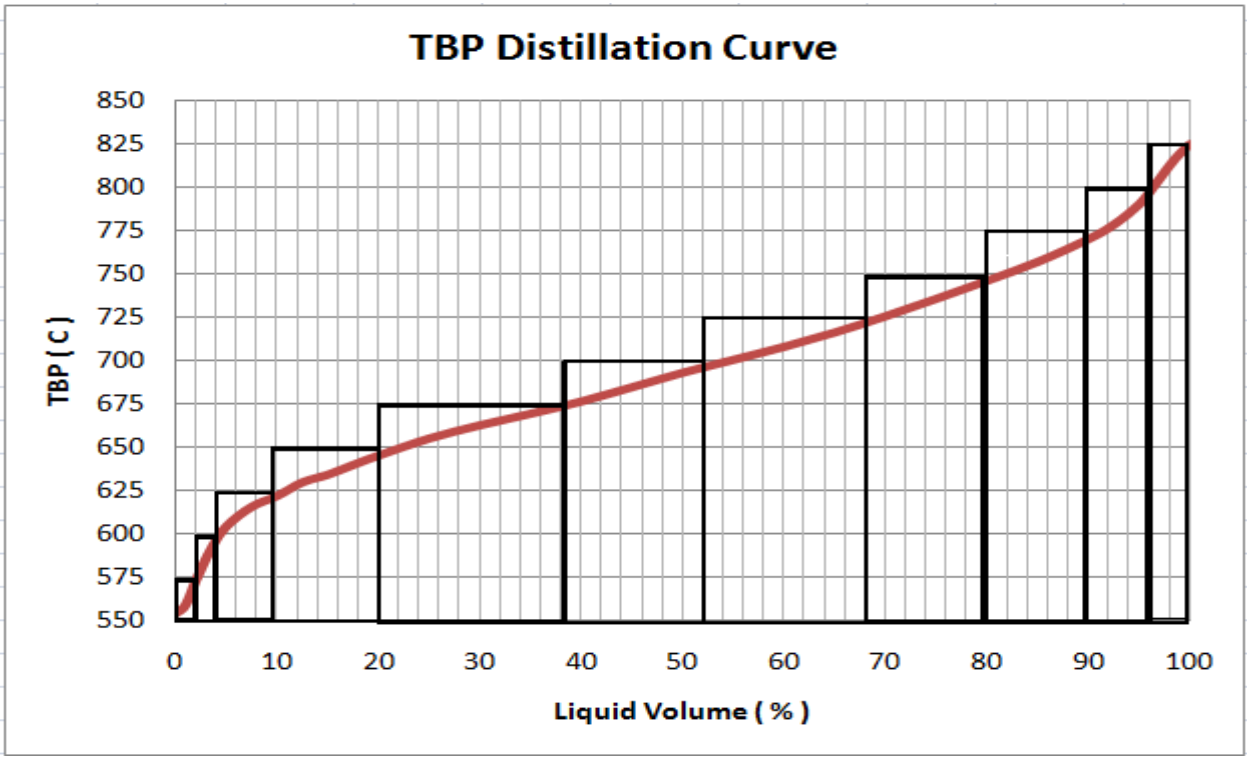

Figure 4.1 Graphical Representation of Pseudocomponent Determination with a 25°C increment

In ASPEN HYSYS Oil Manager, the pseudocomponents breakdown should be specified by either supplying the cut-point ranges with corresponding number of cuts or letting the program do it automatically. In automatic mode, Aspen uses the following ranges and corresponding cuts.

Table 4.1 The temperature ranges of standard cuts and fractionated cuts

Cut-point Range	Number of Cuts
100 - 800°F	28
800 - 1200°F	8
1200 - 1600°F	4

In our study, the cut point ranges were specified as 10 °C increments.

4.3. DETERMINATION OF THE PROPERTIES OF THE PSEUDOCOMPONENTS

Generally, each pseudocomponent is defined by average boiling point (normal boiling point, NBP), specific gravity and molecular weight. The first two properties are obtained experimentally, and the third one is calculated by correlations. After knowing these properties, all other thermophysical and thermodynamic properties can easily be computed with different correlations.

Having determined the cut points, the first step is to calculate the NBP of each pseudocomponents. Since the range is chosen as sufficiently narrow, NBP is found by taking the average of initial and final cut point of each range as follows.

$$NBP_i = \frac{\left[ICP_i + FCP_i\right]}{2} \tag{9}$$

Here, ICP_i and FCP_i stand for initial and final cut point of pseudocomponent i respectively. In fact they are the lowest and highest TBP of the pseudocomponent.

Sometimes the distillation test may include the measurement of specific gravity versus distilled volume. However, in our case the average gravity (API gravity) of the whole petroleum fraction was available. The definition of the API gravity is as follows.

$$API = \frac{141.5}{SG} - 131.5 \tag{10}$$

Hence, we had the average specific gravity of the feed. ASPEN HYSYS Oil Manager uses the constant K (Watson characterization factor) approach for the calculation of each pseudocomponent's specific gravity. The definition of K is as follows.

$$K_i = \frac{MeABP_i^{1/3}}{SG_i} \tag{11}$$

In fact, the $MeABP_i$ stands for mean average boiling point of the pseudocomponent i and since the range for the component is too narrow, $MeABP_i$ is assumed to be equal to NBP_i.

In this method, a constant value of Watson *K* is applied to equation 3 to get the specific gravities of each pseudocomponent. These gravities are then averaged and compared with the available average specific gravity of the whole petroleum fraction. Watson *K* is then adjusted until the resulting average gravity agrees with the given average gravity. The found specific gravity values are used for converting the volume fractions into mass or molar fractions, and also for calculation of other properties that are necessary for modeling.

ASPEN HYSYS Oil Manager has a large variety of correlations to compute physical properties. Among them, Lee-Kesler [43] correlations are used for the calculation of molecular weight (MW), critical temperature (T_c), critical pressure (P_c) and accentric factor (ω_i) of the pseudocomponents. The equations are given below.

$$MW_i = -12272.6 + 9486.4 \times SG_i + (4.6523 - 3.3287 \times SG_i) \times NBP_i + \left[\left(1 - 0.77084 \times SG_i - 0.02058 \times SG_i^2\right) \times \left(1.3437 - \frac{720.79}{NBP_i} \right) \times \frac{10^7}{NBP_i} \right] + \left[\left(1 - 0.80882 \times SG_i + 0.02226 \times SG_i^2\right) \times \left(1.8828 - \frac{181.98}{NBP_i} \right) \times \frac{10^{12}}{NBP_i^3} \right] \quad (12)$$

$$T_{c,i} = 341.7 + 811 \times SG_i + \left[\left(0.4244 \times 0.1174 \times SG_i\right) \times NBP_i \right] + \left[\left(0.4669 - 3.2623 \times SG_i\right) \times \frac{10^5}{NBP_i} \right] \quad (13)$$

$$\ln P_{c,i} = 8.3634 - \frac{0.0566}{SG_i} - \left(0.24244 + \frac{2.2898}{SG_i} + \frac{0.11857}{SG_i^2} \right) \times \frac{10^{-3}}{NBP_i} + \left(1.4685 + \frac{3.648}{SG_i} + \frac{0.47227}{SG_i^2} \right) \times \frac{10^{-7}}{NBP_i^2} - \left(0.42019 + \frac{1.6977}{SG_i^2} \right) \times \frac{10^{-10}}{NBP_i^3} \quad (14)$$

$$\omega_i = -7.904 + 0.1352 \times K_i - 0.007465 \times K_i^2 + 8.359 \times NBP_{r,i} + \frac{\left(1.408 - 0.01063 \times K_i\right)}{NBP_{r,i}} \quad (15)$$

Here, $NBP_{r,i}$ is the reduced boiling point temperature and defined as follows.

$$NBP_{r,i} = \frac{NBP_i}{T_{c,i}} \tag{16}$$

4.4. CHARACTERIZATION BY ASPEN HYSYS OIL MANAGER

The first step was to determine the light end (LE) components of the system. These are the pure components having the highest volatility. For our system, methane, ethane, propane and butane were chosen as LE.

As stated previous sections, distillation data were needed to define the petroleum fractions. In industrial plant, the feed and bottom are characterized by ASTM D1160 method. ASTM D86 is performed for characterization of diesel, kerosene, light naphtha (LN) and heavy naphtha (HN). The gas chromatography data of LE are available as well. ASPEN HYSYS Oil Manager converts ASTM D1160 and ASTM D86 data into TBP data automatically by using the procedures described in API Data Book [42].

After obtaining individual TBP curves, the next step was generation of pseudocomponents. Stangeland [15] formed his pseudocomponents with 50 F (~32.2 °C) ranges and defined them by the TBP of the end of the range. He described the first pseudocomponent by the range 0-50 F (-17.7 °C to 32.2 °C) and assigned it to butanes and lighter products, ie. LE. In this study the cut range was determined as 10 °C and the LE were lumped to the first pseudocomponent in the range 0° to 10 °C TBP. The smaller the increment the better the results are. Feed enters the reactor and then is converted to products by the reactions. Therefore, some entering pseducomponents would not exist in outlet stream and some new pseudocomponents would be generated. The input feed includes heaviest (higher TBP) pseudocomponents only. However, the output products include lighter components. Hence, the feed and product mixture were first divided into pseudocomponents separately. Then, the composite pseudocomponent list including all the pseudocomponents was created.

4.5. CHARACTERIZATION RESULTS

In order to validate the model, simulations should be run and checked against different sets of plant operating data. Therefore, the characterization was performed for the operating conditions obtained from six different days (Days 1-6) and the results were given in the following tables and figures. Some pseudocomponents were not included in the tables for brevity.

Table 4.2 Physical Properties of Pseudocomponents (Day 1)

Component Number	TBP (°C)	NBP (°C)	Molecular Weight (g/mole)	Specific Gravity	Tc (°C)	Pc (kPa)	Accentric Factor
1	10.00	6.03	72.29	0.59	171.39	3749.92	0.13
2	20.00	14.73	72.73	0.60	178.72	3519.87	0.16
3	30.00	25.30	73.40	0.61	188.40	3351.13	0.19
4	40.00	36.64	74.29	0.63	200.21	3261.57	0.22
5	50.00	45.45	75.32	0.65	210.54	3222.04	0.24
6	60.00	54.91	79.18	0.67	222.83	3211.92	0.25
7	70.00	63.63	83.55	0.68	234.16	3177.99	0.26
8	80.00	74.09	87.20	0.69	246.98	3113.87	0.28
9	90.00	86.29	92.66	0.71	263.21	3058.31	0.28
10	100.00	95.47	97.64	0.72	274.90	3003.73	0.29
11	110.00	104.85	101.83	0.73	285.66	2923.43	0.30
12	120.00	114.60	107.03	0.74	296.97	2849.64	0.32
13	130.00	124.74	112.36	0.75	308.49	2771.80	0.33
14	140.00	134.86	117.98	0.76	319.87	2696.95	0.34
15	150.00	145.50	124.52	0.77	331.88	2625.34	0.36
44	440.00	434.95	409.42	0.90	603.05	1146.08	0.96
45	450.00	445.04	423.89	0.90	611.81	1117.86	0.99
46	460.00	455.12	438.33	0.91	620.52	1090.33	1.01
47	470.00	465.03	452.72	0.91	629.03	1064.03	1.04
48	480.00	474.76	466.38	0.92	637.28	1037.71	1.07
49	490.00	484.56	479.80	0.92	645.46	1010.86	1.09
50	500.00	494.87	494.06	0.92	653.97	982.66	1.12
51	510.00	505.42	509.99	0.93	662.66	954.77	1.15
52	521.37	514.52	524.60	0.93	670.08	930.77	1.18
53	530.00	525.19	540.40	0.93	678.49	900.60	1.21
54	540.00	533.86	554.25	0.93	685.23	876.16	1.24
55	550.00	544.77	568.67	0.94	694.20	850.86	1.27
56	560.00	554.37	580.92	0.94	702.25	830.91	1.30
57	570.00	565.14	592.27	0.94	10.96	806.14	1.33
58	580.00	575.40	603.74	0.94	719.30	783.71	1.36
59	590.14	585.22	618.40	0.95	727.71	766.50	1.38

Table 4.3 Physical Properties of Pseudocomponents (Day 2)

Component Number	TBP (°C)	NBP (°C)	Molecular Weight (g/mole)	Specific Gravity	Tc (°C)	Pc (kPa)	Accentric Factor
1	10.00	6.00	71.96	0.59	170.98	3725.80	0.14
2	20.00	15.57	73.64	0.60	179.09	3504.65	0.16
3	30.00	25.03	74.86	0.61	188.37	3360.60	0.19
4	40.00	36.27	75.89	0.63	199.67	3248.85	0.22
5	50.00	44.74	77.34	0.65	210.18	3232.66	0.24
6	60.00	54.91	79.31	0.67	223.10	3221.28	0.25
7	70.00	64.52	83.25	0.68	234.96	3169.79	0.27
8	80.00	75.19	87.45	0.70	248.41	3112.80	0.28
9	90.00	86.28	92.90	0.71	263.44	3065.35	0.28
10	100.00	96.33	97.39	0.72	275.63	2989.22	0.29
11	110.00	104.35	101.42	0.73	285.14	2929.03	0.30
12	120.00	114.63	106.64	0.74	296.97	2848.47	0.32
13	130.00	124.82	112.62	0.75	308.82	2777.29	0.33
14	140.00	135.22	118.00	0.76	320.36	2696.83	0.34
15	150.00	144.99	123.26	0.76	331.09	2623.46	0.36
44	440.00	434.33	408.84	0.90	602.55	1148.34	0.96
45	450.00	445.01	423.63	0.90	611.76	1117.67	0.99
46	460.00	455.04	437.94	0.91	620.41	1090.20	1.01
47	470.00	465.09	452.42	0.91	629.04	1063.36	1.04
48	480.00	474.86	466.24	0.92	637.33	1037.11	1.07
49	490.00	484.77	480.09	0.92	645.63	1010.33	1.09
50	500.00	494.83	493.97	0.92	653.93	982.73	1.12
51	510.00	504.88	508.55	0.92	662.16	955.61	1.15
52	521.37	515.33	525.35	0.93	670.69	928.14	1.18
53	530.00	524.53	540.00	0.93	678.01	902.89	1.21
54	540.00	534.67	555.29	0.93	685.79	873.28	1.24
55	550.00	544.75	569.66	0.93	694.00	849.25	1.27
56	560.00	554.59	583.33	0.94	702.41	830.11	1.30
57	570.00	564.33	595.88	0.94	710.56	810.26	1.32
58	580.00	575.29	607.62	0.94	719.40	785.61	1.36
59	590.14	587.56	624.04	0.95	729.65	761.94	1.39

Table 4.4 Properties of Pseudocomponents (Day 3)

Component Number	TBP (°C)	NBP (°C)	Molecular Weight (g/mole)	Specific Gravity	Tc (°C)	Pc (kPa)	Accentric Factor
1	10.00	5.92	72.50	0.59	170.87	3722.84	0.13
2	20.00	15.61	73.27	0.60	179.09	3502.68	0.16
3	30.00	25.00	74.45	0.61	187.92	3338.29	0.19
4	40.00	36.27	76.22	0.63	199.77	3253.67	0.22
5	50.00	45.15	78.02	0.65	210.20	3218.53	0.24
6	60.00	55.15	79.72	0.67	223.16	3214.71	0.26
7	70.00	63.92	83.22	0.68	234.27	3170.33	0.27
8	80.00	75.29	86.93	0.69	248.05	3098.01	0.28
9	90.00	85.92	92.61	0.71	263.03	3069.33	0.28
10	100.00	95.66	97.74	0.72	275.31	3007.42	0.29
11	110.00	104.60	101.76	0.73	285.58	2931.21	0.30
12	120.00	114.82	106.54	0.74	297.12	2845.12	0.32
13	130.00	124.88	112.14	0.75	308.68	2771.43	0.33
14	140.00	134.94	118.07	0.76	320.17	2701.59	0.34
15	150.00	145.08	123.76	0.77	331.38	2627.66	0.36
44	440.00	434.96	408.68	0.90	602.97	1144.92	0.96
45	450.00	445.08	423.13	0.90	611.75	1116.56	0.99
46	460.00	455.38	438.04	0.91	620.66	1088.74	1.02
47	470.00	465.21	453.10	0.91	629.21	1063.71	1.04
48	480.00	474.58	466.22	0.92	637.14	1038.35	1.07
49	490.00	484.52	479.27	0.92	645.37	1010.43	1.09
50	500.00	494.85	493.51	0.92	653.90	982.16	1.12
51	510.00	505.39	509.61	0.92	662.61	954.55	1.15
52	521.37	515.13	525.41	0.93	670.56	929.00	1.18
53	530.00	525.29	540.12	0.93	678.54	900.02	1.21
54	540.00	535.10	555.10	0.93	686.09	871.73	1.24
55	550.00	545.24	571.22	0.94	695.02	853.84	1.27
56	560.00	553.76	581.65	0.94	702.11	835.54	1.29
57	570.00	565.71	594.18	0.94	711.74	807.71	1.33
58	580.00	573.22	603.36	0.94	717.96	792.18	1.35

Table 4.5 Physical Properties of Pseudocomponents (Day 4)

Component Number	TBP (°C)	NBP (°C)	Molecular Weight (g/mole)	Specific Gravity	Tc (°C)	Pc (kPa)	Accentric Factor
1	10.00	2.02	72.40	0.58	167.85	3709.08	0.11
2	20.00	13.27	72.90	0.60	177.10	3489.36	0.15
3	30.00	25.00	73.66	0.61	188.07	3346.30	0.19
4	40.00	36.17	74.31	0.63	199.57	3247.34	0.22
5	50.00	45.06	75.18	0.65	209.93	3211.03	0.24
6	60.00	55.15	79.35	0.67	223.08	3211.82	0.26
7	70.00	63.84	83.34	0.68	234.16	3169.84	0.26
8	80.00	75.24	86.85	0.69	247.84	3094.27	0.28
9	90.00	85.81	92.61	0.71	262.80	3067.47	0.28
10	100.00	95.81	98.05	0.72	275.47	3005.83	0.29
11	110.00	104.49	101.94	0.73	285.43	2931.49	0.30
12	120.00	114.82	106.78	0.74	297.08	2844.10	0.32
13	130.00	124.74	112.24	0.75	308.45	2770.80	0.33
14	140.00	134.81	118.00	0.76	319.87	2698.50	0.34
15	150.00	145.27	123.81	0.76	331.42	2621.91	0.36
44	440.00	435.50	410.34	0.90	603.55	1144.77	0.96
45	450.00	445.11	424.83	0.90	611.97	1118.97	0.99
46	460.00	454.39	437.68	0.91	619.93	1092.96	1.01
47	470.00	464.78	451.48	0.91	628.72	1063.52	1.04
48	480.00	474.88	465.43	0.92	637.26	1036.00	1.07
49	490.00	484.90	479.47	0.92	645.65	1009.04	1.09
50	500.00	494.92	493.69	0.92	653.97	982.07	1.12
51	510.00	504.97	508.37	0.92	662.21	955.05	1.15
52	520.00	515.03	523.61	0.93	670.35	927.88	1.18
53	530.00	525.64	542.41	0.93	678.92	900.15	1.21
54	540.00	534.36	553.24	0.93	685.51	873.71	1.24
55	550.00	545.05	568.34	0.93	694.00	846.25	1.27
56	560.00	555.73	585.14	0.94	703.42	828.27	1.30
57	570.00	563.55	599.45	0.94	710.49	817.08	1.32
58	580.00	575.24	610.47	0.95	719.73	788.98	1.35
59	593.00	587.65	625.66	0.95	729.93	763.37	1.39

Table 4.6 Physical Properties of Pseudocomponents (Day 5)

Component Number	TBP (°C)	NBP (°C)	Molecular Weight (g/mole)	Specific Gravity	Tc (°C)	Pc (kPa)	Accentric Factor
1	10.00	6.13	72.63	0.59	171.32	3741.22	0.14
2	20.00	14.05	73.10	0.60	178.11	3514.52	0.16
3	30.00	25.54	73.86	0.61	188.75	3359.18	0.19
4	40.00	36.57	74.53	0.63	200.21	3263.79	0.22
5	50.00	45.30	75.17	0.65	210.43	3222.57	0.24
6	60.00	54.95	79.17	0.67	222.85	3211.33	0.25
7	70.00	63.96	83.56	0.68	234.40	3173.12	0.26
8	80.00	74.08	87.51	0.70	247.21	3121.27	0.28
9	90.00	86.31	92.67	0.71	263.35	3061.48	0.28
10	100.00	95.61	97.83	0.72	275.15	3005.28	0.29
11	110.00	104.77	101.97	0.73	285.67	2927.25	0.30
12	120.00	114.63	106.86	0.74	296.95	2847.64	0.32
13	130.00	124.81	112.29	0.75	308.53	2770.23	0.33
14	140.00	134.93	117.96	0.76	319.95	2696.35	0.34
15	150.00	145.20	123.91	0.76	331.39	2623.46	0.36
44	440.00	434.98	409.26	0.90	603.06	1145.71	0.96
45	450.00	445.03	423.56	0.90	611.77	1117.46	0.99
46	460.00	455.28	438.30	0.91	620.62	1089.60	1.02
47	470.00	464.94	452.31	0.91	628.93	1063.87	1.04
48	480.00	474.81	466.07	0.92	637.28	1037.14	1.07
49	490.00	484.69	479.61	0.92	645.53	1010.09	1.09
50	500.00	494.90	493.94	0.92	653.97	982.44	1.12
51	510.00	505.18	509.86	0.93	662.49	955.62	1.15
52	520.00	514.43	524.62	0.93	670.03	931.13	1.18
53	530.00	525.09	540.23	0.93	678.41	900.86	1.21
54	540.00	534.19	553.61	0.93	685.36	873.97	1.24
55	550.00	544.61	567.95	0.94	694.16	852.16	1.27
56	560.00	554.32	580.08	0.94	702.28	831.65	1.29
57	570.00	565.34	591.26	0.94	711.14	805.85	1.33
58	580.00	575.44	602.58	0.94	719.35	783.81	1.36
59	593.00	585.17	617.22	0.95	727.71	766.92	1.38

Table 4.7 Physical Properties of Pseudocomponents (Day 6)

Component Number	TBP (°C)	NBP (°C)	Molecular Weight (g/mole)	Specific Gravity	Tc (°C)	Pc (kPa)	Accentric Factor
1	10.00	6.21	72.65	0.59	171.49	3748.22	0.14
2	20.00	16.36	73.23	0.60	180.39	3543.42	0.17
3	30.00	26.53	73.61	0.61	189.35	3349.64	0.20
4	40.00	35.53	74.28	0.63	198.85	3237.38	0.22
5	50.00	44.02	75.00	0.65	208.86	3203.78	0.24
6	60.00	54.91	79.24	0.67	222.81	3211.03	0.25
7	70.00	64.43	82.96	0.68	234.96	3173.45	0.27
8	80.00	73.99	87.67	0.70	247.30	3127.20	0.27
9	90.00	86.35	92.54	0.71	263.28	3057.91	0.28
10	100.00	95.71	98.08	0.72	275.39	3007.50	0.29
11	110.00	104.45	101.87	0.73	285.35	2930.81	0.30
12	120.00	114.80	106.88	0.74	297.11	2845.28	0.32
13	130.00	124.88	112.31	0.75	308.61	2769.43	0.33
14	140.00	134.94	117.99	0.76	319.97	2696.67	0.34
15	150.00	145.00	123.75	0.76	331.14	2624.38	0.36
44	440.00	434.97	409.65	0.90	603.10	1146.33	0.96
45	450.00	444.96	423.82	0.90	611.75	1118.18	0.99
46	460.00	454.89	437.79	0.91	620.29	1090.71	1.01
47	470.00	464.85	451.66	0.91	628.79	1063.41	1.04
48	480.00	474.78	465.43	0.92	637.19	1036.41	1.07
49	490.00	484.89	479.27	0.92	645.62	1008.81	1.09
50	500.00	495.13	493.78	0.92	654.12	981.27	1.12
51	510.00	504.91	509.27	0.92	662.25	956.16	1.15
52	520.00	514.49	524.46	0.93	670.06	930.75	1.18
53	530.00	525.18	540.31	0.93	678.47	900.55	1.21
54	540.00	534.06	553.38	0.93	685.25	874.25	1.24
55	550.00	544.81	567.59	0.94	694.22	850.65	1.27
56	560.00	554.43	580.07	0.94	702.33	830.94	1.30
57	570.00	564.76	591.60	0.94	710.76	808.01	1.33
58	580.00	575.59	603.78	0.94	719.48	783.54	1.36
59	593.00	588.73	621.09	0.95	730.54	758.96	1.39

As can be observed in Figure 4.2., feed contains heavier pseudocomponents, i.e components having higher boiling points. Apart from Day 4, the compositions are similar for other days.

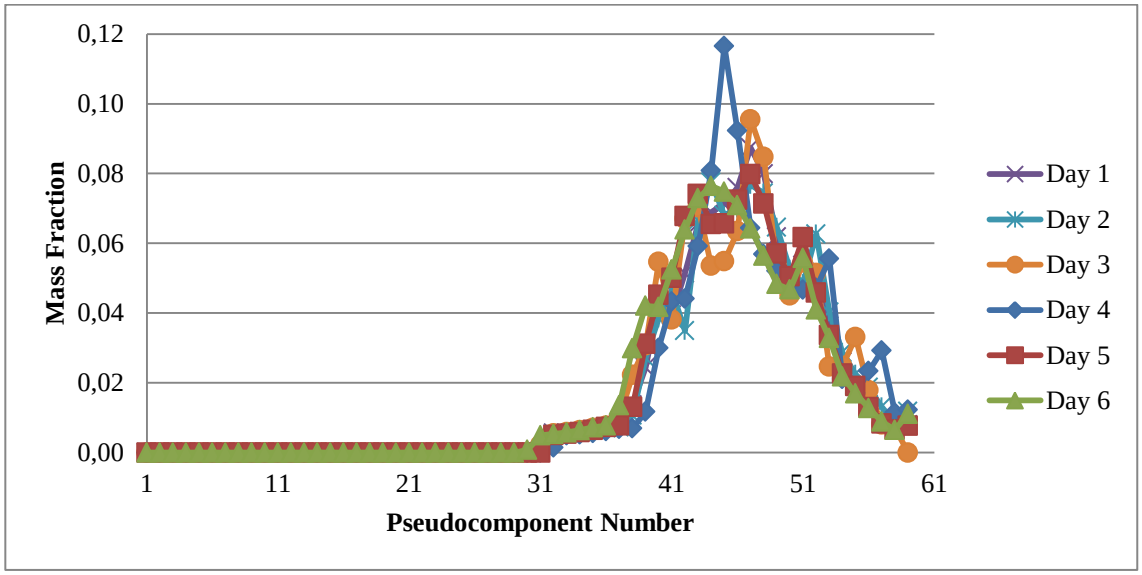

Figure 4.2 Feed Compositions with respect to pseudocomponents for 6 different days

When the product mixture compositions for different days are investigated, they are similar to each other as can be seen in Figure 4.3. Although the feed composition of Day 4 is different from the others, it gives similar distribution of pseudocomponents in products. This is due to the fact that operating conditions (e.g. bed inlet temperatures) are adjusted by the actual system to yield similar products.

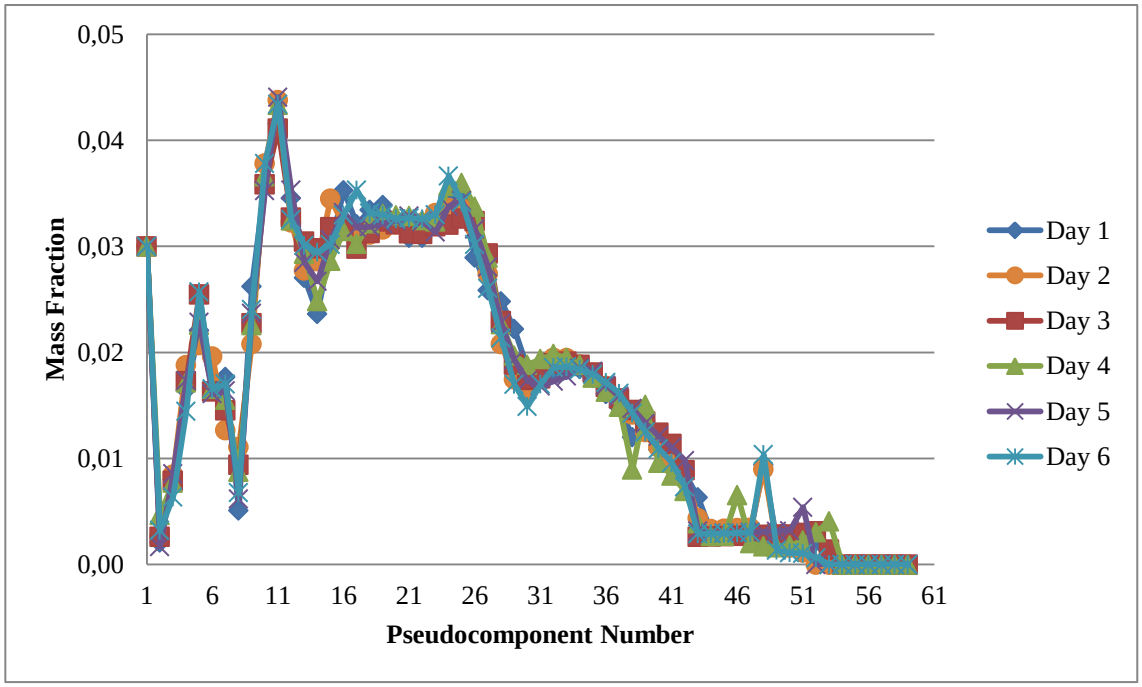

Figure 4.3 Product Mixture Compositions with respect to pseudocomponents for 6 different days

Chapter 5

5. MODELING OF A HYDROCRACKER REACTOR

In this study, discrete lumping approach was employed to model an industrial hydrocracker reactor. In the literature several discrete lumped models have been proposed. Among them Stangeland's [15] kinetic model has been widely used in fuel processing industry because it has the capability to predict product yield, reactor temperature profile and make-up hydrogen requirement satisfactorily.

Mohanty [17] adopted Stangeland's model for the simulation of a two-stage hydrocracker unit. Pacheco and Dassori [16] improved Mohanty's model by introducing two additional parameters by which the overall mass balance is satisfied as well. In this thesis the starting point is this model.

At the beginning, the Mohanty's model with Pacheco and Dassori's additional parameter was adopted and simulations were performed by the industrial data given in Mohanty's paper [17]. Since the results matched well enough with those given in that paper [17], this model was used to simulate the industrial hydrocracker reactor. However, the results were not satisfactory. Therefore, some modifications were introduced into the model. The modeling details were explained step by step in the following sections.

5.1. FIRST PRINCIPLE MODEL DEVELOPMENT

The following modeling assumptions are used in order not to overcomplicate the resulting model.

- Steady-state operation is assumed.
- Reactor operates under adiabatic conditions.
- Reactor is an ideal plug flow reactor without axial and radial dispersion.
- Hydrocracking is a first order pseudo-homogeneous reaction [10,15]
- Components having a boiling point less than 400 K are assumed not to undergo cracking [17]
- A pseudo-component can not crack into an adjacent pseudo-component but it can crack into at least once removed pseudo-component. For instance, pseudocomponent 60 can not crack into pseudocomponent 59 but it can crack into pseudocomponent 58 and lighters.

- Hydrodesulfurization (HDS), hydrodenitrogenation (HDN) and polymerization reactions are assumed to be negligible.
- Total mass flow rate of liquid feed is assumed to be constant.
- Due to excess amount of hydrogen, the rate of hydrocracking is taken to be independent of hydrogen concentration.
- Make-up and recycle gases are assumed to be pure hydrogen.

5.2. MASS BALANCE

According to above assumptions, the component mass balance can be written as;

$$M_{total} \times \frac{dC_i}{dW} = \left[-k_i \times C_i\right] + \left[\sum_{j=r}^{N} k_j \times P_{ij} \times C_j\right] \quad (17)$$

The first term on the right hand side of the equation shows the disappearance of component i due to cracking reaction and the second term represents the formation of component i from cracking of component j. M_{total} represents total mass flow rate of liquid feed in kg/h, C_i stands for mass fraction of components,W is the catalyst weight in kg , $k_{i,j}$ is the first order rate constant in kg-reactant/(kg-catalyst×h) and P_{ij} is the probability of formation of component i from cracking of component j [15].

Subscripts are defined as follows.

i=1,2,…N where N is the heaviest component

r = i+2 for i≥p and r=p for i<p where p is the lightest component undergoes cracking, i.e the first component after crack limit. Crack limit is the boiling point below which no cracking occurs.

When the boiling point of component i is smaller than crack limit, it will not crack. It will be formed by cracking of other components starting from the lightest cracking component (p) until to the heaviest one (N). When the boiling point of component i is higher than crack limit, it will both crack into lighter components and be formed by other heavier components starting from the i+2th component to the heaviest one (N).

5.2.1. Correlations for Kinetics and Product Distribution

The rate constant, k_i, depends on the type of feed and catalyst. There are several studies on kinetics of cracking reactions [10,15,76]. However, due to diversity of catalyst and operating conditions, the applications of those studies are limited. Mohanty [17] assumed a simple expression for rate constant k_i which is the product of a relative rate constant, K_i, and estimated rate constant, k. The relative rate constant is defined as Rapaport [76]

$$K_i = D_1 + D_2 \times T_{b,i} + D_3 \times T_{b,i}{}^2 + D_4 \times T_{b,i}^3 \quad \text{for i=1,2...N} \tag{18}$$

Here, $T_{b,i}$ represents the boiling point of pseudocomponent i. The constants $D_1 - D_4$ are adjusted to match the predictions and real plant data. The initial estimate for them were taken from Mohanty [17]

The estimated rate constant expression is as follows;

$$k = \left(\frac{\rho_{HVGO}}{\rho_{catalyst}} \right) \times A \times e^{-E/RT} \tag{19}$$

Here, A stands as frequency factor and E stands as activation energy. Quader and Hill [10] reported values for A and E for hydrocracking of a vacuum gas oil, having an average boiling point of 643 K. Those values were used as first estimates and then adjusted again to match the predictions with real plant data.

Then the rate constant is calculated from:

$$k_i = K_i \times k \text{ for i=1,2...N} \tag{20}$$

The product distribution of each pseudo-component is evaluated by correlations of Mohanty [17] which are in fact very similar to those of Stangeland [15]. The probability of butanes and lighter components (ie. LE) formed from cracking of component j is as follows;

$$P_{1j} = C \times \exp\left[w \times \left(1.8 \times T_{b,j} - 229.5 \right) \right] \quad \text{for j=p,...N} \tag{21}$$

where $T_{b,j}$ is the boiling point of component j, C and w are tuning parameters.

The yields of all other components are evaluated by one expression. However, the boiling point range should be normalized. The normalization equation is as follows [15] ;

$$y_{ij} = \frac{\left(T_{b,i} - T_{b,1} \right)}{\left(T_{b,j-2} - T_{b,1} \right)} \quad \text{where i=2,3...(j-2) and j=p,...N} \tag{22}$$

Here, $T_{b,1}$ is the boiling point of first pseudo-component and y_{ij} is the normalized temperature for the i^{th} component formed from j^{th} component.

The distribution can be found by the following correlation [16]

$$P'_{ij} = \left[y_{ij}^2 + B1 \times y_{ij}^3 - B2 \times y_{ij}^2 \right] \times \left[1 - P_{1j} \right] \quad (23)$$

Here P'_{ij} is the cumulative yield until the component i from cracking of component j. B1 and B2 are again tuning parameters. Then, the actual yield is evaluated as [15];

$$P_{ij} = P'_{ij} - P'_{i-1,j} \quad (24)$$

5.2.2. Energy Balance

The energy balance for the system can be expressed as;

$$\sum_{i=1}^{N+1} \left(m_i \times Cp_i \right) \times \frac{dT}{dW} = \sum_{j=p}^{N} \left(\Delta H_R \right)_j \times k_j \times C_j \quad (25)$$

In the equation, m_i is the mass flow rate of component i, Cp_i is the heat capacity of component i, T is the temperature, W is the catalyst weight, N is the number of pseudo-components, N+1 stands for hydrogen, p is the smallest component that undergoes cracking, $(\Delta H_R)_J$ is the heat of reaction for cracking of component j, k_j is first order rate constant and C_j is the mass fraction of component j.

5.2.2.1. Evaluation of Heat Capacity

The procedure given by Mohanty [17] was followed. After evaluation of properties such as molecular weight, critical temperature, critical pressure, accentric factor (the evaluation details are given in chapter 4), Peng-Robinson Equation of state was used in the calculation of enthalpy and heat capacity of components. In order to find the fugacity coefficient of a pure component, the following equations from Peng-Robinson, was used.

$$\kappa_i = 0.37464 + 1.54226 \times \omega_i - 0.26992 \times \omega_i^2 \quad (26)$$

Here, ω_i is the accentric factor of component i computed by eqn. 15.

$$\alpha_i = \left[1+\kappa_i \times \left(1-T_{r,i}^{1/2}\right)\right]^2 \tag{27}$$

Here, $T_{r,i}$ is reduced temperature for component i.

$$a_i = 0.45724 \times \frac{R^2 \times T_{c,i}^{\ 2}}{P_{c,i}} \times \alpha_i \tag{28}$$

Here, $T_{c,i}$ and $P_{c,i}$ are critical temperature and pressure for component i respectively.

$$b_i = 0.07780 \times \frac{R \times T_{c,i}}{P_{c,i}} \tag{29}$$

$$A_i = \frac{a_i \times P}{R^2 \times T^2} \tag{30}$$

Here, P and T stand for bed pressure and temperature respectively.

$$B_i = \frac{b_i \times P}{R \times T} \tag{31}$$

Then, we have the compressibility factor equation as follows;

$$Z_i^3 - (1-B_i) \times Z_i^2 + \left(A_i - 3 \times B_i^2 - 2 \times B_i\right) \times Z_i - \left(A_i \times B_i - B_i^2 - B_i^3\right) = 0 \tag{32}$$

The smallest positive root for each component was picked as compressibility factor because it was the one stands for liquid. Fugacity coefficient of a pure component can be written as;

$$\ln \phi_i = Z_i - 1 - \ln(Z_i - B_i) - \frac{A_i}{2\sqrt{2} \times B_i} \times \ln\left[\frac{Z_i + 2.434 \times B_i}{Z_i - 0.414 \times B_i}\right] \quad (33)$$

There is a thermodynamic relation with enthalpy and fugacity coefficient.

$$H_i = H_i^{idl} - R \times T^2 \times \frac{\delta \ln \phi_i}{\delta T} \quad (34)$$

In the equation H_i^{idl} is the ideal enthalpy of component i and can be calculated by using the following correlation given by Weir and Eaton [77]

$$H_i^{idl} = 2.326 \times \left[(15 \times SG_i - 26) - (0.465 \times SG_i - 0.811) \times T + 0.000290 \times T^2\right] \quad (35)$$

Here, SG_i is the specific gravity of component i at 60 F, T is the temperature in F.
After computation of H_i, the heat capacity can be easily evaluated by;

$$Cp_i = \frac{H_i}{\left(T - T_{ref}\right)} \quad (36)$$

The reference temperature was taken as 273 K.

5.2.2.2. Evaluation of Heat of Reaction

Since the composition of the reaction mixture is undefined, heat of reaction for the system can not be evaluated by using standard heat of combustion. Studies by Zohorov [13] and [Kurganov [78] showed that the standard heat of reaction for hydrocracking can be assumed to be 42000 joules per mole of hydrogen reacted. To estimate the hydrogen consumption, the carbon to hydrogen (C/H) ratio of each pseudocomponent should be determined first. Different correlations for C/H ratio can easily be found in the literature. Since all these correlations are approximations, it is important to choose the correlation that describes the feed and products the best. Hence, C/H ratios of pseudocomponents were computed by different correlations. According to Brown [79] and Tushar [80], the ratio is given by equation 21 and equation 22 respectively.

$$\left(\frac{C}{H}\right)_i = 15.89 - 0.0502 \times \rho_i - 0.626 \times K_i \quad (37)$$

$$\left(\frac{C}{H}\right)_i = \frac{\left[100-\left(26.25\times SG_i + 0.0013\times TBP_i + 35.2\right)\right]}{\left(26.25\times SG_i + 0.0013\times TBP_i + 35.2\right)} \tag{38}$$

where ρ_i and K_i are density and Watson constant of ith component respectively and SG_i and TBP_i are specific gravity and boiling point temperature in Fahrenheit of ith component.

Each correlation gave different C/H ratios ranging from 5 to 12. The total rate of hydrogen consumption can easily be calculated by subtracting the hydrogen content of the feed from the hydrogen content of the products as follows.

$$HCON = \sum_{i=1}^{N}\left[\frac{m_i}{\left(R_i+1\right)}\right] - \sum_{j=1}^{N}\left[\frac{m_j}{\left(R_j+1\right)}\right] \tag{39}$$

where m_i and R_i are the mass flow rates and C/H ratio of component i at the exit and m_j and R_j are the mass flow rates and C/H ratio of component j at the inlet.

The C/H ratios found by equation 21 and equation 22 were plugged into equation 23. However, in both cases the evaluated hydrogen consumption did not match with the real hydrogen consumption value. Therefore, a new correlation was generated for calculating C/H ratios of pseudocomponents.

Firstly, the C/H ratios that were computed by Tushar correlation (equation 22) were plotted with respect to TBP of the pseudocomponents as follows.

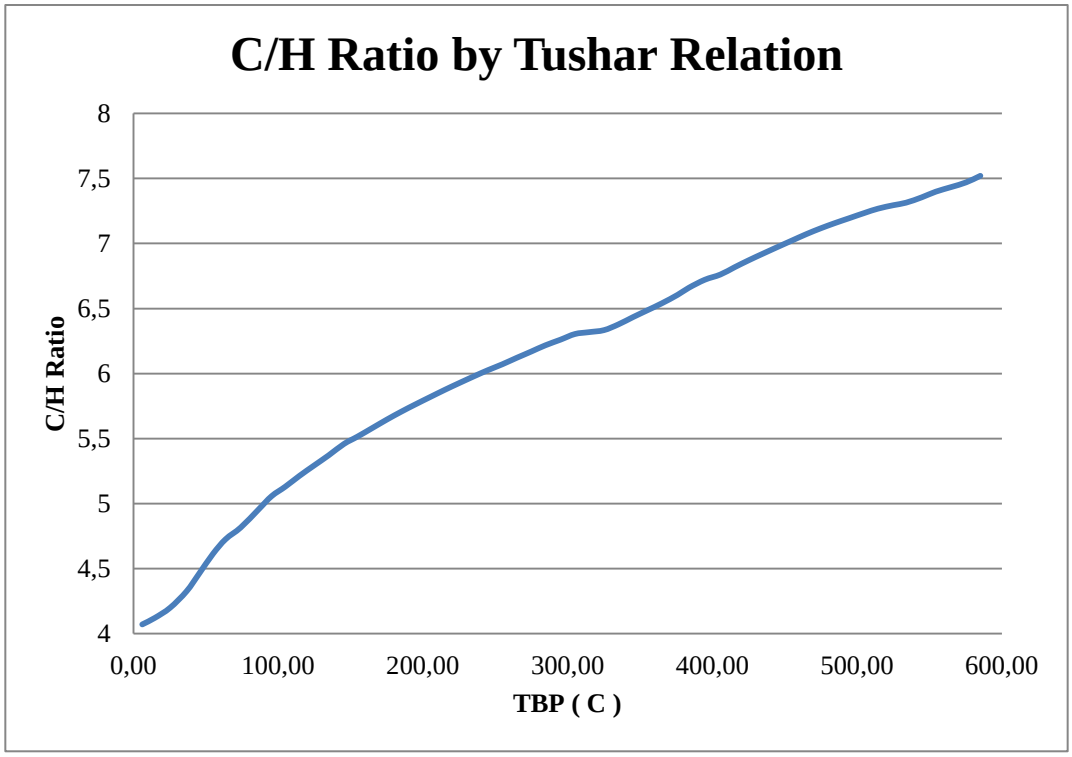

Figure 5.1 Relationship between TBP and C/H ratios

From Figure 3.1, it can easily be assumed that there is a linear correlation between TBP and C/H ratio. Hence, a linear fit in the form of $a \times TBP_i + b$ can be used for calculating C/H ratios of our system. After deciding the type of new correlation, the constants should be determined. Since the real total hydrogen consumption amount was available, the constants a and b were tuned in order to match that amount with the evaluated amount by equation 23. The final correlation was found to be:

$$\left(\frac{C}{H}\right)_i = 0.004 \times TBP_i + 5.9 \qquad (40)$$

In order to solve the energy balance (equation 9), the value of heat released by cracking of j^{th} pseudocomponent is needed. Therefore, the hydrogen consumption for j^{th} pseudocomponent should be evaluated. Since C/H ratios of each component are known, the hydrogen consumption for each component can be found by the following correlations easily.

When 1 kg of component j cracks, P_{ij} kg of component i form. Therefore, the total carbon content of cracked j can be written as follows.

$$(TCC)_j = \sum_{i=1}^{j-2} \left[P_{ij} \times \frac{\left(C/H\right)_i}{\left(C/H\right)_i + 1} \right] \quad \text{j=p,...N} \tag{41}$$

Similarly, the hydrogen content of products that are formed by craking of component j can be written as follows.

$$(THC)_j = \sum_{i=1}^{j-2} \left[P_{ij} \times \frac{1}{\left(C/H\right)_i + 1} \right] \quad \text{j=p,...N} \tag{42}$$

Hence, the hydrogen consumption for cracking reaction of component j can be found as follows.

$$(HCON)_j = (THC)_j - \left[\frac{(TCC)_j}{\left(C/H\right)_j} \right] \tag{43}$$

As can be observed in Figure 5.2, hydrogen consumption increases with an increasing C/H ratio.

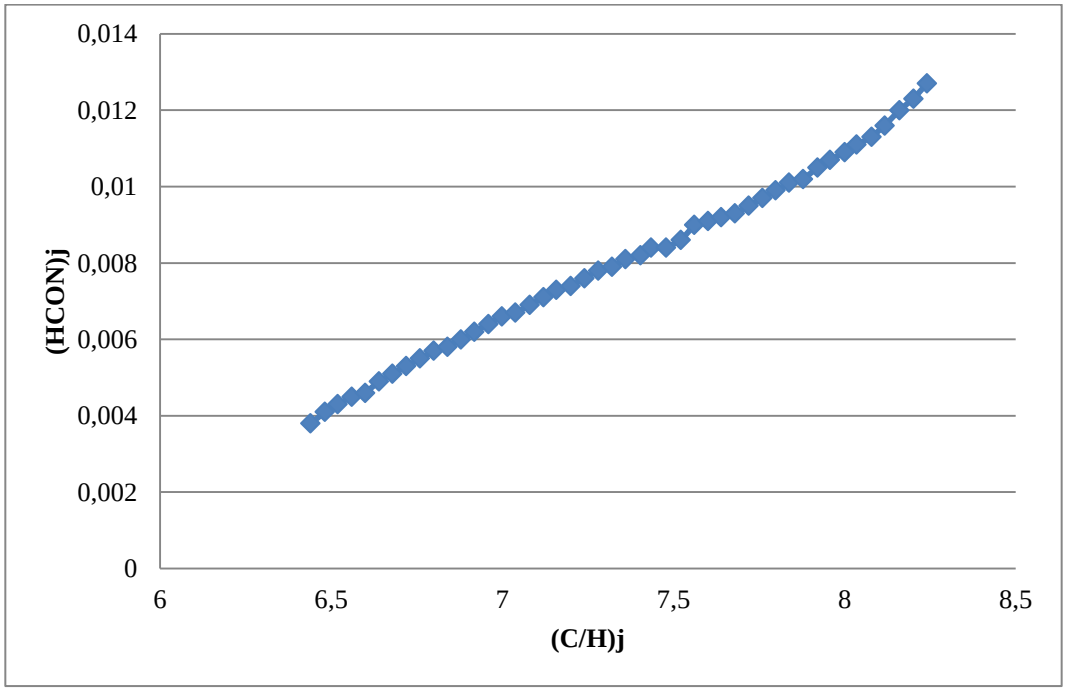

Figure 5.2 Hydrogen consumption for cracking reaction of component j with respect to C/H of component j.

The standard heat of reaction for j^{th} reaction can be expressed as follows.

$$\left(\Delta H_R^0\right)_j = \left(HCON\right)_j \times \left(\frac{-42000}{2}\right) \text{ kJ/kg} \qquad \text{j=p,...N} \tag{44}$$

Due to the effects of temperature and pressure on the heat of reaction, the enthalpy of both reactants and products were evaluated first at standard conditions and then at reaction conditions. The enthalpy of hydrogen at reaction conditions and standard conditions were calculated by available literature data. The enthalpies at reaction condition were evaluated by Peng-Robinson Equation of State as given in evaluation of heat capacity section. The enthalpies at standard conditions were calculated by Zhvanestskii and Platnov [81] equation as follows.

$$H_i^0 = \frac{0.3897 \times T + 0.0004638 \times T^2}{\rho_i^{2/3}} \times \left(0.3265 + \frac{0.4515}{\rho_i} \times \left(\frac{T_{b,i}}{273.2} + 1\right)^{1/3}\right) \tag{45}$$

In the above equation $T = 25\ \text{C}$ as the enthalpy at standard condition was evaluated. ρ_i and $T_{b,i}$ represent the density and boiling point of component i respectively.

Therefore, the heat of reaction at reaction condition was evaluated by the following equation.

$$\left(\Delta H_R^T\right)_j = \left(\Delta H_R^0\right)_j + \left[\sum_{i=1}^{j-2}\left(H_i - H_i^0\right) \times P_{ij}\right] - \left[H_j - H_j^0\right] - \left[\left(H_{H2} - H_{H2}^0\right) \times \left(HCON\right)_j\right] \tag{46}$$

Here, i denotes the products and j denotes the reactants. For the system hydrogen is also a reactant. Therefore, in calculation of heat of reaction the enthalpy of reactants were subtracted from the enthalpy of products and the standard heat of reaction was added to that value.

5.2.3. Model Modifications

The model for this study was formed by the set of equations 1 through 30. In order to complete the modeling process, the model parameters had to be tuned parameter estimation. The model parameters were given in the following table.

Table 5.1 Tuning parameters of the model

Parameter	Description
A1	Frequency factor of the estimated rate for Bed 1
A2	Frequency factor of the estimated rate for Bed 2
A3	Frequency factor of the estimated rate for Bed 3
A4	Frequency factor of the estimated rate for Bed 4
D1	The first constant of relative rate equation
D2	The second constant of relative rate equation
D3	The third constant of relative rate equation
D4	The fourth constant of relative rate equation
C	Product Distribution parameter
w	Product Distribution parameter
B1	Product Distribution parameter
B2	Product Distribution parameter

Parameter estimation was performed by the parameters given in Table 5.1. Although many trials were done, the results were poor as given in Table 5.2.

Table 5.2 Comparison of bed exit temperatures

	PLANT	PREDICTION
T1	205.08	208.76
T2	204.17	206.04
T3	205.08	206.74
T4	204.74	207.64

Predictions deviate from plant data by 3-7 °C which cannot be tolerable for an HCU operation. Therefore, some modifications were done. These modifications allowed the model to be simpler and gave satisfactory results with the help of newly generated tuning parameters.

Since the temperature difference between inlet and outlet streams were small (around 10.5 °C) enough, it would be reasonable to neglect the temperature effect on heat capacities of individual pseudocomponents. Therefore, instead of calculating heat capacity with respect to

temperature, an average heat capacity value would serve our purpose. As the pseudocomponents were defined by their true boiling points, the calculated heat capacities of pseudocomponents were plotted with respect to their true boiling points.

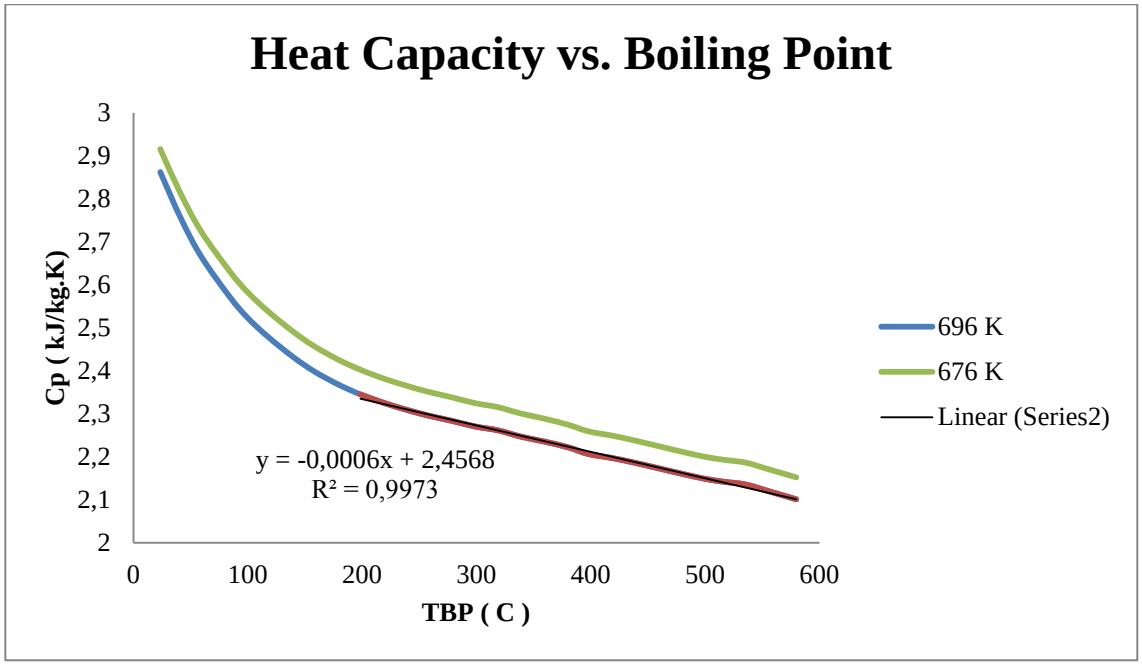

5.3 Relation between heat capacity and boiling point

It can easily be observed from the Figure 5.3 that heat capacity decreases with increasing boiling point and it does not significantly vary in the temperature range of interest. Since hydrocracking process maximizes middle distillates, it would be more important to propose an average heat capacity describing middle distillates than light distillates. Hence, the range between 200 and 600 °C was used to generate relation for heat capacity. As can be seen from Figure 5.3, this portion of the graph has a linear trend. The final heat capacity relation obtained by parameter estimation is as follows.

$$Cp_i = -0.0004 \times TBP_i + 3.12 \quad (47)$$

The second modification was performed on the calculation of heat of reaction. The pressure along the reactor beds was assumed to be constant. Moreover, the temperature effect can be neglected as stated in heat capacity case. Under these conditions, the standard heat of reaction dominated over the other terms in the heat of reaction equation. Table 5.3 shows the values for components from 25 to 35. The negative sign means that the reaction is exothermic. Therefore, the heat of reaction would be more or less equal to standard heat of reaction.

Table 5.3 Comparison of Standard Heat of Reaction values with the Heat of Reaction at operating temperatures

Component Number	Standard Heat Term (kj/kg)	Sum of Other Terms (kj/kg)
25	-129.90	13.59
26	-133.57	11.92
27	-137.58	9.81
28	-141.30	8.03
29	-144.40	6.53
30	-148.59	5.30
31	-152.40	4.15
32	-154.70	1.30
33	-158.85	1.99
34	-162.80	1.23
35	-165.65	0.36

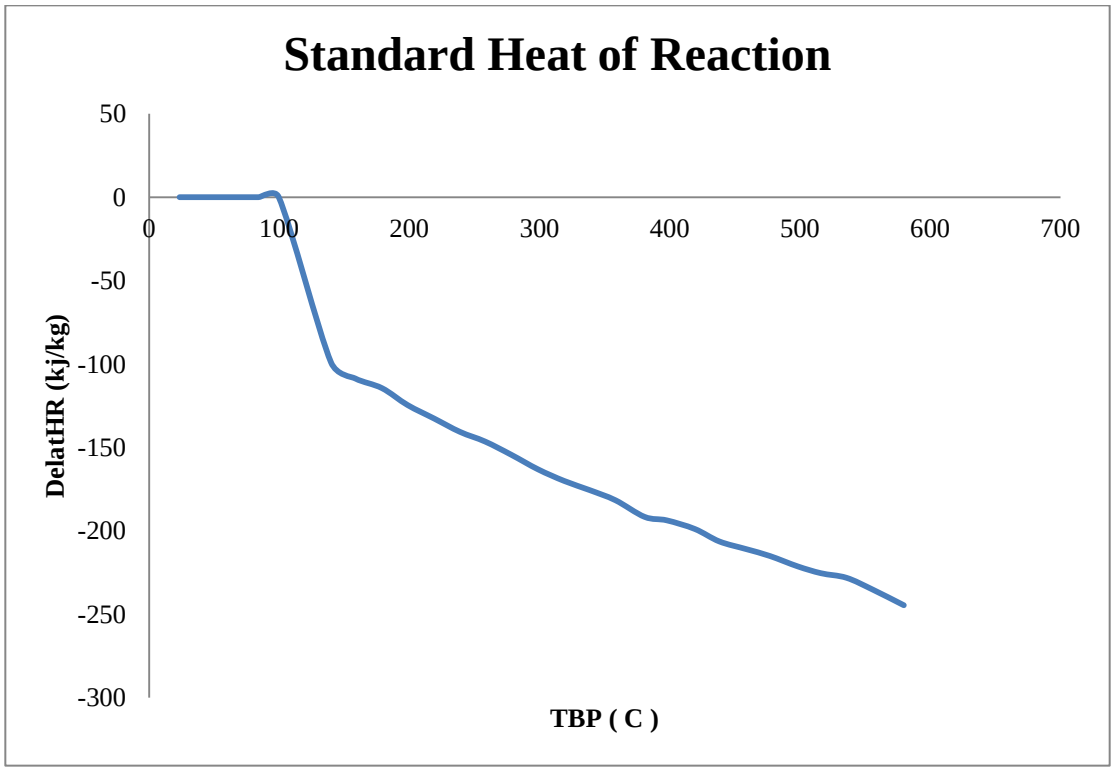

Figure 5.4 Relation between Standard Heat of Reaction and Boiling Point

In the figure above, a linear trend is observed. In fact this is not surprising because standard heat of reaction depends on consumed hydrogen which is a function of C/H ratio. And as mentioned earlier, C/H ratio increases with an increasing boiling point. Therefore, the components having higher boiling points will have higher standard heat of reaction. The values are negative due to the exothermic nature of the reaction. On the other hand, in cracking reactions, there is a cracking limit. The components having lower boiling point than that cracking limit do not undergo cracking. Hence, in Figure 5.3, the standard heat of reaction is zero for these components.

Due to the linearity observed in above figure, the heat of reaction can be expressed as

$$(\Delta H_R)_i = HR1 \times TBP_i + HR2 \quad (48)$$

Here, $HR1$ and $HR2$ were newly generated tuning parameters. The final set of model parameters were tabulated in the following table.

Table 5.4 Final set of tuning parameters

Parameter	Description
A1	Frequency factor of the estimated rate for Bed 1
A2	Frequency factor of the estimated rate for Bed 2
A3	Frequency factor of the estimated rate for Bed 3
A4	Frequency factor of the estimated rate for Bed 4
D1	The first constant of relative rate equation
D2	The second constant of relative rate equation
D3	The third constant of relative rate equation
D4	The fourth constant of relative rate equation
C	Product Distribution parameter
w	Product Distribution parameter
B1	Product Distribution parameter
B2	Product Distribution parameter
HR1	Constant 1 in heat of reaction equation
HR2	Constant 1 in heat of reaction equation

Chapter 6

6. PARAMETER ESTIMATION

6.1. INTRODUCTION

Parameter estimation is the process of determination of model parameters by matching the model-based calculated values with the experimental (real) data. When the model equations are linear functions of the parameters, the problem is called linear estimation. Nonlinear estimation refers to the more general and most frequently encountered situation where the model equations are nonlinear functions of the parameters. For linear models, the estimation procedure allows for development of analytic solutions. However, for nonlinear models, the analytic solutions are not available and numerical iterative methods should be used. Therefore, the solution is more difficult for nonlinear models. Hibbert [44] stated that the size of parameter space, the existence of local minima, the continuity of objective function and the sensitivity of objective function to each of the model parameters should be taken into consideration carefully in the case of nonlinear models. The first two points indicate that the determination of initial guesses plays a very important role in parameter estimation.

After defining the parameter space and the associated objective function, several non linear optimization methods can be used. Mostly, these methods are derivative-based and the minimization is performed along a direction that combines gradient vector (vector of first derivatives with respect to model parameters) and the Hessian matrix (the matrix of second derivatives with respect to model parameters) [45]. In direct search methods, the objective function is evaluated without the calculation of derivatives. Although, the search methods are simpler, Bard [46-47] reported that derivative-based methods perform better due to speed of convergence and reliability. After Bard's [47] work in 1970, Edgar and Himmelblau [48] presented a good comparison between these methods in their book.

Both derivate-based and direct search methods start from an initial guess which makes them local search methods. In the field of chemical engineering, parameter estimation problems become difficult due to the large number of parameters, high correlation between parameters and multimodal nature of objective function [45]. The heuristic optimization methods such as genetic algorithm (GA), simulated annealing (SA) and particle swarm optimization (PSA) can be used in order to overcome the difficulties. These methods are promising because they do not use derivatives and do not need initial guesses for the parameters. Moreover, they are able

to perform a global optimization. The GA became popular through the book *Adaptation in Natural and Artificial Systems* [49]. Thereafter, it has been applied successfully to many problems. Goldberg [50] and Deb [51] provided a detailed information on GA. Balasubramanian [52] used GA with sequential quadratic programming in hydrocracking process, Kasat [53] applied GA to FCC units, Mitra [54] performed an multi-objective optimization of an industrial semi-batch naylon-6 reactor by using GA, Nandi [55] modeled benzene iso-propylation process with GA, Pina [56] worked on a glass furnace operation again by using GA, Rajesh [57] optimized a steam reformer performance by applying GA, Sarkar [58] used GA for optimization of bioreactors, Tarafder [59] applied GA to an industrial styrene reactor. SA mimics the cooling of molten metals in its search procedure. The method works with a single point at a time and is effective in finding global optimal solution when slow cooling procedure is used [51]. The PSO was originally proposed by Kennedy and Eberhart [60] based on the social behavior of collection of animals. Costa [61] used PSO for optimization of styrene polymerization process, Parsopoulos [62] performed PSO for multi-objective optimizations.

The results obtained by parameter estimation are also uncertain to some extent. For the evaluation of final results, the characterization of this uncertainty, which is defined as confidence region, is very important. In order to construct confidence region, different methods have been proposed in the literature such as *likelihood method* [63], *lack-of-fit method* [64-66] and *profiling t-plots* [67]. The likelihood method is exact only for linear models which have an elliptical confidence region. The lack-of-fit model can produce exact confidence regions for all model parameters. However, since it requires derivatives, it is more computational than likelihood method. Profiling t-plots was designed for computation of confidence intervals. Therefore, the confidence region can be found by interpolation easily.

6.2. CONSTRUCTION OF OBJECTIVE FUNCTION

The unknown model parameters are determined by minimizing a function called objective function. It is the overall departure of model outputs from real data. In this study, the minimization of objective function was performed by least squares (LS) estimation in which weighted sum of least squares of errors (WSSE) was minimized. Model predicts the final product composition (for 59 pseudocomponents), the outlet temperatures of beds (4 beds), the amount of quench flows (3 quench flows) and the amount of total consumed hydrogen. Hence, the objective function consisted of these items. Since the units of outputs differ, the normalized values of items are used in objective function as given below.

$$\text{F=Min}\left[w_1 \times \sum_{i=1}^{59}\left(1-\frac{fC_{i,M}}{fC_{i,R}}\right)^2 + w_2 \times \sum_{i=1}^{4}\left(1-\frac{T_{i,M}}{T_{i,R}}\right)^2 + w_3 \times \sum_{i=1}^{3}\left(1-\frac{Q_{i,M}}{Q_{i,R}}\right)^2 + w_4 \times \left(1-\frac{H_{2,M}}{H_{2,R}}\right)^2 \right] \quad (49)$$

In the above equation, w_1, w_2, w_3 and w_4 are elements of weighting matrix, the subscript M and R represent model predictions and real data respectively. The first term stands for product composition, the second one for bed outlet temperature, the third one for quench flows and the last one for total hydrogen consumption.

Although it is not clear how to select the weights, it is obvious that the highest weight should be given to the term that has highest priority. The total hydrogen consumption depends on C/H ratio and final composition. The quench flows are cold hydrogen flows to cool the bed effluent and depend on both the outlet temperatures and intermediate composition between beds. Therefore, when the outlet temperatures and final composition are achieved, the quench flows and total hydrogen consumption will also be achieved. Hence, the weight for them was selected as 1. As final composition and outlet temperatures are equally important, their weights are to be equal as well. After many trials, the weight for them was chosen as 100.

6.3. INPUT DATA FOR PARAMETER ESTIMATION

The industrial plant under study has numerous sets of steady state operating data including feed and product distillation data, their flow rates, reactor temperatures and total hydrogen consumption. The model calibration and validation were performed by using these data. It should be noted that the industrial data were verified first for consistency (overall mass balance) before using for calibration and validation.

The model uses feed and inlet temperatures of beds as input and gives the products distribution and exit temperatures of beds as output. It also computes the needed quench flows and total hydrogen consumption as well.

In the following figure, the TBP curves of feeds for three different days of operation are presented. As can be observed, feeds' TBP change within a small range. Therefore, it can be concluded that feeds are similar in terms of their TBPs. Moreover, TBP curves for other days which are not shown here are similar as well.

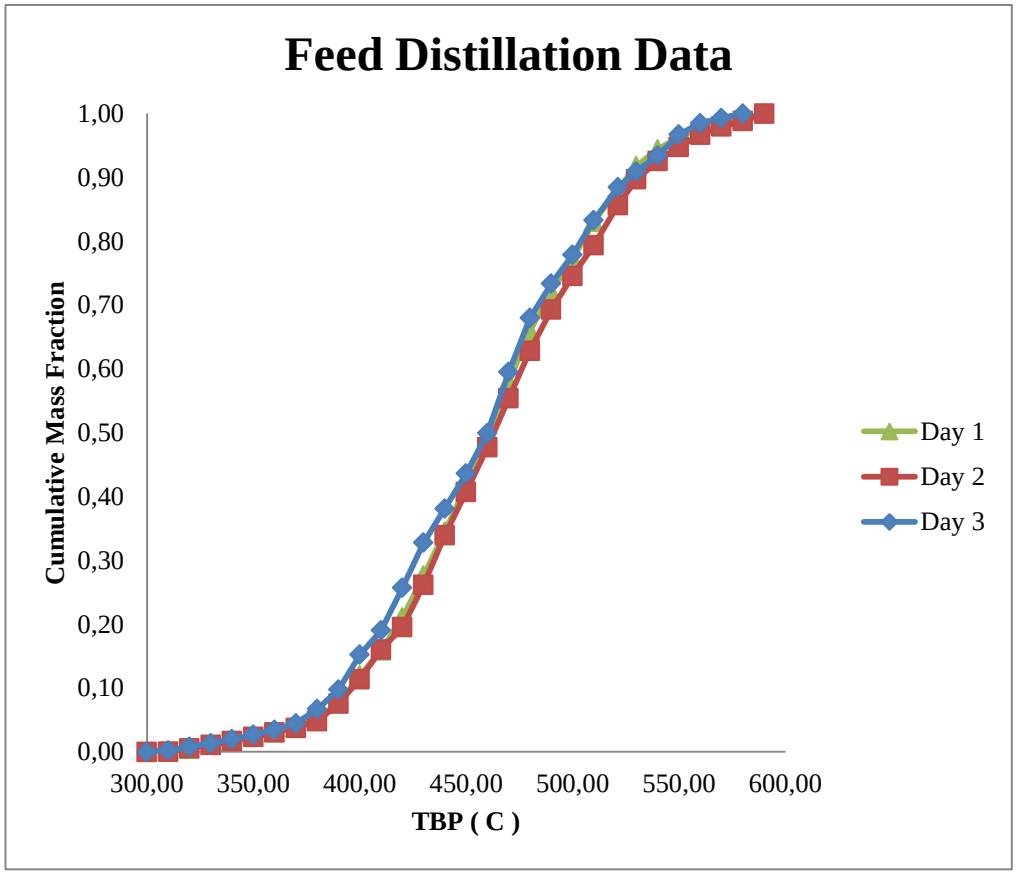

Figure 6.1 Feed Distillation Data for different days of operation

Bed inlet temperatures are also very important for the process. As can be seen from Figure 6.6, the values at bed 1 and bed 2 are smaller than the values at bed 3 and bed 4. In fact, since the reactions are exothermic in nature, the increasing trend of bed inlet temperatures is to be expected.

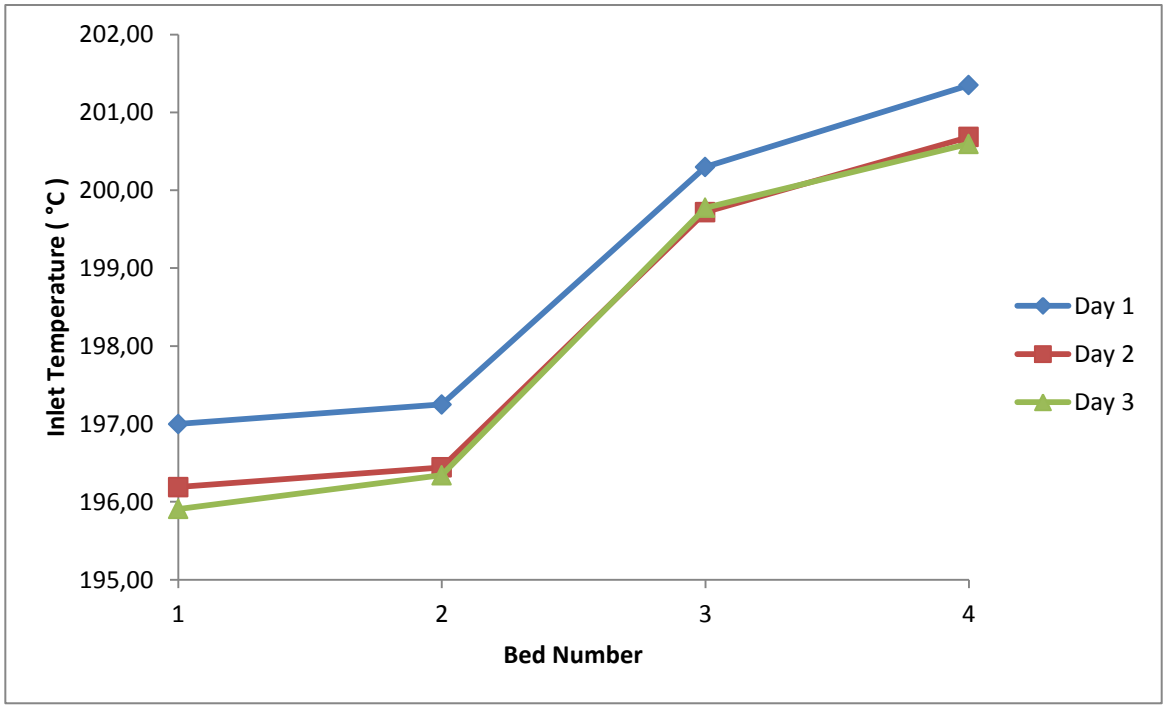

Figure 6.2 Bed Inlet Temperatures for different days of operation

6.4. THE ALGORITHM USED IN THE STUDY

In this study, parameter estimation was performed by using MATLAB fminsearch solver. This solver uses the Nelder-Mead Simplex algorithm which is one of the derivative-free methods. Firstly, a set of parameters were found in order to match just a day of operation (Day 1). The values were tabulated in the following table.

Table 6.1 Estimated Parameters by using Day 1 plant data only

Parameter	Value	Description
A1	2018677.3200	Frequency factor of the estimated rate for Bed 1
A2	2754481.9370	Frequency factor of the estimated rate for Bed 2
A3	2757569.7538	Frequency factor of the estimated rate for Bed 3
A4	3369786.0506	Frequency factor of the estimated rate for Bed 4
D1	4.4968	The first constant of relative rate equation
D2	-0.0414	The second constant of relative rate equation
D3	0.0002	The third constant of relative rate equation
D4	-1.67E-07	The fourth constant of relative rate equation
C	0.0004	Product Distribution parameter
w	-0.0064	Product Distribution parameter
B1	0.5251	Product Distribution parameter
B2	0.5248	Product Distribution parameter
HR1	-0.3254	Constant 1 in heat of reaction equation
HR2	-38.4199	Constant 2 in heat of reaction equation

The results found by the parameters given in Table 6.1 were satisfactory. However, in order to decide on the final parameter set, the estimation should be repeated by an extended set of data. That is, instead of one data set, more data sets should be used. Therefore, the estimation algorithm was re-performed to match three sets of steady state data (Day 1, Day 2 and Day 3) simultaneously. The new set of model parameters is given in Table 6.2.

Table 6.2 Estimated Parameters by using Day 1,Day 2 and Day 3 plant data together

Parameter	Value	Description
A1	2066024.0484	Frequency factor of the estimated rate for Bed 1
A2	2746550.0936	Frequency factor of the estimated rate for Bed 2
A3	2661407.9350	Frequency factor of the estimated rate for Bed 3
A4	3330575.6629	Frequency factor of the estimated rate for Bed 4
D1	4.2372	The first constant of relative rate equation
D2	-0.0393	The second constant of relative rate equation
D3	0.0002	The third constant of relative rate equation
D4	-1.73E-07	The fourth constant of relative rate equation
C	0.0006	Product Distribution parameter
w	-0.0060	Product Distribution parameter
B1	0.5230	Product Distribution parameter
B2	0.5223	Product Distribution parameter
HR1	-0.3243	Constant 1 in heat of reaction equation
HR2	-37.7335	Constant 2 in heat of reaction equation

This process should be repeated until the changes in the parameters become insignificant. Therefore the first set and the second set values were compared as can be seen in Table 6.3. Since the values remained almost constant, the process was ended. The second parameter set would be the final parameter set for the model. In fact, the process could be continued a bit further. However, since the feeds and operation conditions for different days are very similar, this was not necessary.

Table 6.3 Comparison of two parameter sets

	1	2	1/2		
A1	2018677.3200	2066024.0484	0.9771		
A2	2754481.9370	2746550.0936	1.0029		
A3	2757569.7538	2661407.9350	1.0361		
A4	3369786.0506	3330575.6629	1.0118		
D1	4.4968	4.2372	1.0613		
D2	-0.0414	-0.0393	1.0537		
D3	0.0002	0.0002	0.9982		
D4	-1.67E-07	-1.73E-07	0.9678		
C	0.0004	0.0006	0.8017		
w	-0.0064	-0.0060	1.0738		
B1	0.5251	0.5230	1.0041		
B2	0.5248	0.5223	1.0047		
HR1	-0.3254	-0.3243	1.0032		
HR2	-38.4199	-37.7335	1.0182		
1: Parameter Estimation by Day 1 data only					
2: Parameter Estimation by Day 1-Day2-Day 3					

6.5. SENSITIVITY ANALYSIS

After determination of model parameters, the examination of the impact of each parameter on the output results is very crucial. By performing sensitivity analysis, one can readily decide which parameters have significant effect on results and which parameters can be ignored or fixed at some nominal value.

Sensitivity analysis is mainly categorized in two groups; local and global. In recent years, global sensitivity analysis has received considerable attention. It analyzes the whole set of parameters and aims to give an overall indication about how the outputs vary in response to the input variations within the range of parameter uncertainty [69]. Cukier, Schaibly and coworkers [70-73] developed Fourier Amplitude Sensitivity Test (FAST). After 1990s, researchers developed Monte-Carlo based FAST approach and Sobol [74] is famous for his formulation of this approach.

As Saltelli [75] discussed most of the sensitivity analysis in the literature are local analysis. In this method, the effect of a parameter is evaluated locally while assuming all other parameters fixed. Therefore, it is also called as one-at-a-time (OAT) method. Although sensitivity is generally defined by derivatives, in the literature there are studies in which sensitivity analysis has been performed by incremental ratios (for instance 5%).

Due to its simplicity, local sensitivity analysis was performed in this study. The model parameters were perturbed by ±10% in order to determine their effects. Sensitivity was found by the following equation.

$$S_{ij} = \frac{\Delta Y_j}{\Delta X_i} \tag{50}$$

Here, ΔY_j denotes % change in output j and ΔX_i denotes % change in input i.

There are fifteen outputs of the model. In the following figures, the effects of each parameter on these outputs were presented. The simulations were performed by using Day 1 data.

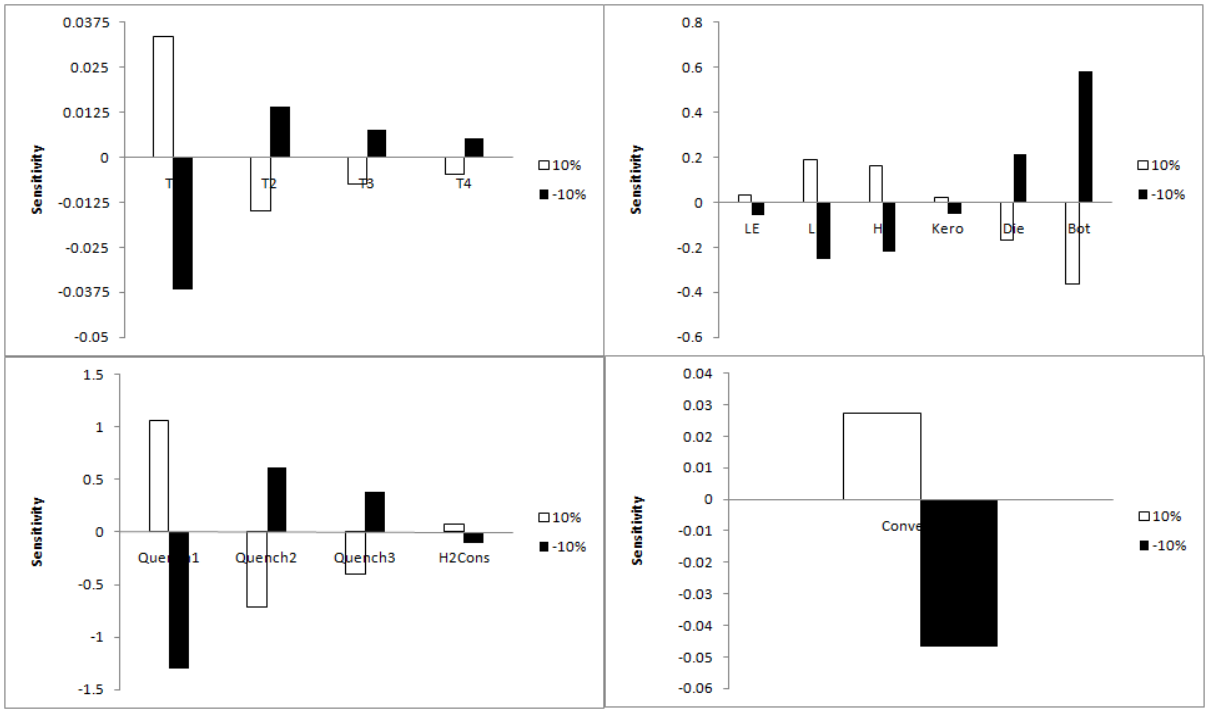

Figure 6.3 Effect of A1 on model outputs for a perturbation ±10%

A1 is used in the calculation of reaction rate constant and there is a linear relation between A1 and rate constant. Hence, an increase in A1 will result in an increase in rate constant and increasing rate constant means more cracking. Therefore, it is reasonable that the exit temperature of bed 1 increases. Since most of the cracking occurs in bed 1, the exit

temperatures of other beds will decrease as observed in Figure 6.7. More cracking will lead to lighter products. Therefore, a decline in flow rates of bottom and diesel is seen. Since the flow rate of bottom decreases, the conversion increases as in Figure 6.7. Due to more cracking, more hydrogen is consumed as shown above. The quench flows have a linear relation with bed exit temperatures. They are the flows given to the system to cool down the bed effluent streams. When the exit temperatures increase, more quench flows are needed to cool the stream and vice versa. Therefore, the same trend in bed exit temperatures is observed in quench flows. A 10% decline in parameter A1 shows the opposite effects on each output.

The effects of parameters A2-4 are given in the following three figures. They can be analyzed with the same perspective as in parameter A1 case and it will easily be concluded that the results are rational.

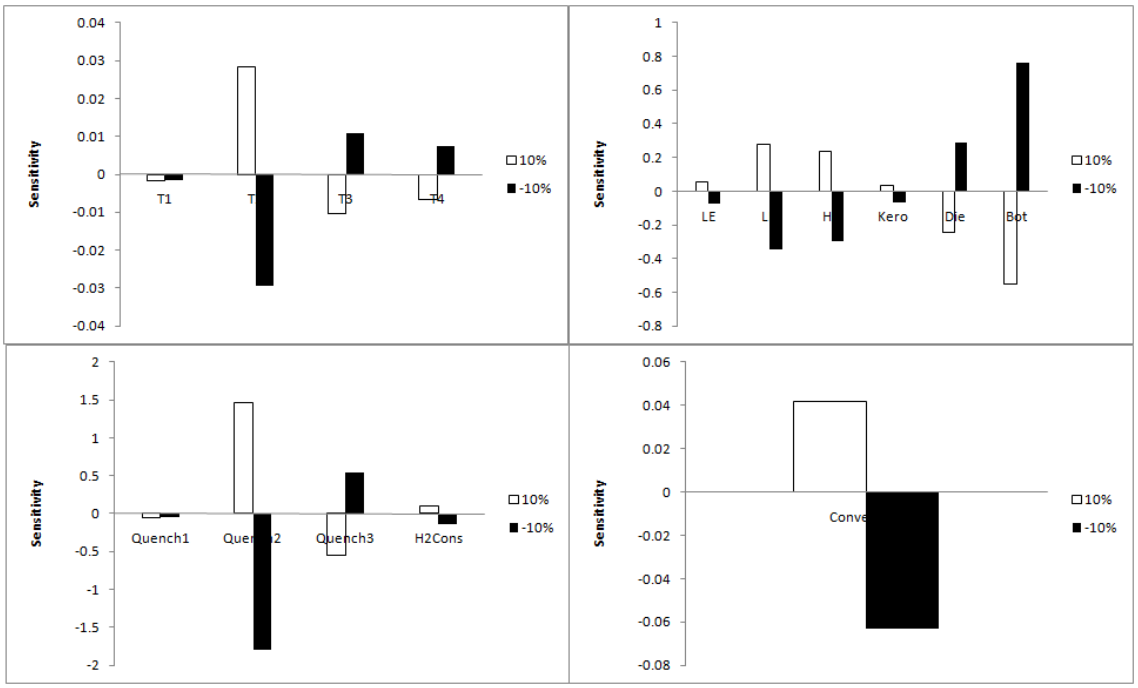

Figure 6.4 Effect of A2 on model outputs for a perturbation ±10%

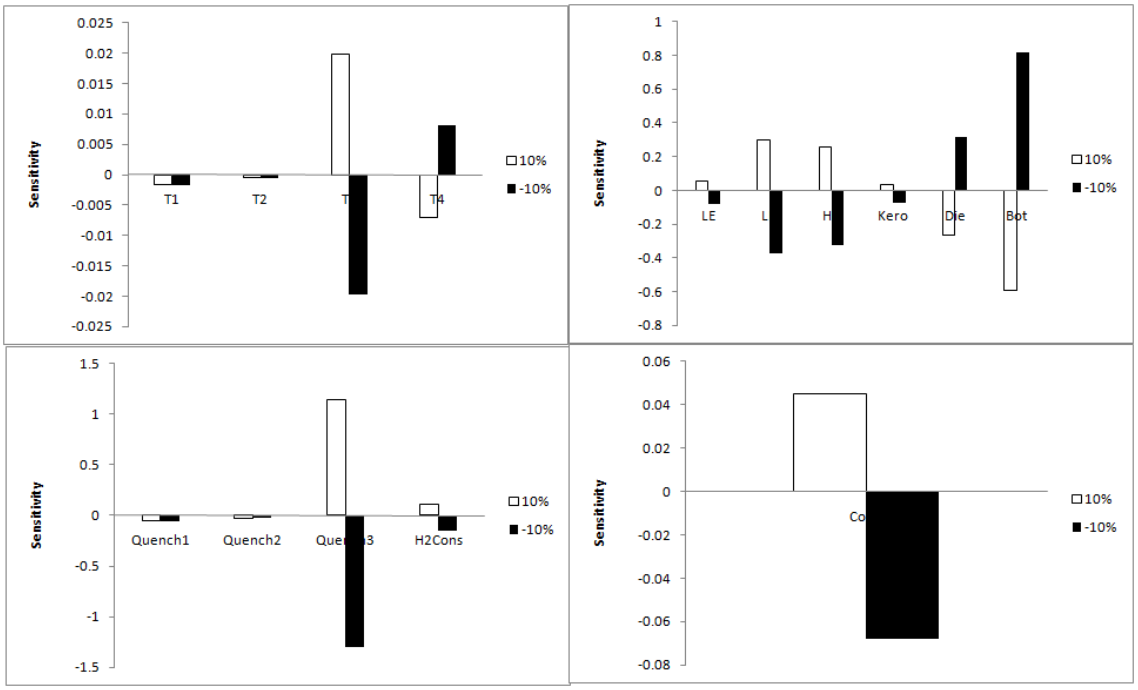

Figure 6.5 Effect of A3 on model outputs for a perturbation ±10%

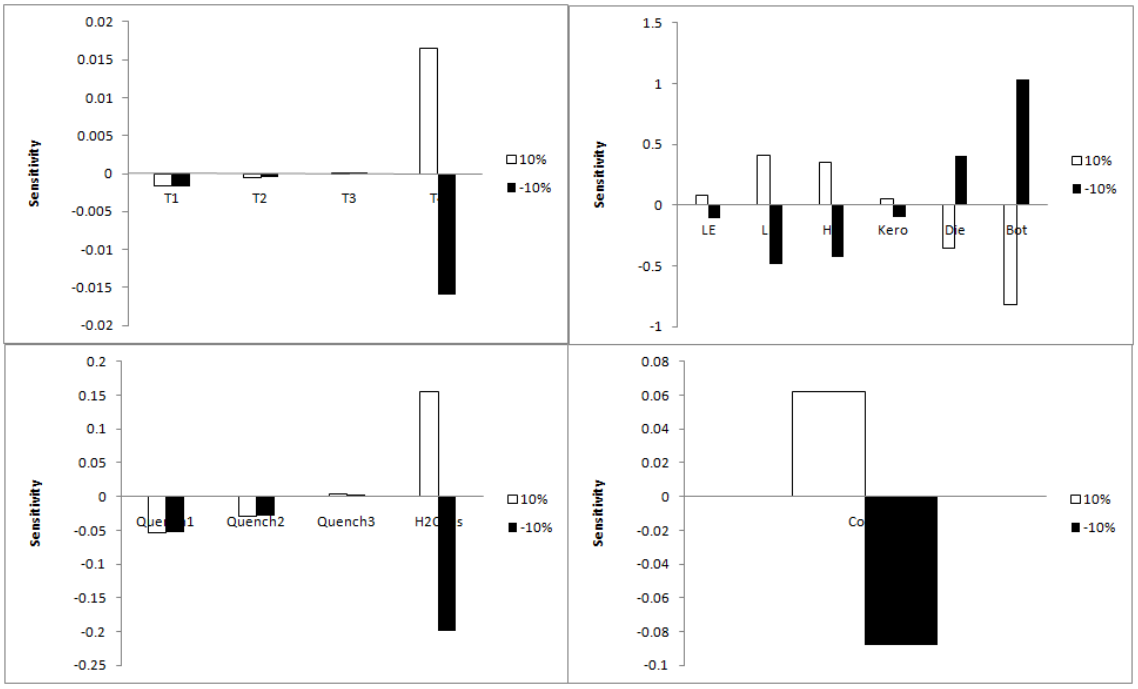

Figure 6.6 Effect of A4 on model outputs for a perturbation ±10%

In the model, relative rate constant is evaluated by using the parameters D1-4. The expression (eqn. 18) is a third order polynomial depending on TBP and the parameters D1-4 are the constants for that polynomial. From the expression, it can be claimed that D1 has the least and D4 has the most effect on rate constant due to the order of their multipliers (TBPs). However, as can be seen in Table 6.3, D4 is very small. Hence, D4 effect on rate constant can be

neglected. In the following graphs, it is observed that D3 affects the outputs most and the results are consistent with each other.

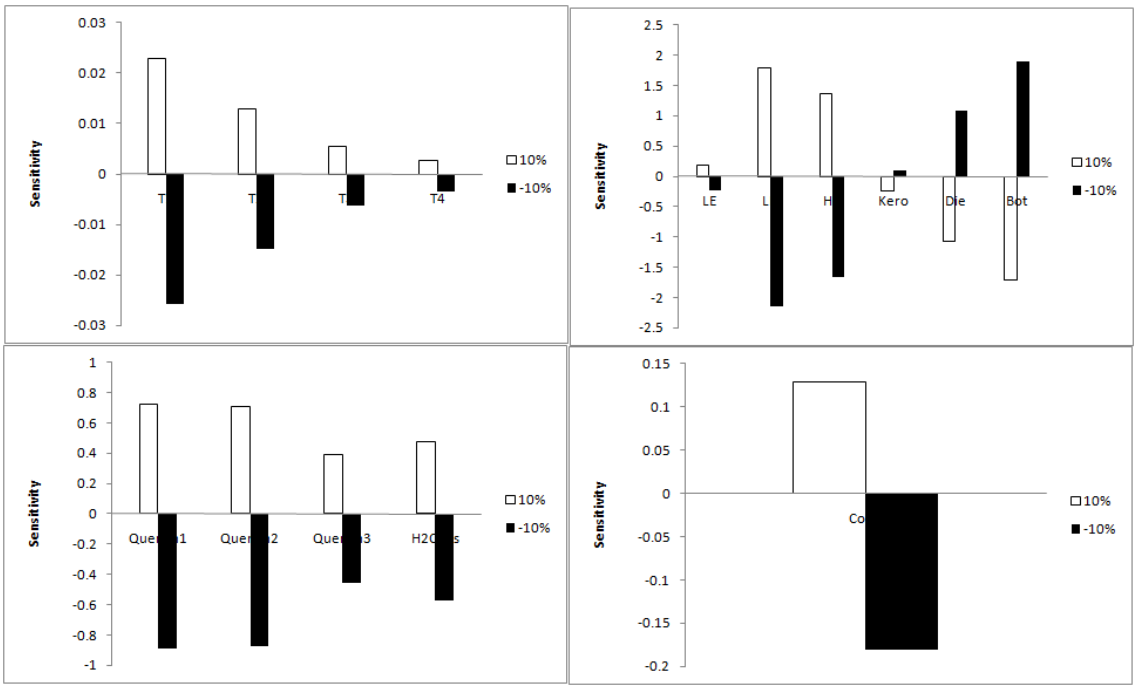

Figure 6.7 Effect of D1 on model outputs for a perturbation ±10%

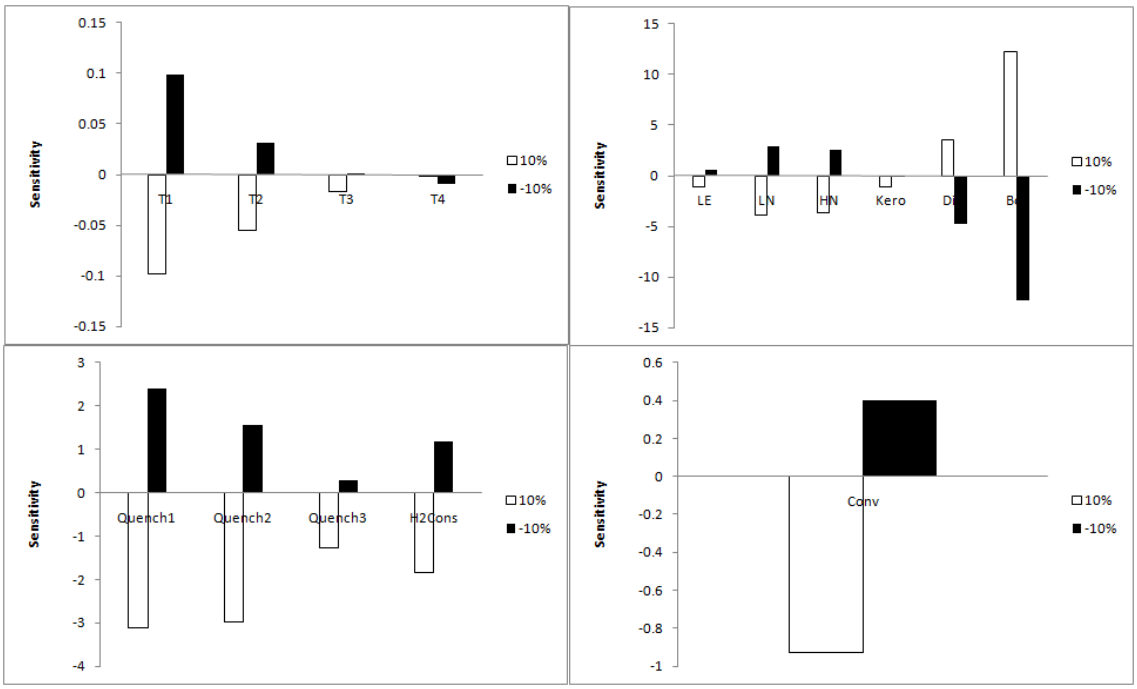

Figure 6.8 Effect of D2 on model outputs for a perturbation ±10%

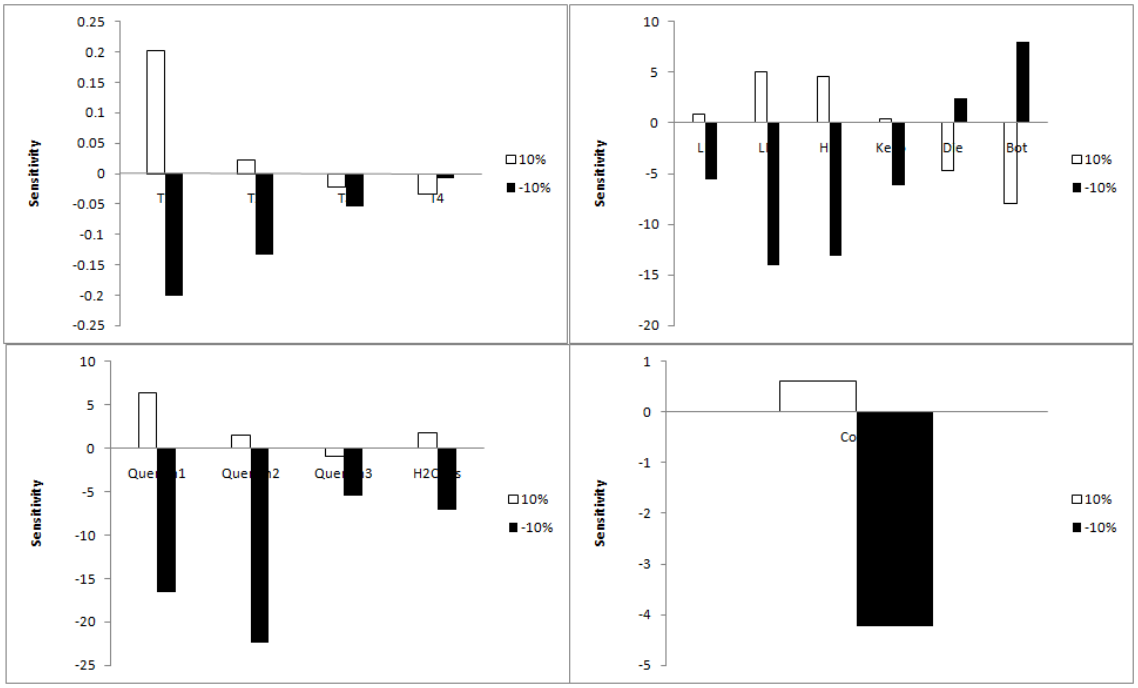

Figure 6.9 Effect of D3 on model outputs for a perturbation ±10%

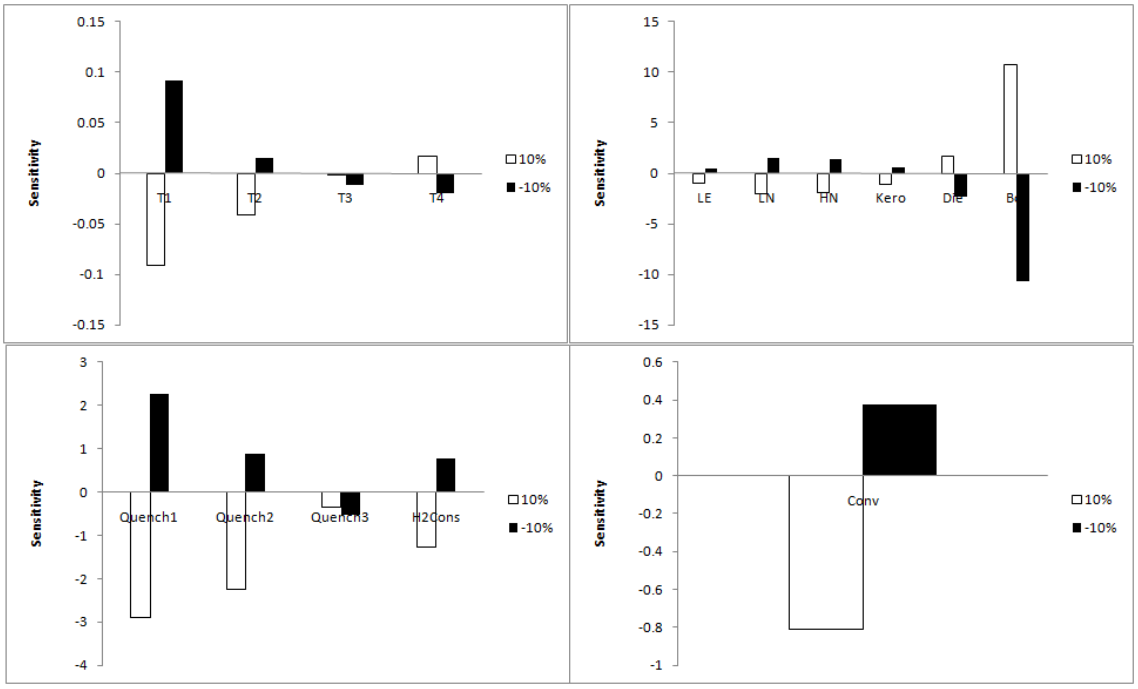

Figure 6.10 Effect of D4 on model outputs for a perturbation ±10%

C-w-B1 and B2 are the parameters that describe the product distribution. While C and w are used to compute LE composition, B1 and B2 are used for calculating heavier fractions compositions. Therefore, in the following four figures, it is observed that C and w have significant effect on LE and B1 and B2 have evident effect on the other products.

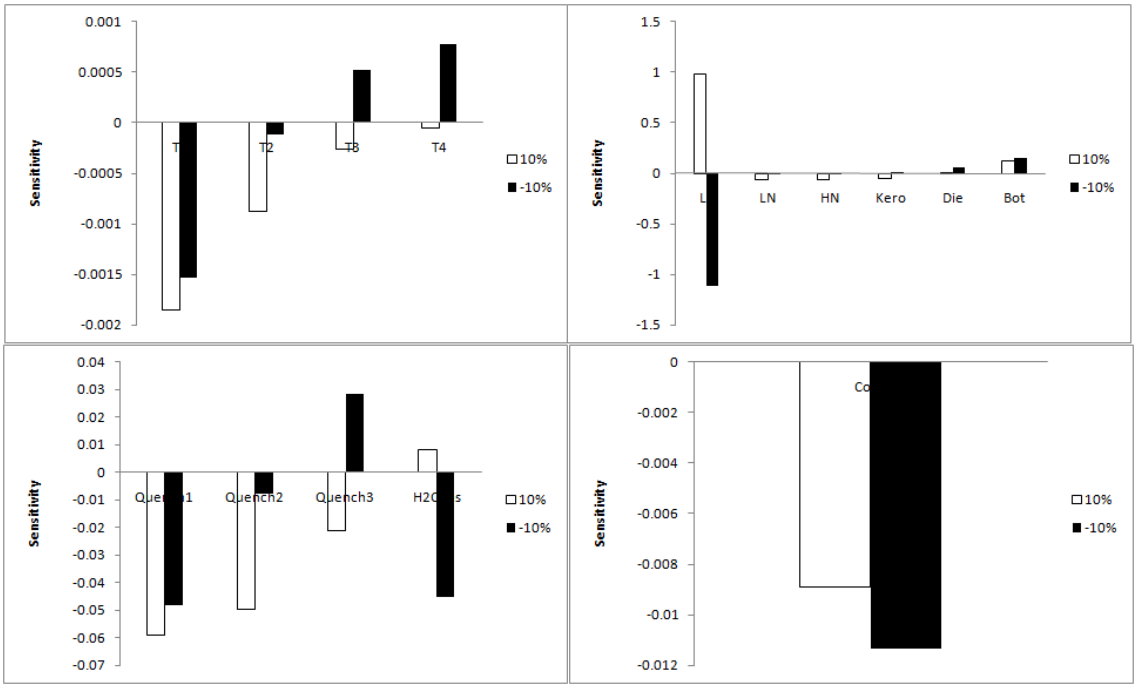

Figure 6.11 Effect of C on model outputs for a perturbation ±10%

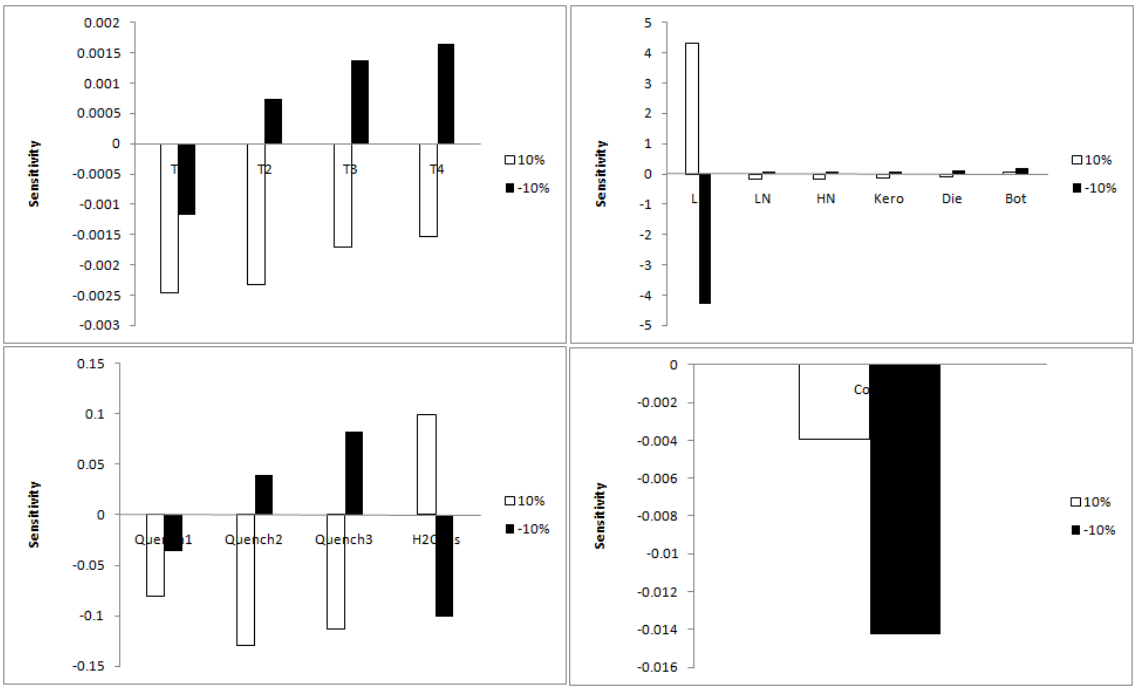

Figure 6.12 Effect of w on model outputs for a perturbation ±10%

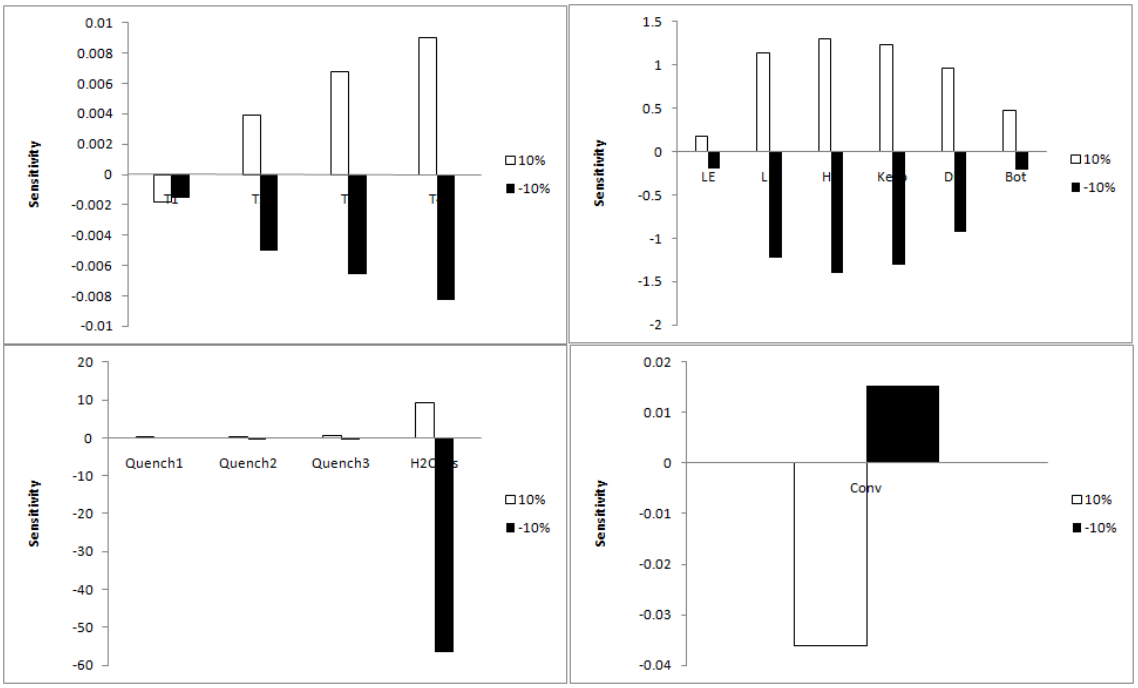

Figure 6.13 Effect of B1 on model outputs for a perturbation ±10%

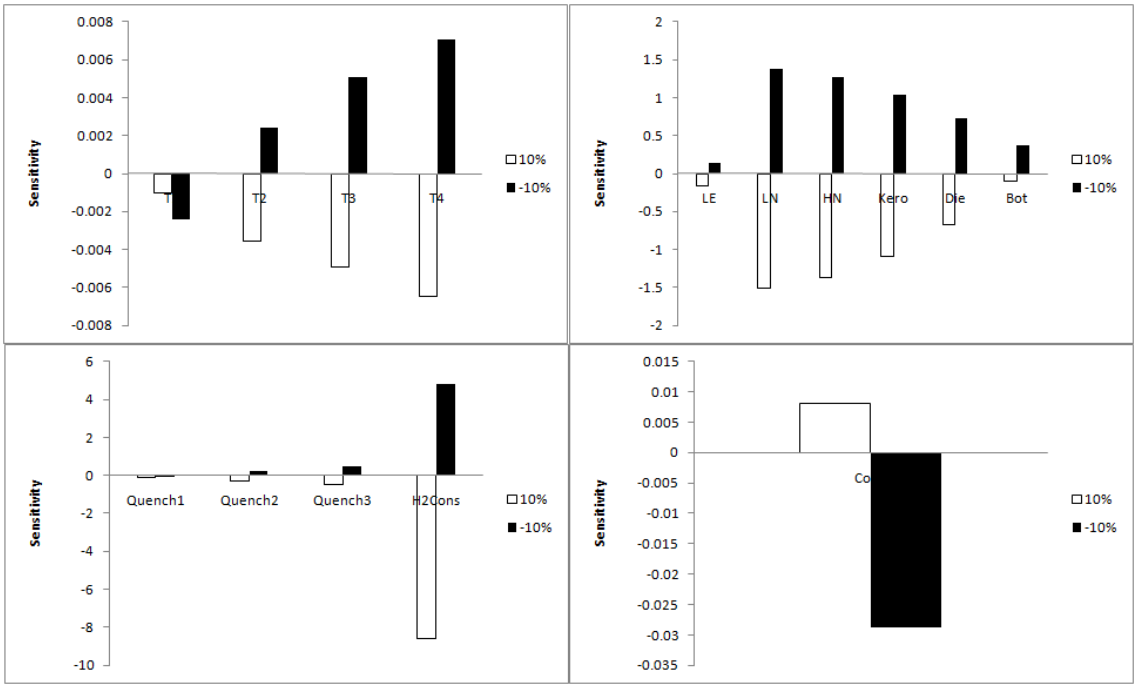

Figure 6.14 Effect of B2 on model outputs for a perturbation ±10%

The parameters HR1 and HR2 are used in the calculation of heat of reaction which affects temperature directly. Therefore, a perturbation on both HR1 and HR2 show a remarkable result on temperatures as seen in Figures 6.19 and 6.20. The other results are consistent with temperature effect.

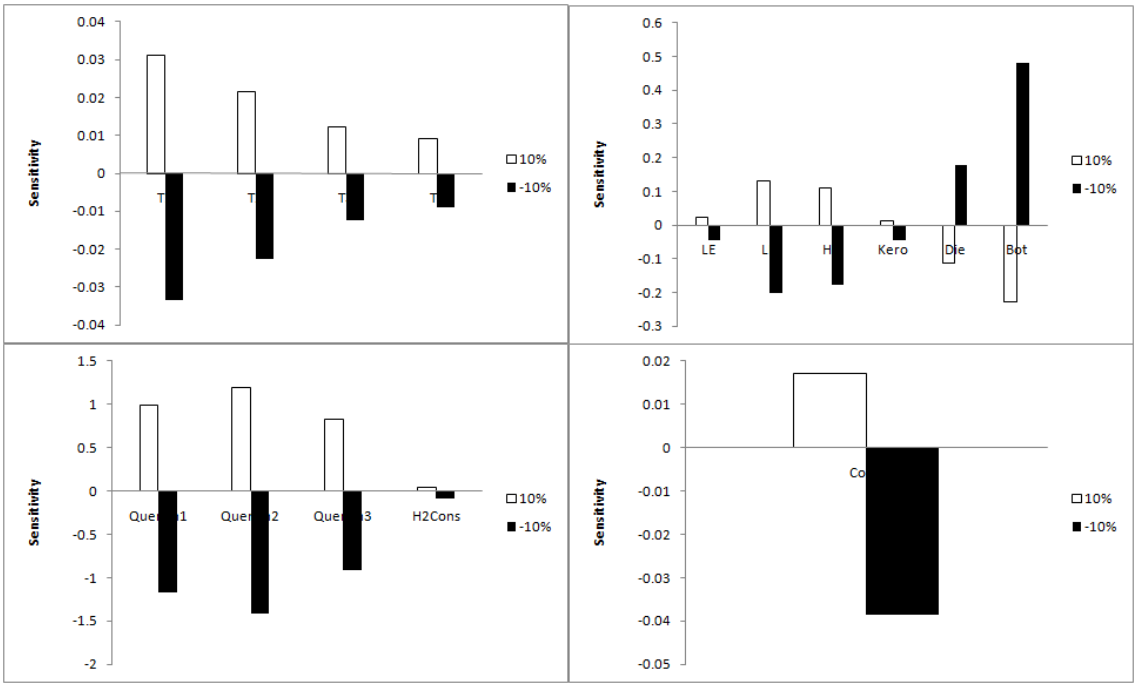

Figure 6.15 Effect of HR1 on model outputs for a perturbation ±10%

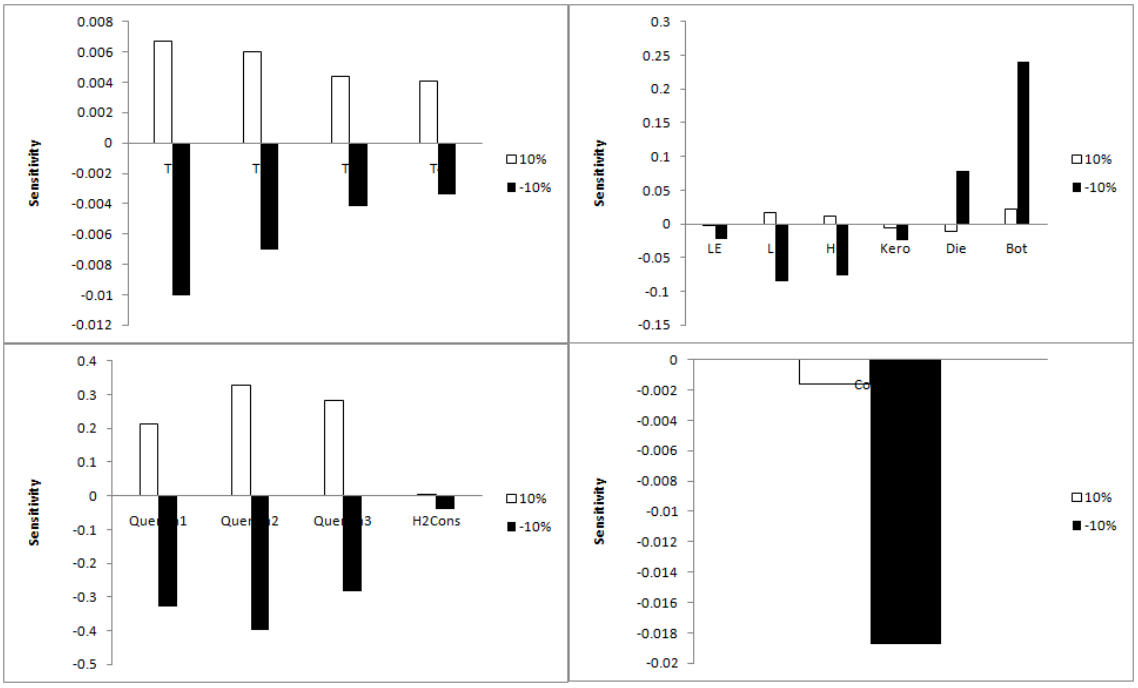

Figure 6.16 Effect of HR2 on model outputs for a perturbation ±10%

In order to decide which parameters have significant effect on results, the average sensitivity of each parameter for each output was computed and ranked from highest to least as given in the following tables. It can be concluded from the tables that D3 has the largest effect on results and since the parameters C and w affect the product LE only, they can be fixed at a nominal value.

Table 6.4 Ranking of parameters according to effects on exit temperatures

	T1	T2	T3	T4
1	D3	D3	D3	D3
2	D2	D2	A3	D4
3	D4	A2	HR1	A4
4	A1	D4	A2	HR1
5	HR1	HR1	D2	B1
6	D1	A1	A1	A3
7	HR2	D1	D4	A2
8	w	HR2	B1	B2
9	B1	B1	D1	D2
10	B2	B2	B2	A1
11	A2	w	HR2	HR2
12	A3	A3	w	D1
13	A4	A4	C	W
14	C	C	A4	C

Table 6.5 Ranking of parameters according to effects on product flows

	LE	LN	HN	Kero	Die	Bot
1	w	D3	D3	D3	D2	D2
2	D3	D2	D2	B1	D3	D4
3	C	D1	D4	B2	D4	D3
4	D2	D4	D1	D4	D1	D1
5	D4	B2	B1	D2	B1	A4
6	D1	B1	B2	D1	B2	A3
7	B1	A4	A4	w	A4	A2
8	B2	A3	A3	A4	A3	A1
9	A4	A2	A2	A3	A2	HR1
10	A3	A1	A1	A2	A1	B1
11	A2	HR1	HR1	A1	HR1	B2
12	A1	w	w	C	w	C
13	HR1	HR2	HR2	HR1	HR2	HR2
14	HR2	C	C	HR2	C	w

Table 6.6 Ranking of parameters according to effects on quench flows, hydrogen consumption and conversion

	Quench1	Quench2	Quench3	H2Cons	Conv
1	D3	D3	D3	B1	D3
2	D2	D2	A3	B2	D2
3	D4	A2	HR1	D3	D4
4	A1	D4	D2	D2	D1
5	HR1	HR1	B1	D4	A4
6	D1	D1	A2	D1	A3
7	HR2	A1	B2	A4	A2
8	B1	B1	D4	A3	A1
9	W	HR2	D1	A2	HR1
10	A2	B2	A1	w	B1
11	A3	w	HR2	A1	B2
12	A4	A3	w	HR1	HR2
13	C	A4	C	C	C
14	B2	C	A4	HR2	w

Chapter 7

7. RESULTS AND DISCUSSION

7.1. CONSTANT CONVERSION TRAINING DATA

As mentioned in the previous chapter, the final model parameters were found by matching three days of operation data (Day 1-Day 2 and Day 3) simultaneously. The available data and the chosen training data are shown in the following figures. It should be noted that the data presented in this thesis were manipulated due to confidential issues.

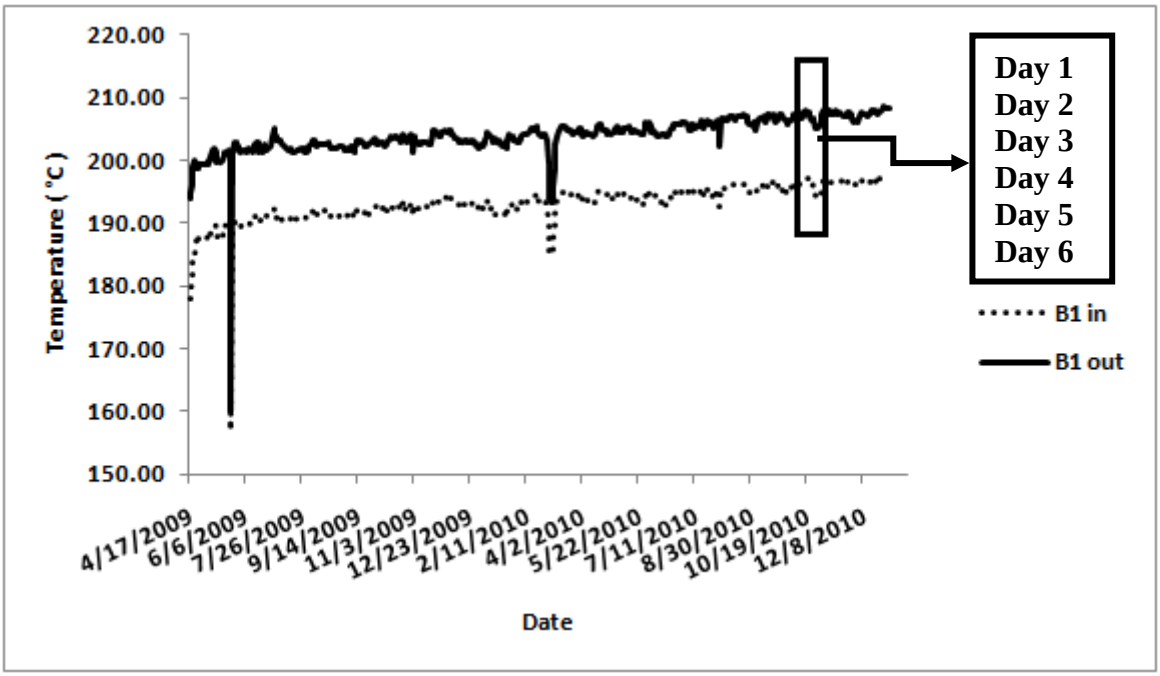

Figure 7.1 Plant data for first bed inlet and outlet temperatures with the chosen data window

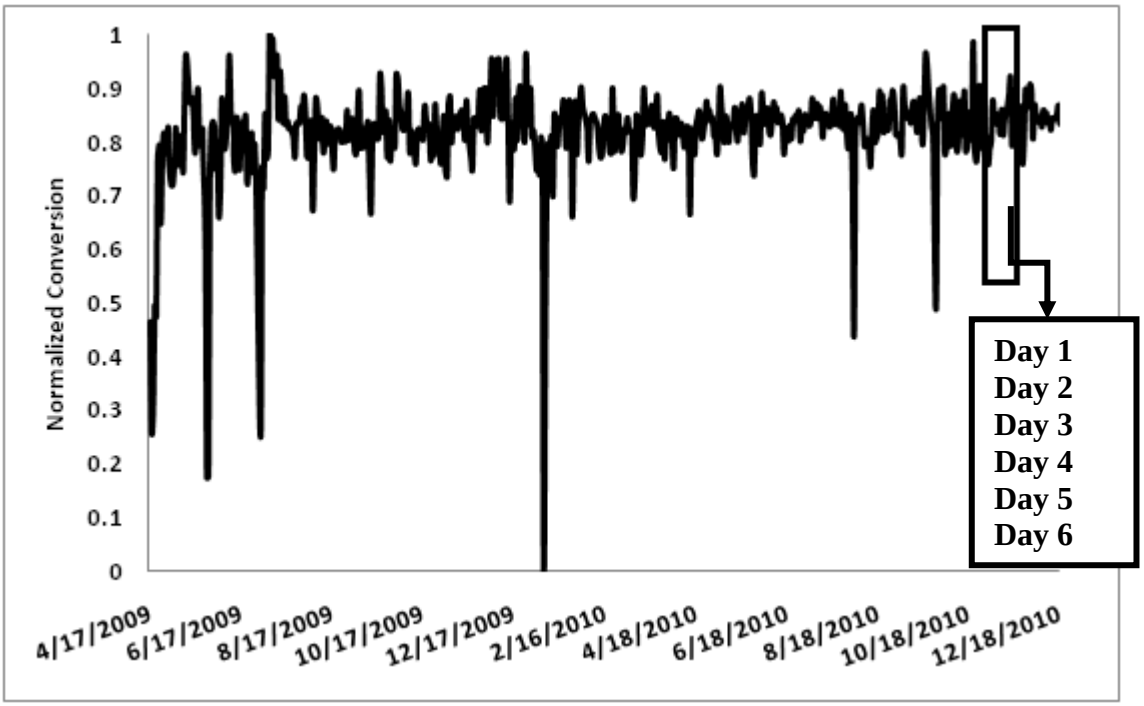

Figure 7.2 Conversion data of the plant data with the chosen data window

The model outputs and plant data for these three different days were compared in the following sections.

7.1.1.1. Day 1 Simulations

As can be seen in the Figure 7.3, the model gives higher exit temperatures for the first two beds. The difference is significant in the second bed exit temperature. The model predicts the third and fourth bed exit temperatures successfully.

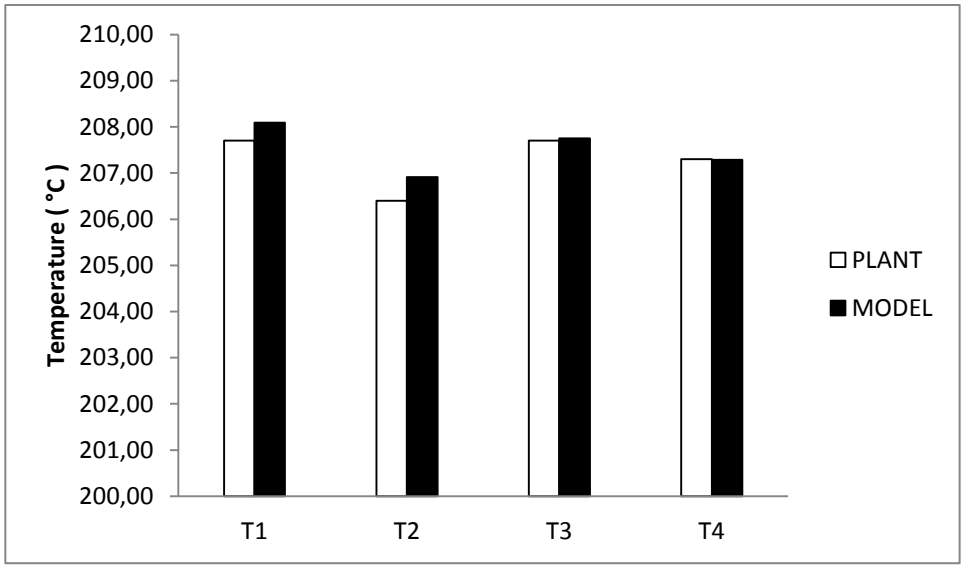

Figure 7.3 Comparison of bed exit temperatures for Day 1

Due to higher bed exit temperatures in the first two beds, more quench flows are needed to cool the exit streams of those beds. This expected result is observed in the following figure.

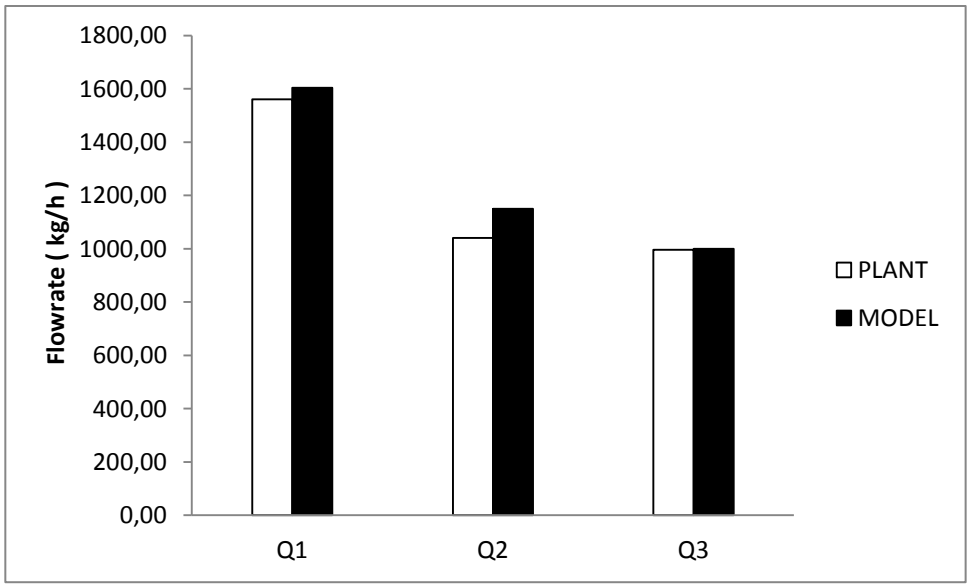

Figure 7.4 Comparison of quench flows for Day 1

Since the reaction is exothermic in nature, higher exit temperatures will imply more cracking and hence favor lighter products. As can be seen in Figure 7.5, the model predicts higher flow rates for the product Naphtha. Since the bottom flow rate is smaller, the conversion computed by model will be higher as observed in Figure 7.6.

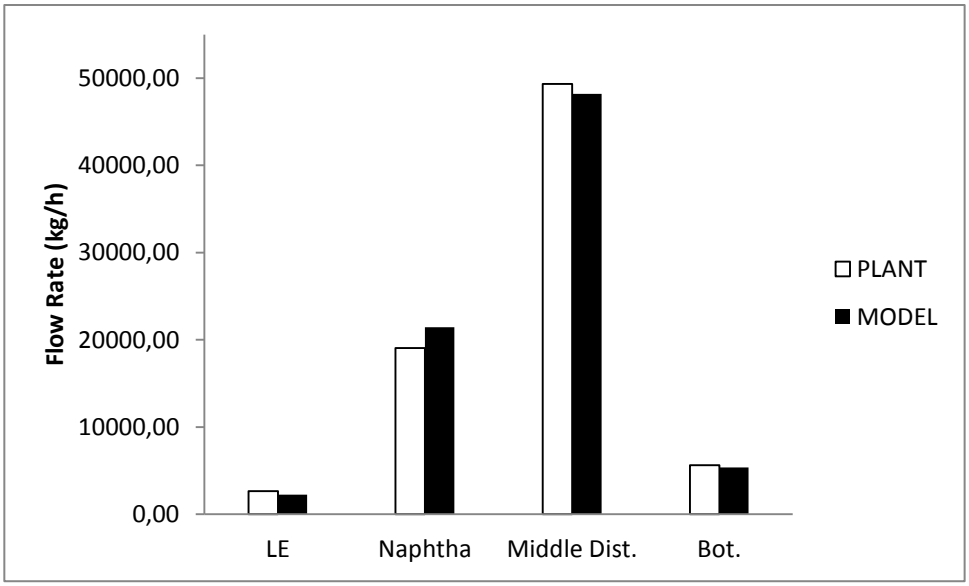

Figure 7.5 Comparison of products flow rates for Day 1

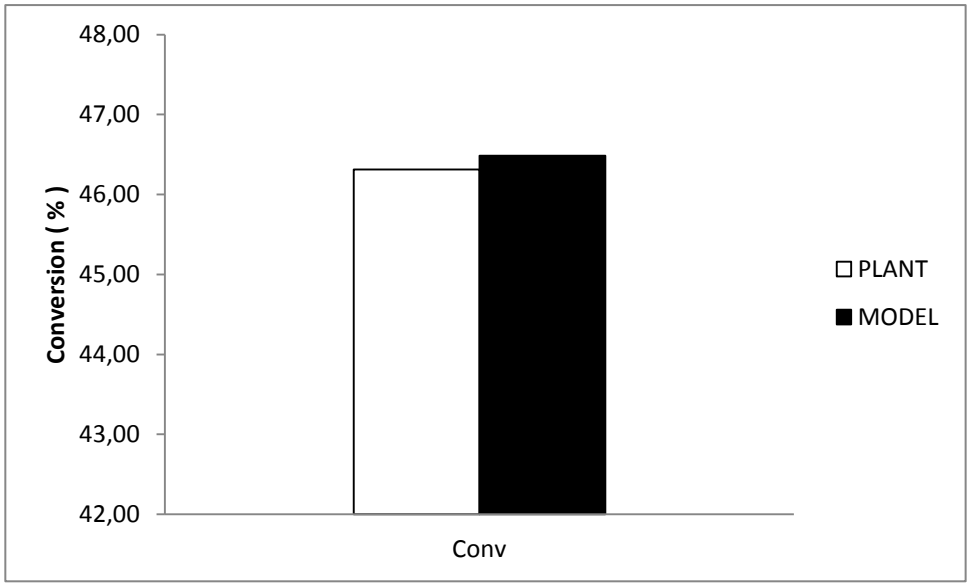

Figure 7.6 Comparison of conversion for Day 1

As the model foresees more cracking, the hydrogen consumption given by model will be higher than plant data. This expected result can also be seen in Figure 7.7.

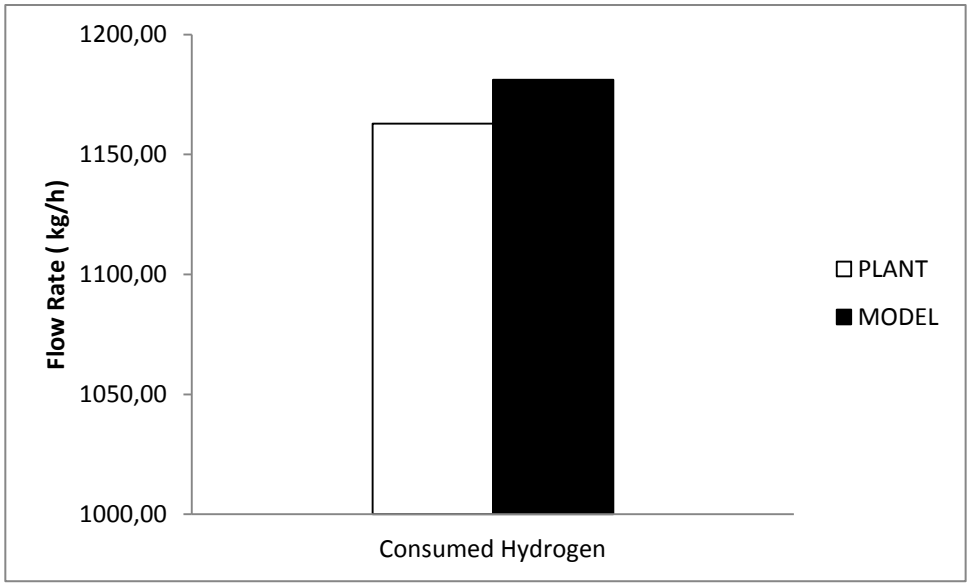

Figure 7.7 Comparison of hydrogen consumption for Day 1

Since products prices and operating expenses are available, daily profit can easily be computed as follows;

$$\Pr ofit = \sum_{i=1}^{5} P_i \times F_i - \sum \left[\left(P_{Feed} \times F_{feed} \right) + \left(P_{Hydrogen} \times F_{Hydrogen} \right) \right] \quad (51)$$

where P stands for price in \$/ton and F stands for amount in ton.

As can be seen in Table 7.1, the model predicts daily profit with a small error.

Table 7.1 Daily profit prediction of Model for Day 1

PLANT ($)	MODEL PREDICTION ERROR %
*	4.84

**Confidential*

7.1.2. Day 2 Simulations

Figure 7.8 shows that exit temperatures computed by model are lower than the plant data. However, the differences are reasonable when the profit prediction of model is taken into account.

Table 7.2 Daily profit prediction of Model for Day 2

PLANT ($)	MODEL PREDICTION ERROR %
*	3.72

**Confidential*

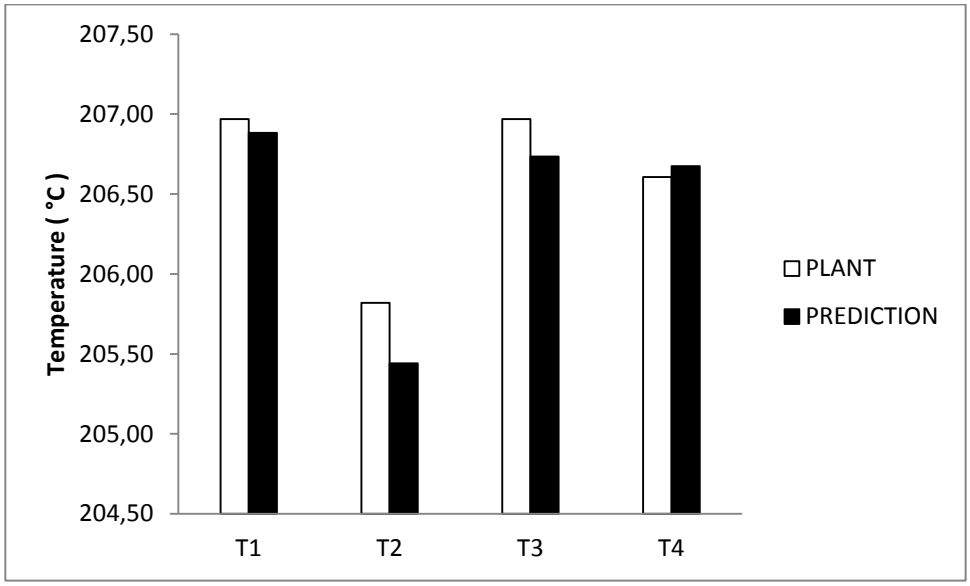

Figure 7.8 Comparison of bed exit temperatures for Day 2

Since the bed exit temperatures match well with plant values, the quench flows of model and plant will be almost equal as seen in the following figure.

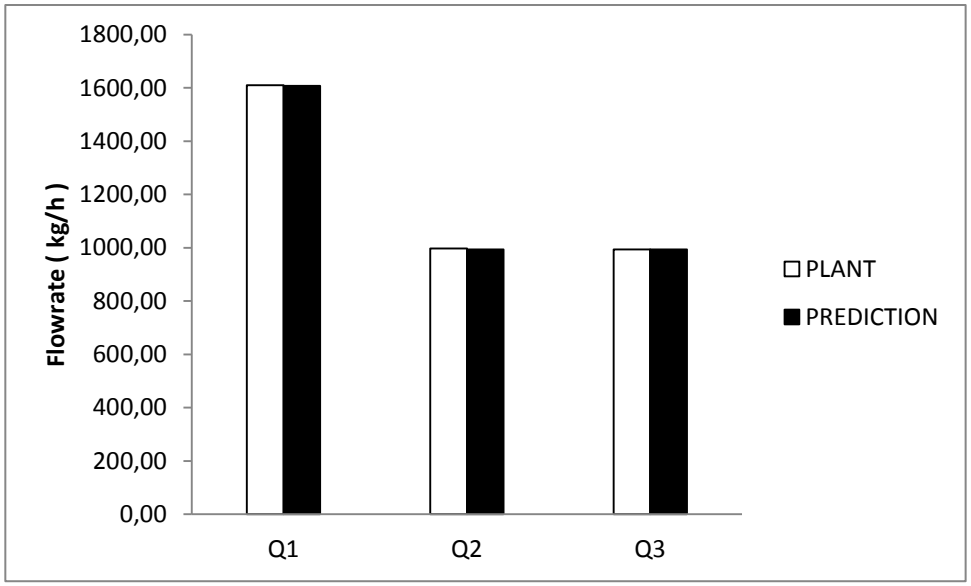

Figure 7.9 Comparison of quench flows for Day 2

The product distribution can be seen in the following figure. Since the bottom flow of model is a bit higher than the plant data, the conversion computed by model will be a bit lower than the plant data as observed in Figure 7.11.

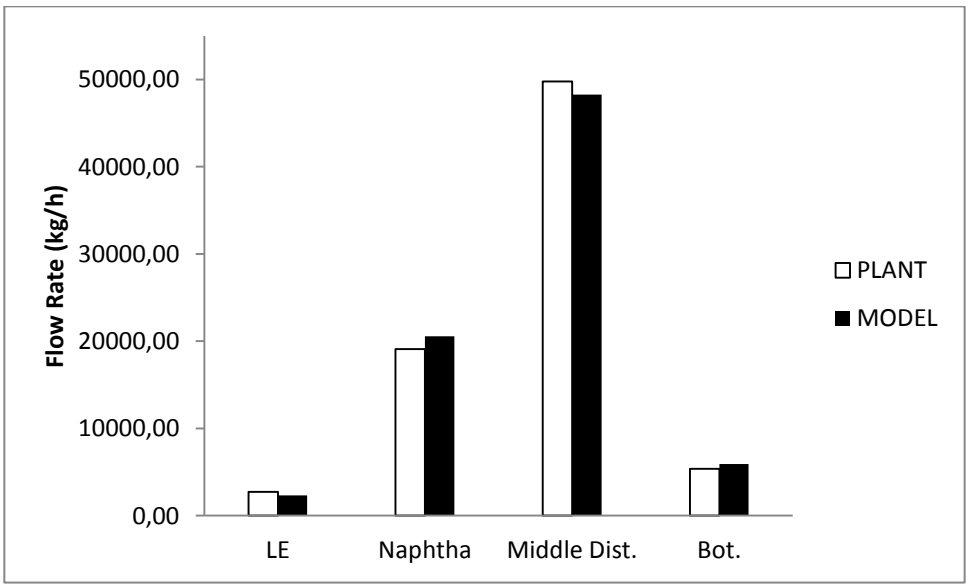

Figure 7.10 Comparison of product flows for Day 2

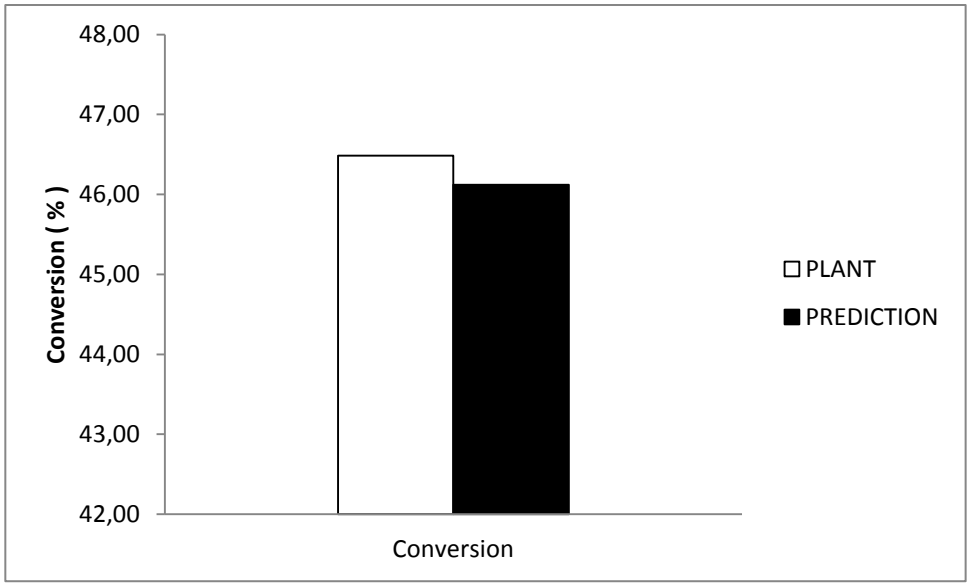

Figure 7.11 Comparison of conversion for Day 2

As in the previous outputs, the model predicts the hydrogen consumption closely as well. The result can be observed in the following figure.

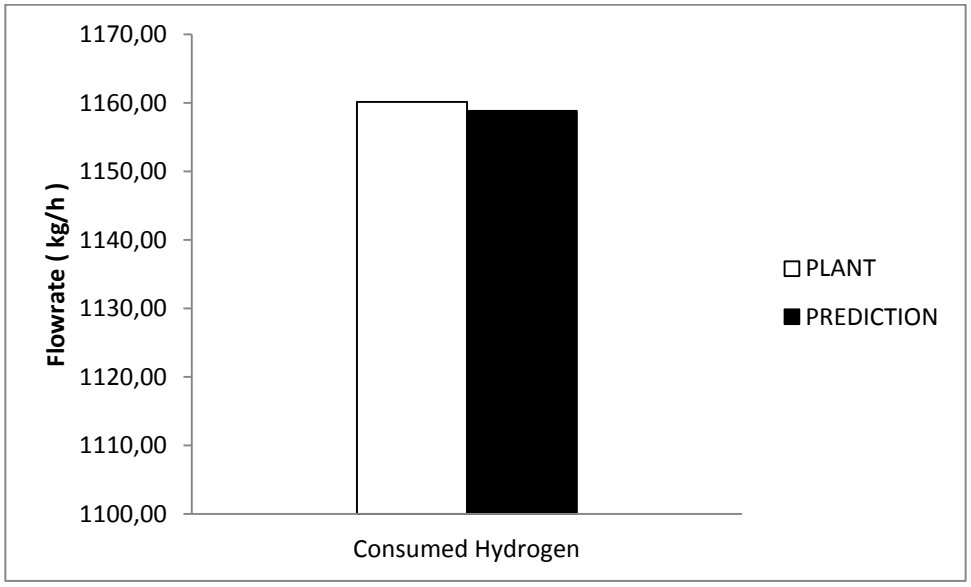

Figure 7.12 Comparison of hydrogen consumption for Day 2

Since daily profit prediction for Day 2 is better than the prediction for Day 1, it can be concluded that model has better predictions for Day 2.

7.1.3. Day 3 Simulations

Temperature predictions are shown in Figure 7.13.

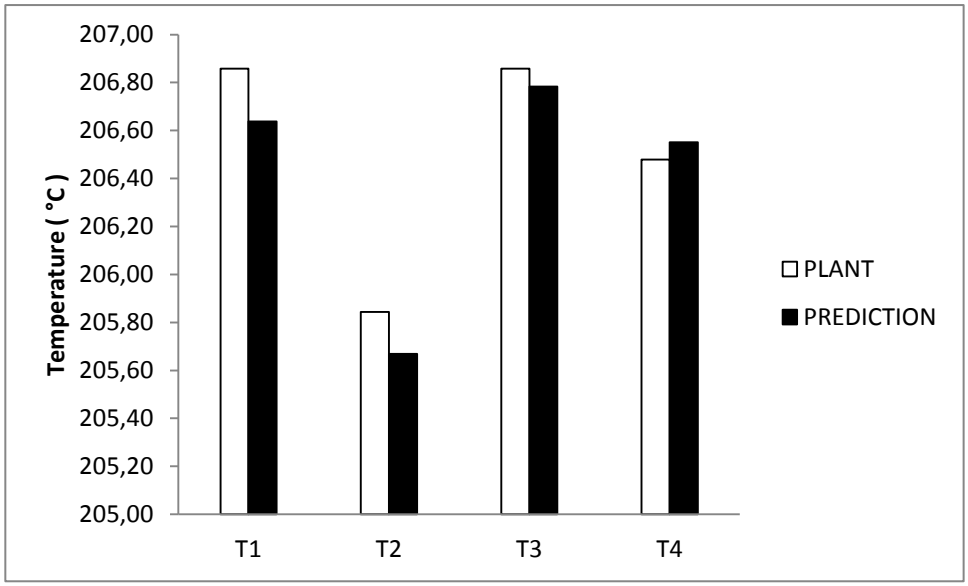

Figure 7.13 Comparison of bed exit temperatures for Day 3

The bed exit results are coherent with the other results as can be followed in the next figures below.

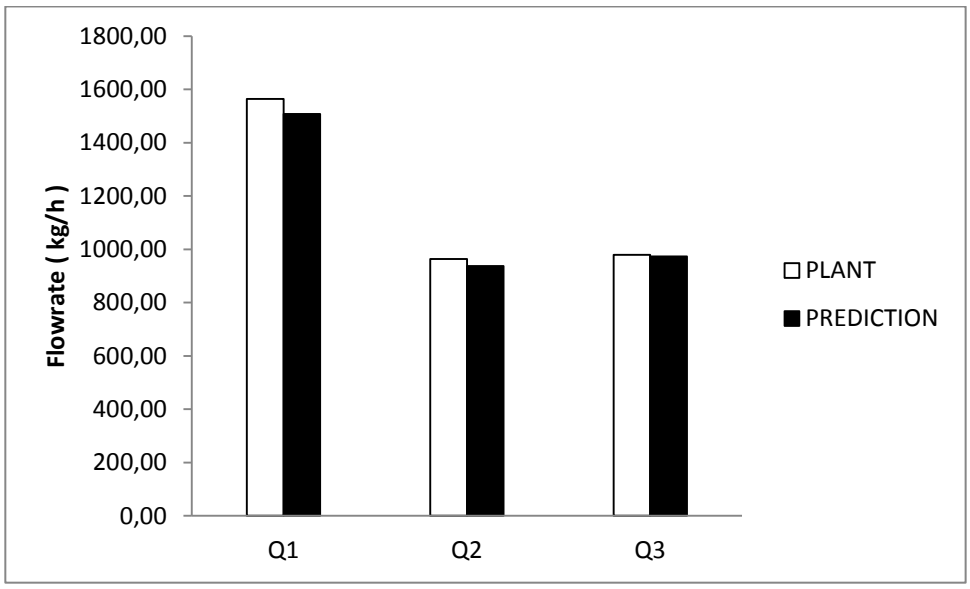

Figure 7.14 Comparison of quench flows for Day 3

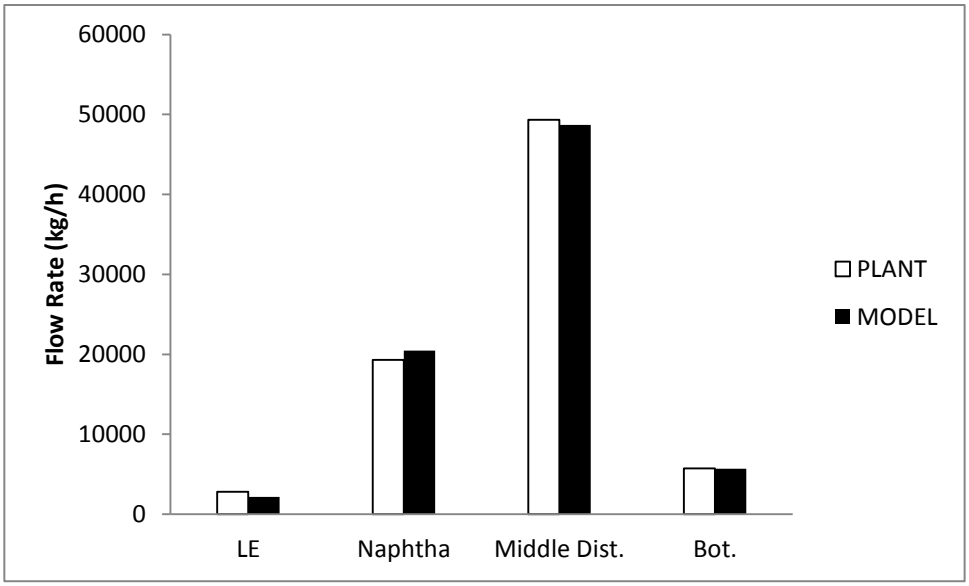

Figure 7.15 Comparison of product flows for Day 3

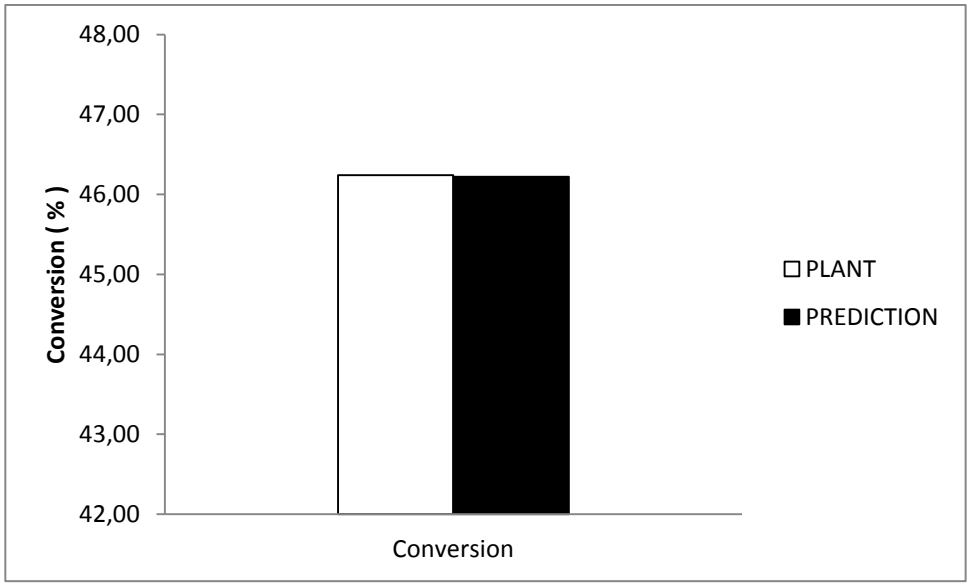

Figure 7.16 Comparison of conversion for Day 3

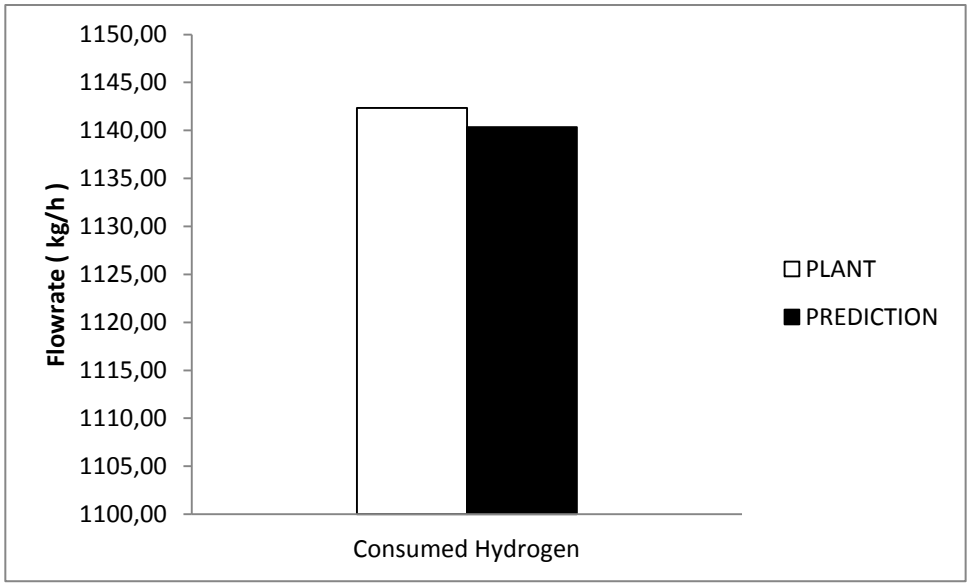

Figure 7.17 Comparison of hydrogen consumption for Day 3

Table 7.3 Daily profit prediction of Model for Day 3

PLANT ($)	MODEL PREDICTION ERROR %
*	1.92

**Confidential*

To sum up, according to results presented above, it can easily be claimed that the final model gives quite satisfactory predictions for the training data that was used in determination of model parameters.

7.2. PREDICTIONS

The model parameters should be tested by performing simulations for the operation data different than those used in estimation. Unless the reliability of parameter set is proved, the modeling cannot be finalized. Here, providing the distillation data of feed and inlet temperatures for all days will be useful to visualize the variability of data. Although the distillation curves look similar, the first bed inlet temperature of Day 4 is out of range when compared with the other days. Hence, it is expected that the simulations by Day 4 will be distinct.

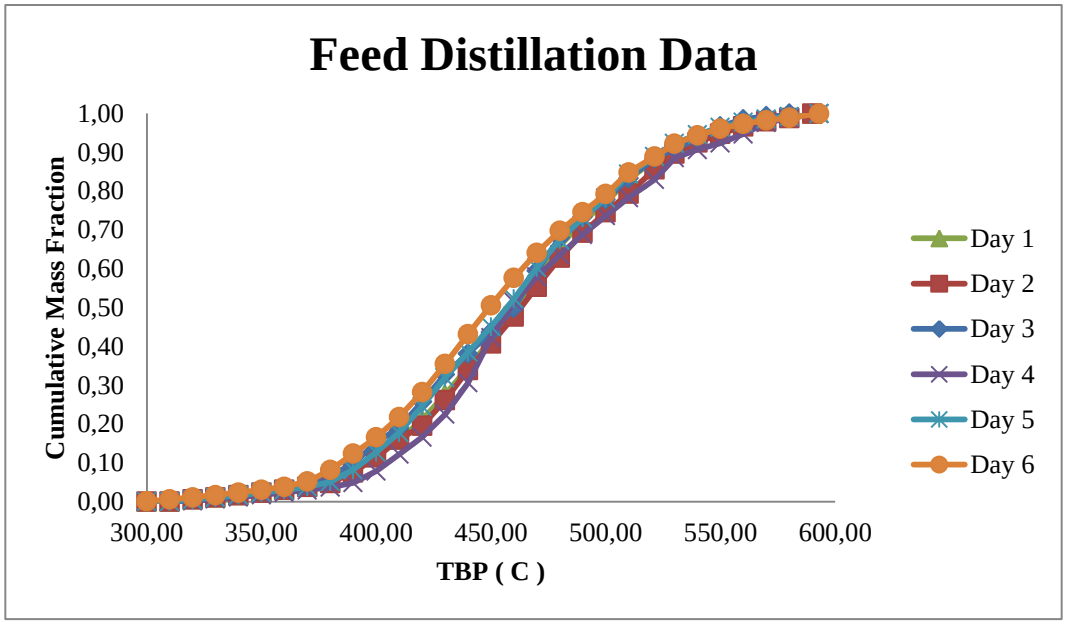

Figure 7.18 Variability of feed for six different days of operation

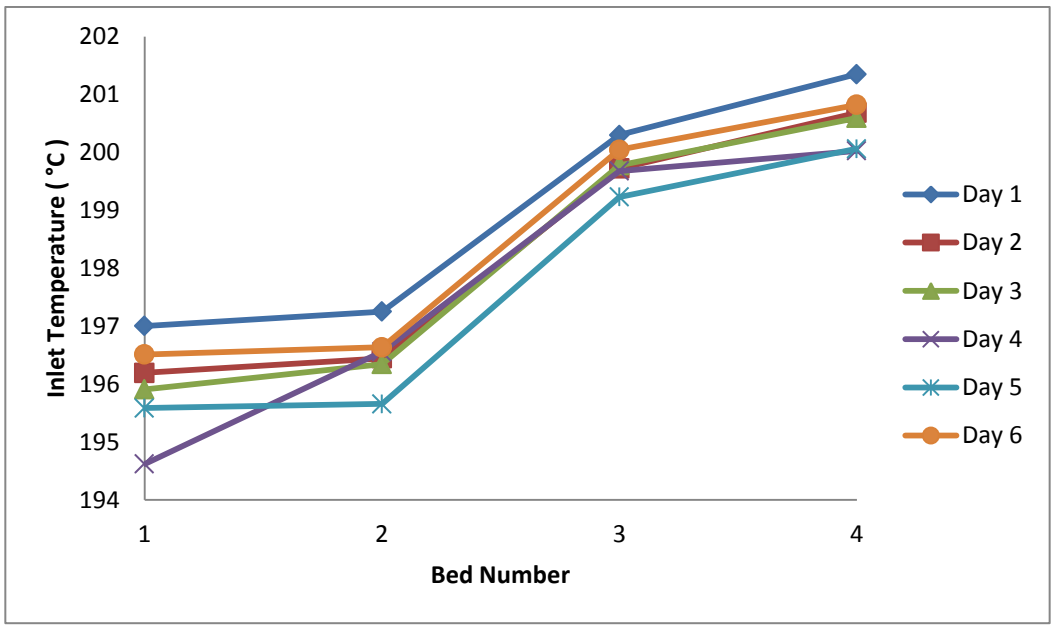

Figure 7.19 Variability of inlet temperatures for six different days of operation

The model predictions for Day 4, Day 5 and Day 6 were given in the following sections respectively.

7.2.1. Day 4 Simulations

As can be observed in Figure 7.20, first bed exit temperature of the model is dramatically lower than the plant value. Although the difference in distillation cannot be realized by Figure 7.18, Figure 7.19 implies that the characteristic of feed on Day 4 is very distinct. Therefore,

the model prediction for first bed is compatible with this distinction. Other exit temperatures match the plant data more closely.

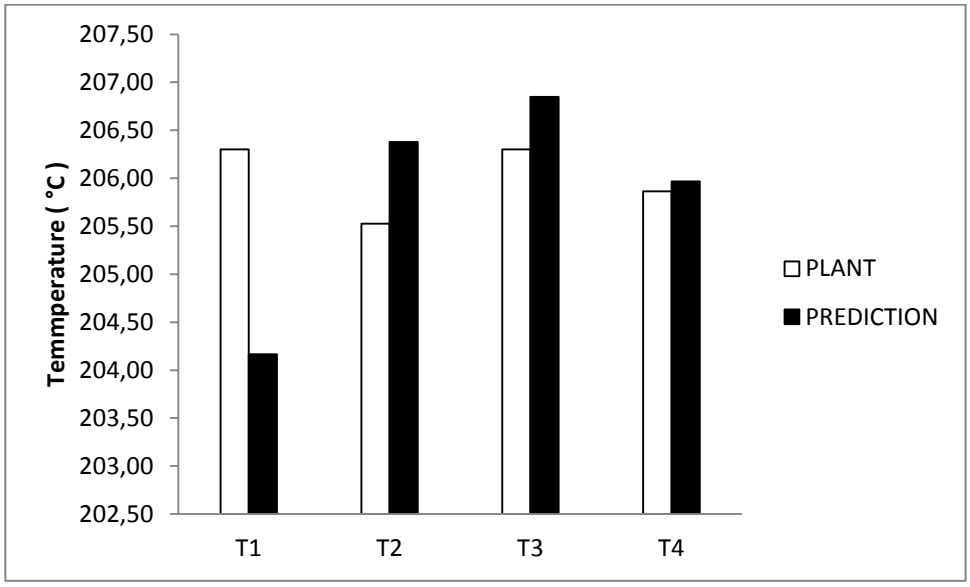

Figure 7.20 Comparison of bed exit temperatures for Day 4

Since the exit temperature of the first bed is lower markedly, the first quench flow will be lower than the plant value as observed in Figure 7.21. Likewise, the other quench flows are a little bit higher than the plant values due to the little differences in bed exit temperatures observed.

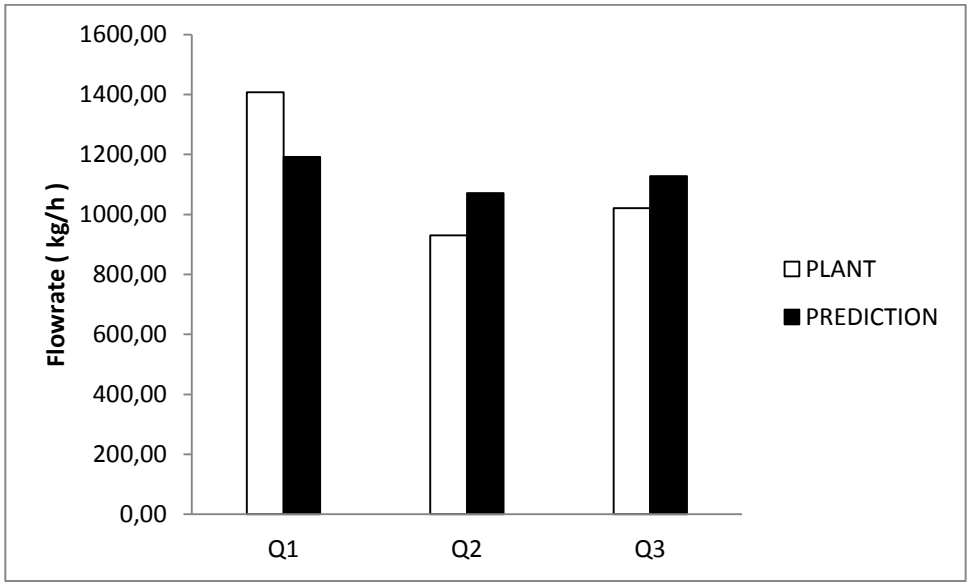

Figure 7.21 Comparison of quench flows for Day 4

The following figure shows that bottom and middle distillate flows are higher and the other flows are lower than the plant data. In fact, it implies that less cracking occurred. This may be concluded that first bed is the key for cracking.

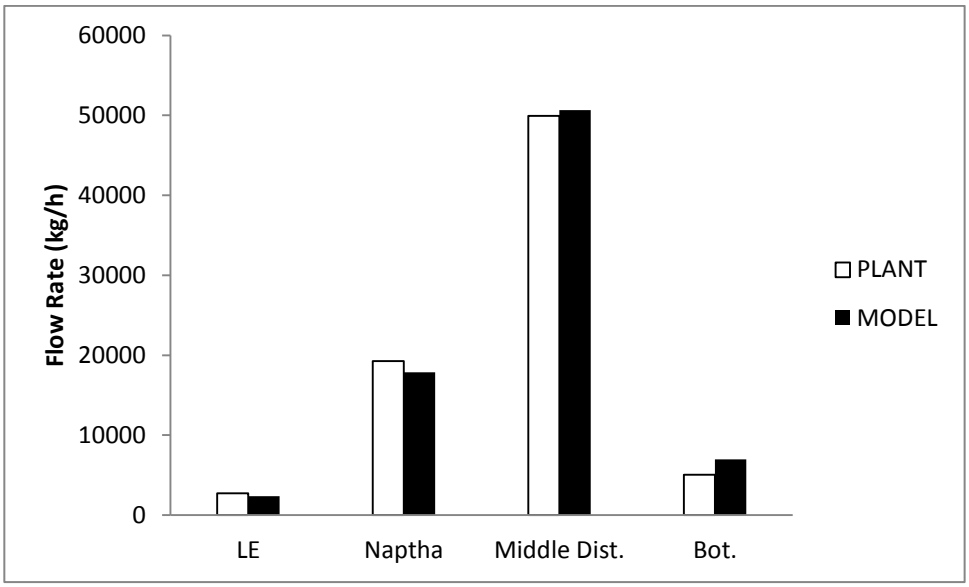

Figure 7.22 Comparison of product flows for Day 4

The more bottom flow means the less conversion as can be seen in the following figure.

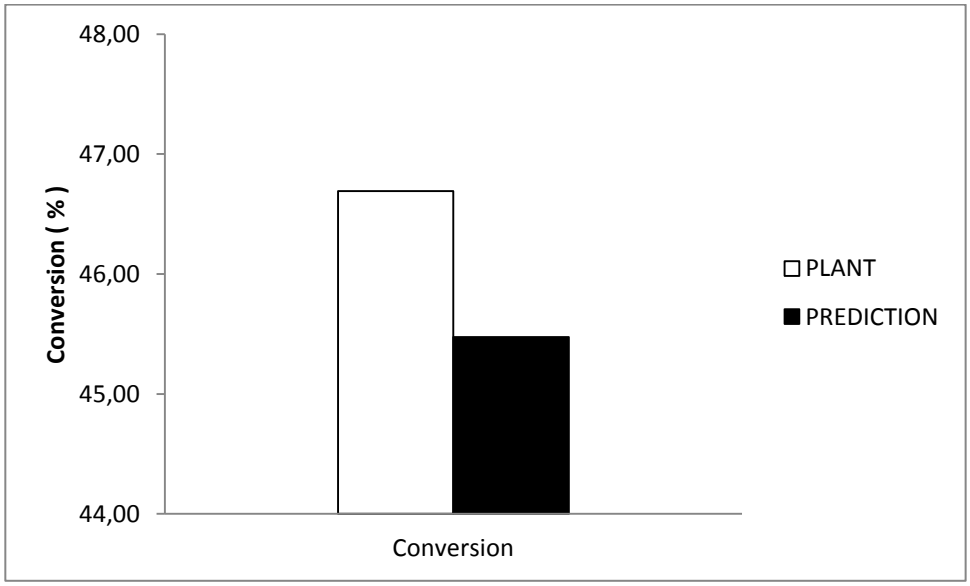

Figure 7.23 Comparison of conversion for Day 4

Due to the less cracking, less hydrogen will be consumed as Figure 7.24 shows.

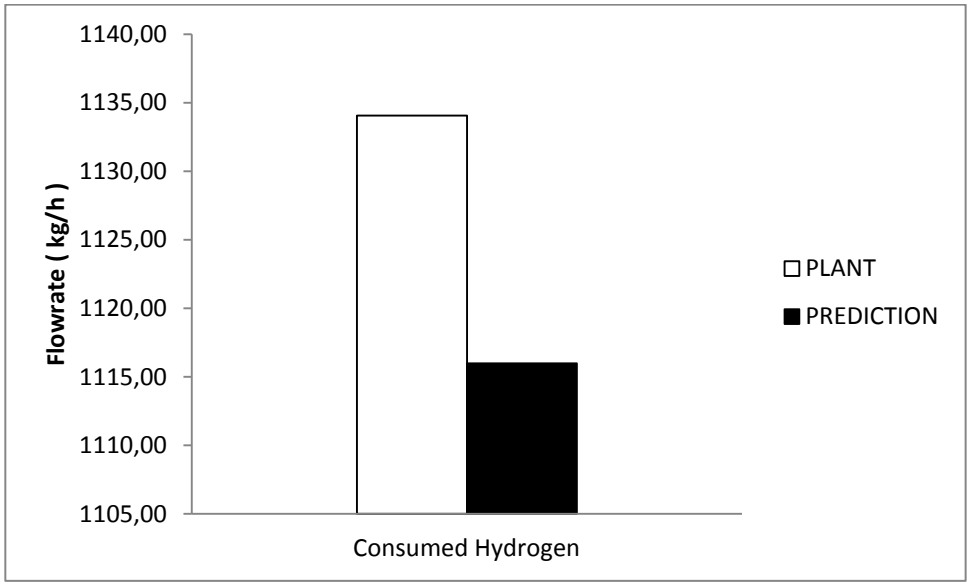

Figure 7.24 Comparison of hydrogen consumption for Day 4

Table 7.4 Daily profit prediction of Model for Day 4

PLANT ($)	MODEL PREDICTION ERROR %
*	12.6

**Confidential*

It can be concluded here that bed inlet temperatures affect the model predictions and first bed has a critical role for the model.

7.2.2. Day 5 Simulations

When the following figures are analyzed, it can easily be observed that the model prediction for Day 5 is remarkably satisfactory.

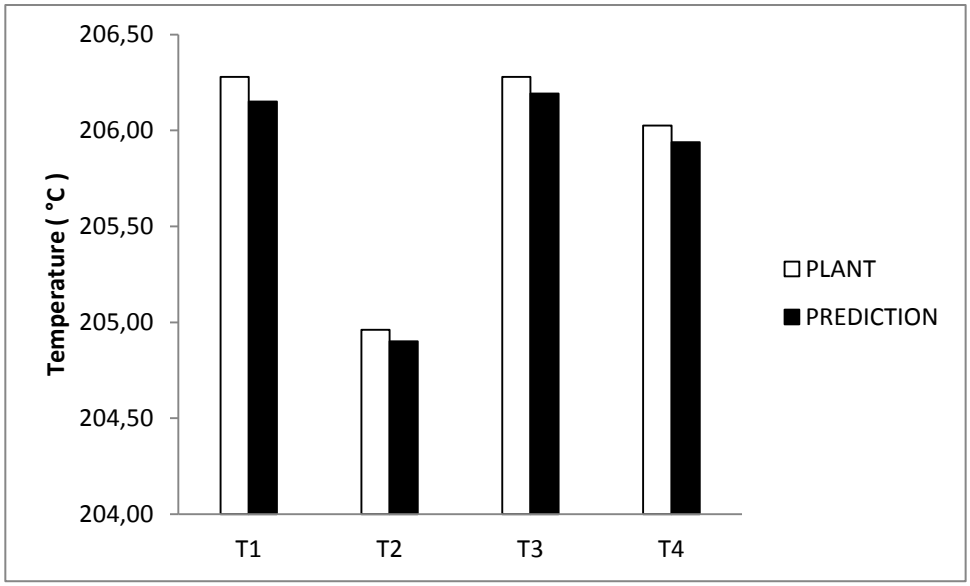

Figure 7.25 Comparison of bed exit temperatures for Day 5

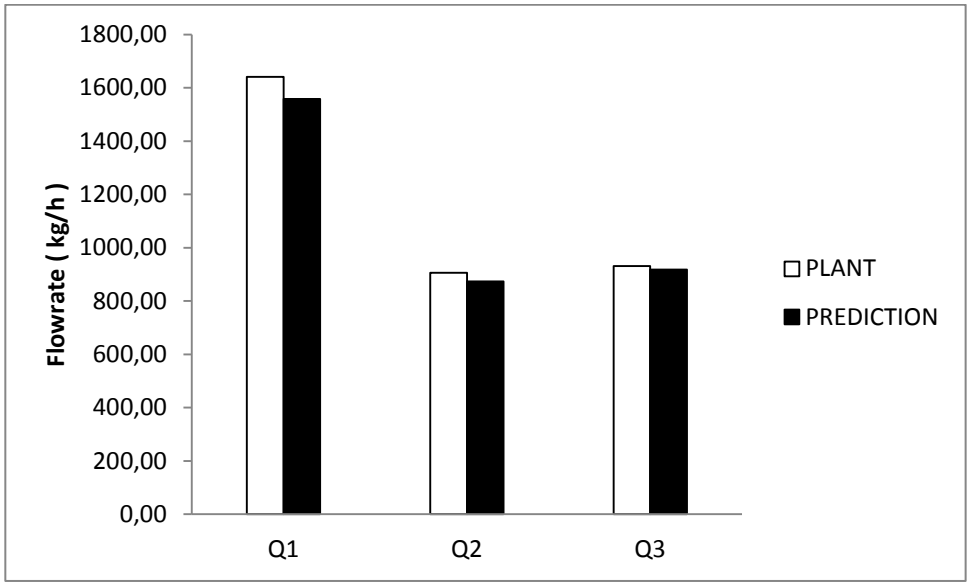

Figure 7.26 Comparison of quench flows for Day 5

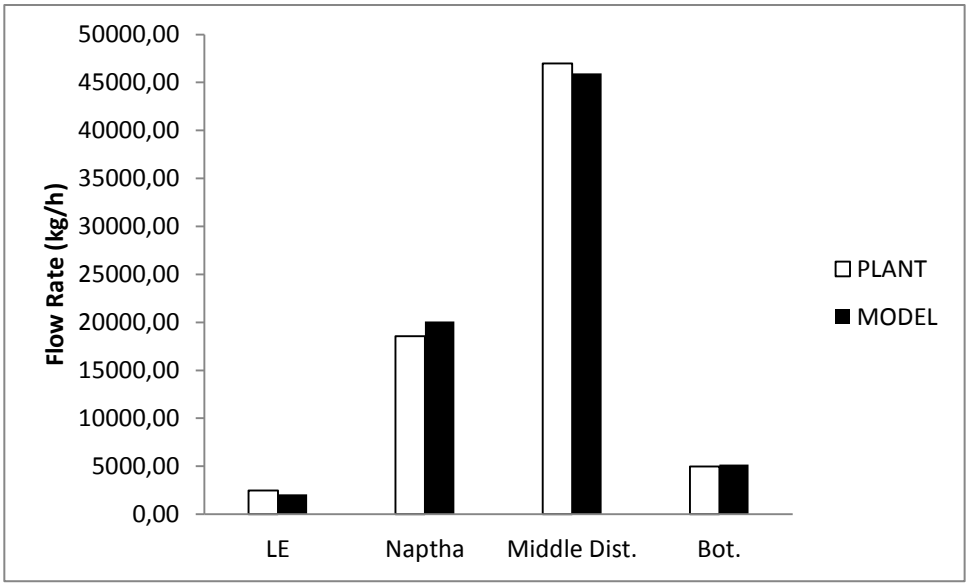

Figure 7.27 Comparison of product flows for Day 5

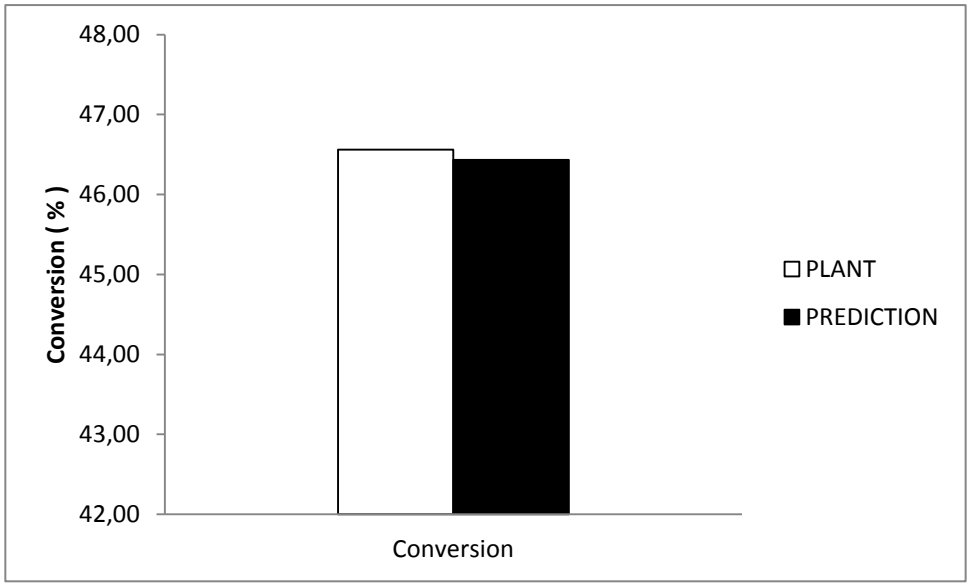

Figure 7.28 Comparison of conversion for Day 5

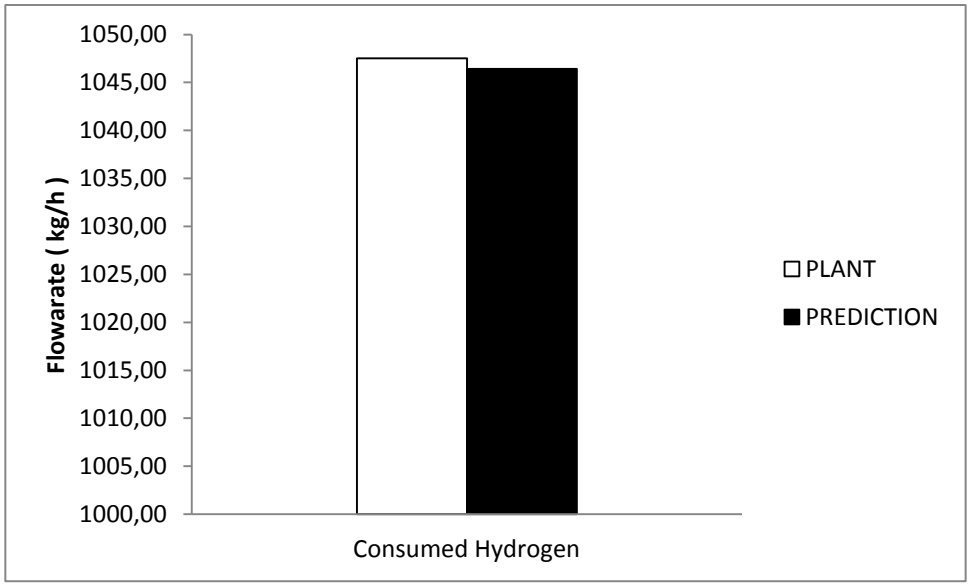

Figure 7.29 Comparison of hydrogen consumption for Day 5

Table 7.5 Daily profit prediction of Model for Day 5

PLANT ($)	MODEL PREDICTION ERROR %
*	1.15

**Confidential*

7.2.3. Day 6 Simulations

As in the case Day 5, model predictions for Day 6 are also successful. The results are given in the following figures.

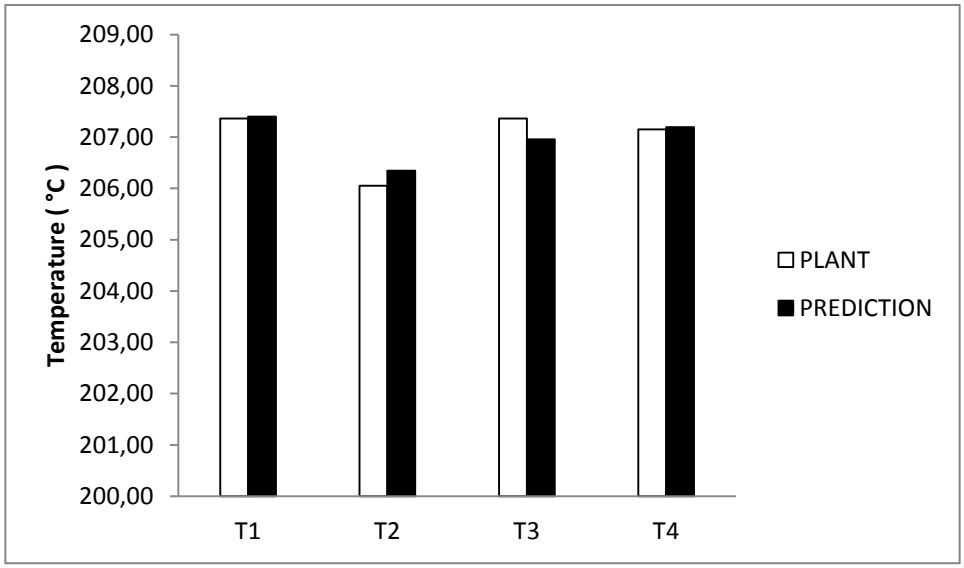

Figure 7.30 Comparison of bed exit temperatures for Day 6

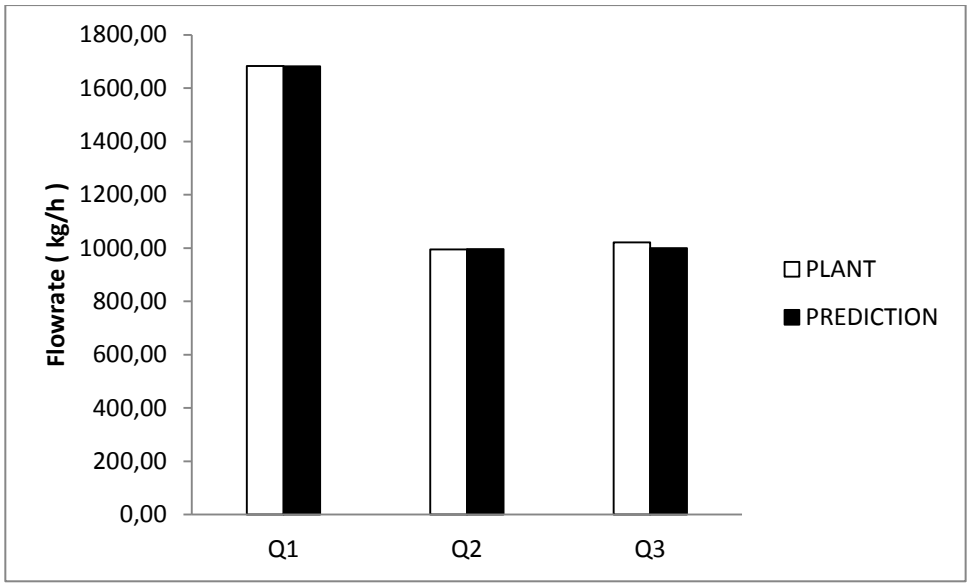

Figure 7.31 Comparison of quench flows for Day 6

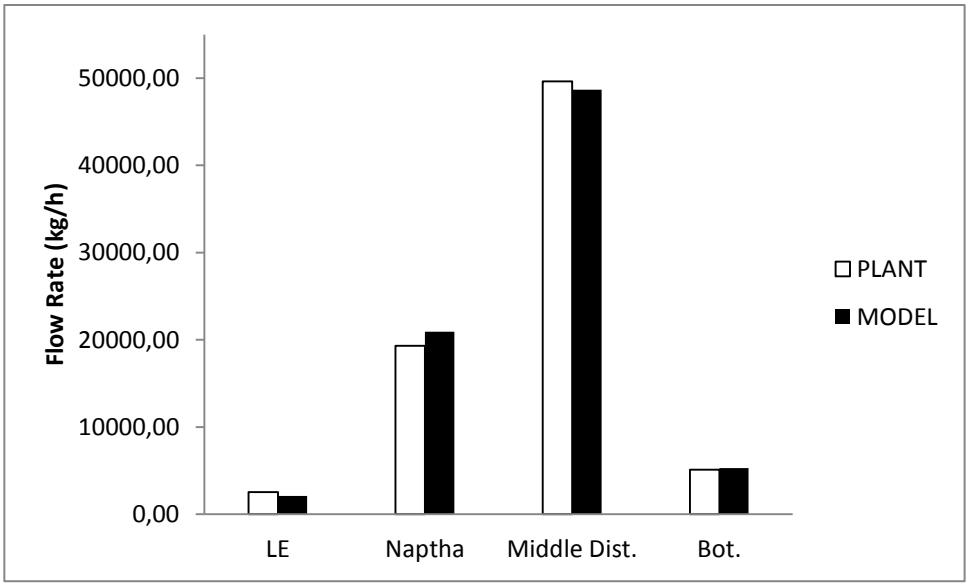

Figure 7.32 Comparison of product flows for Day 6

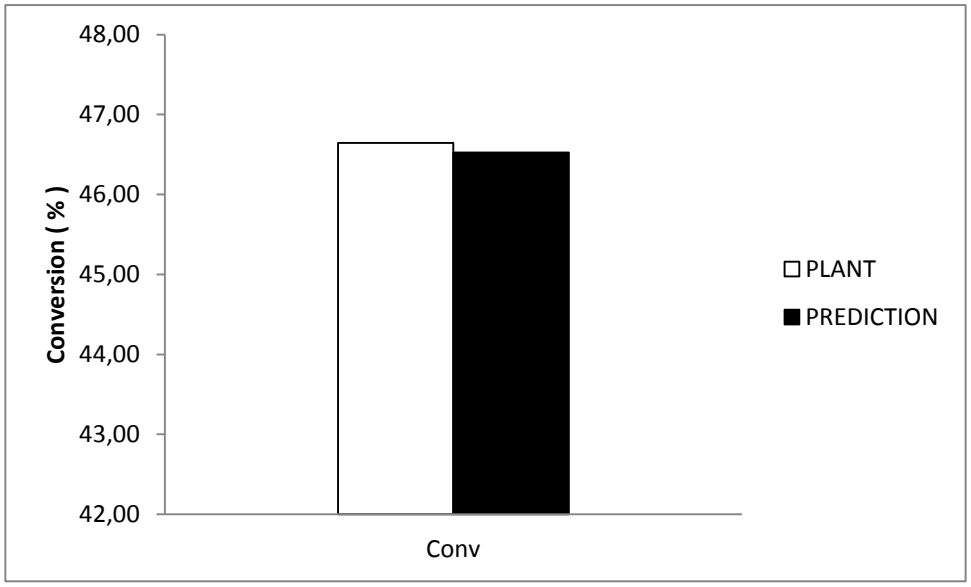

Figure 7.33 Comparison of conversion for Day 6

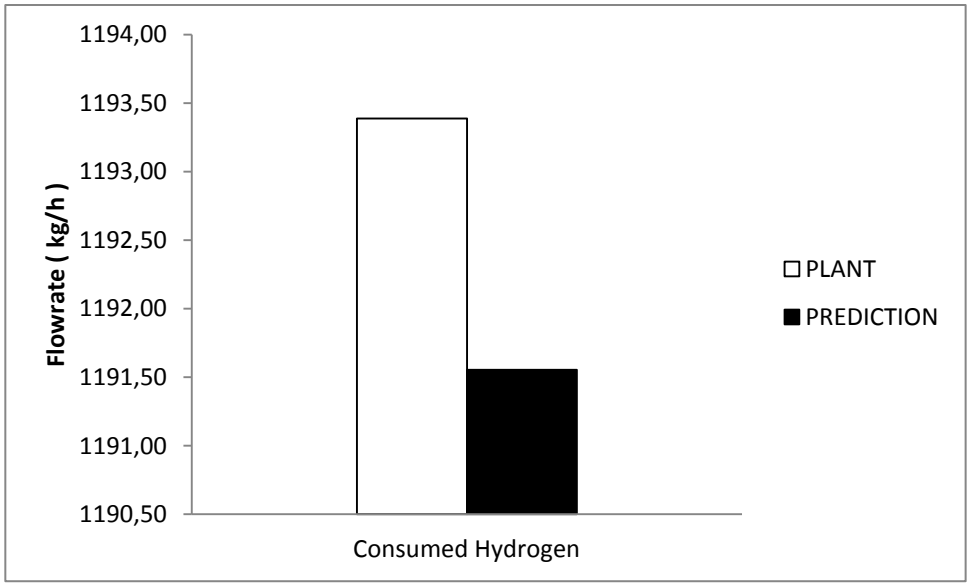

Figure 7.34 Comparison of hydrogen consumption for Day 6

Table 7.6 Daily profit prediction of Model for Day 6

PLANT ($)	MODEL PREDICTION ERROR %
*	0.81

**Confidential*

The results show that model predictions are successful enough when the feed that simulations performed by, has similar characteristics with the feeds used in determination of model parameters. As in the case Day 4, the model predictions deviate from the plant data. It seems that it is a limitation of model. However, since the plant aims to produce same products, the feed treated in the plant should also have similar properties. Therefore, dissimilar feed cases are very rare indeed and it can surely be claimed that the developed model is successful in predicting the process behavior. Otherwise parameters have to be estimated on-line.

7.3. EFFECT OF CATALYST DEACTIVATION ON MODEL PARAMETERS

As the HCU operates, the catalyst loses its activity. In fact, catalyst activity determines the temperature that is required to obtain a fixed conversion. When the catalyst is deactivated, higher inlet temperatures are needed in order to achieve the same conversion as can be observed in the following figure.

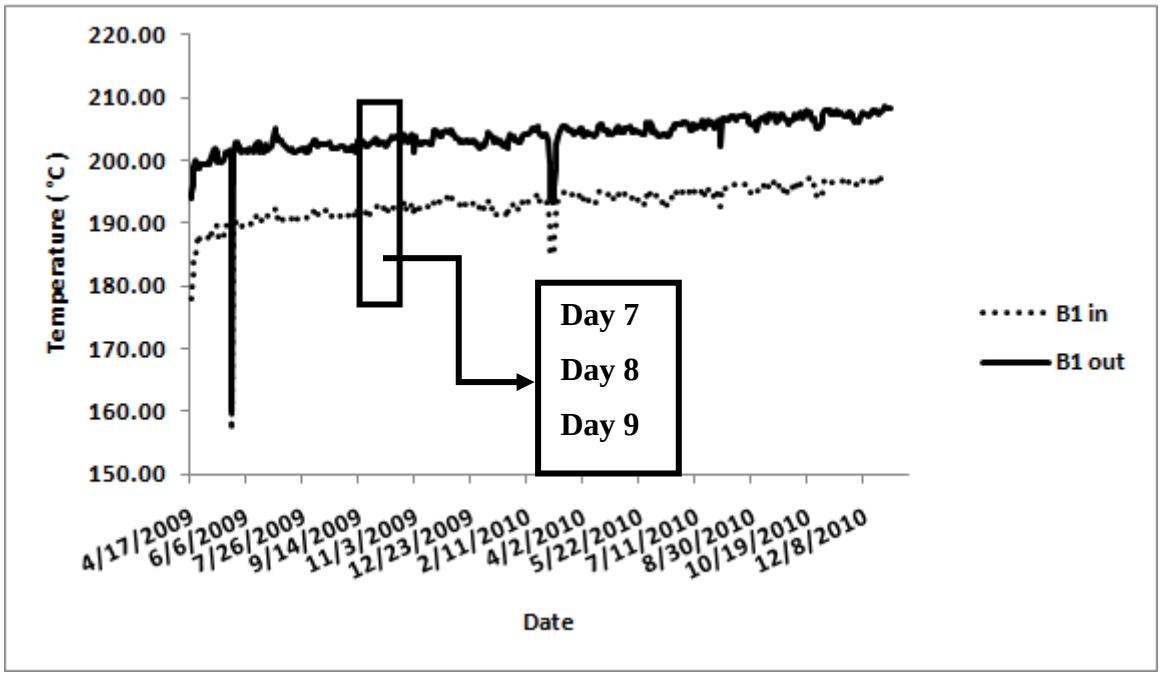

Figure 7.35 Plant data for first bed inlet and outlet temperatures with the chosen data window

Since operating conditions change, the model parameters should be updated as well. Therefore, a new training data window was chosen as shown in Figure 7.35. Firstly, the simulations were performed by using the previous model parameters. The model predictions were poor as expected. Then, model parameters were updated by using the new training data. The updated parameters were compared with the previous ones in order to observe the effect of catalyst deactivation on parameters. The results are presented in the following sections.

7.3.1. Predictions by Using Previously Found Model Parameters

The predictions for Days 7-8-9 are given in the following figures. As can be observed in the figures, model gives less conversion which means less cracking. In fact, this is reasonable since the parameters were estimated at the time when the catalyst was less active. Therefore, the reaction rate was lower. And low reaction rate results in less cracking.

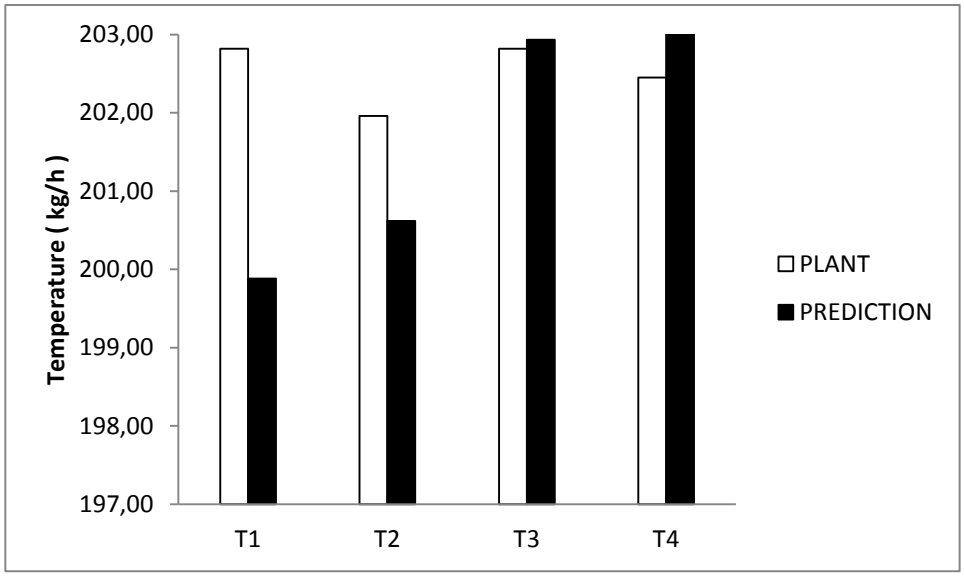

Figure 7.36 Comparison of bed exit temperatures for Day 7

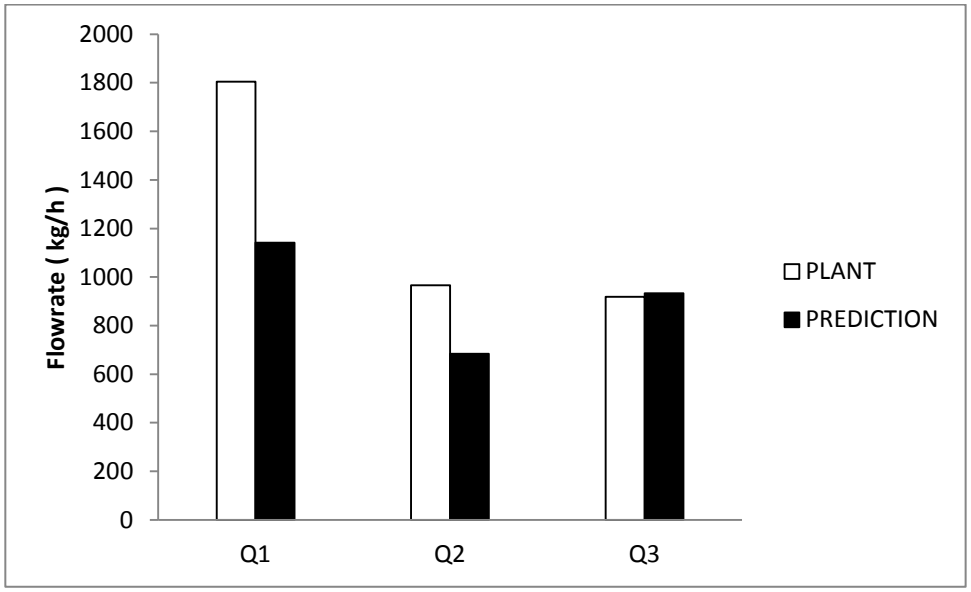

Figure 7.37 Comparison of quench flows for Day 7

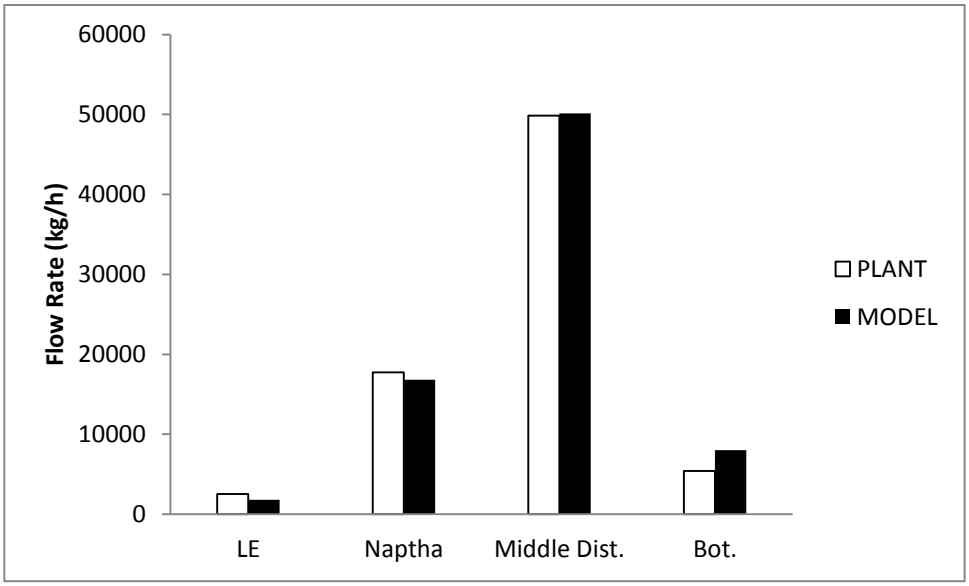

Figure 7.38 Comparison of product flows for Day 7

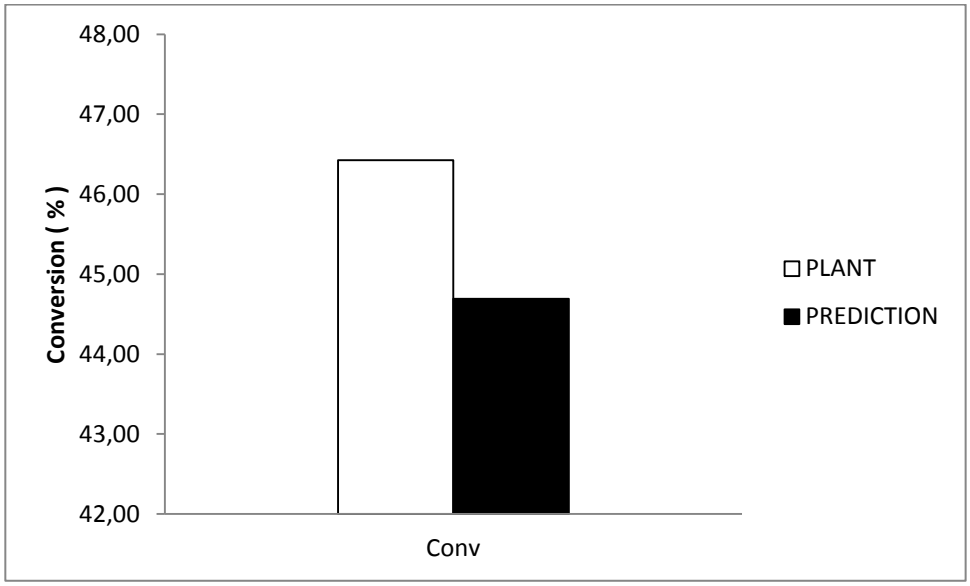

Figure 7.39 Comparison of conversion for Day 7

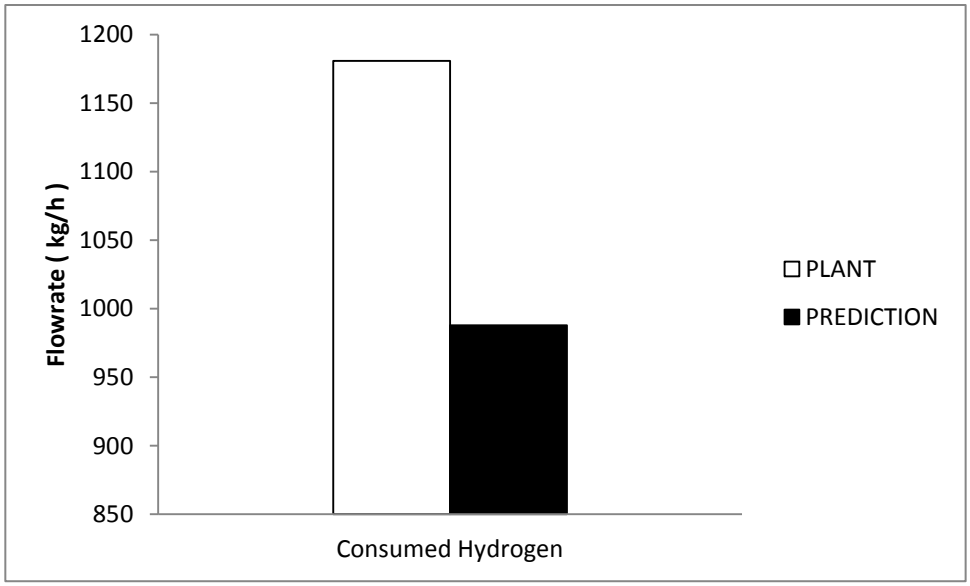

Figure 7.40 Comparison of hydrogen consumption for Day 7

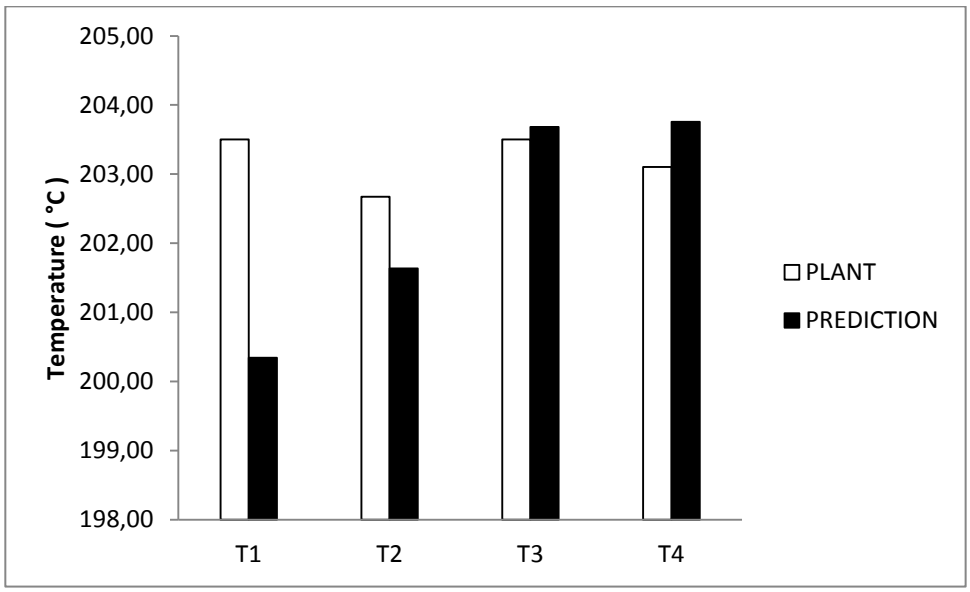

Figure 7.41 Comparison of bed exit temperatures for Day 8

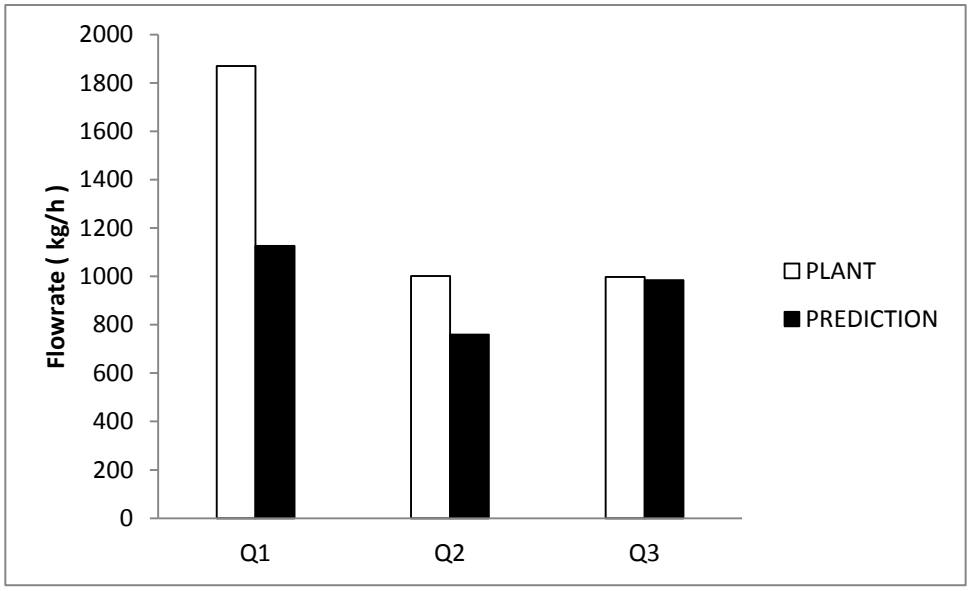

Figure 7.42 Comparison of quench flows for Day 8

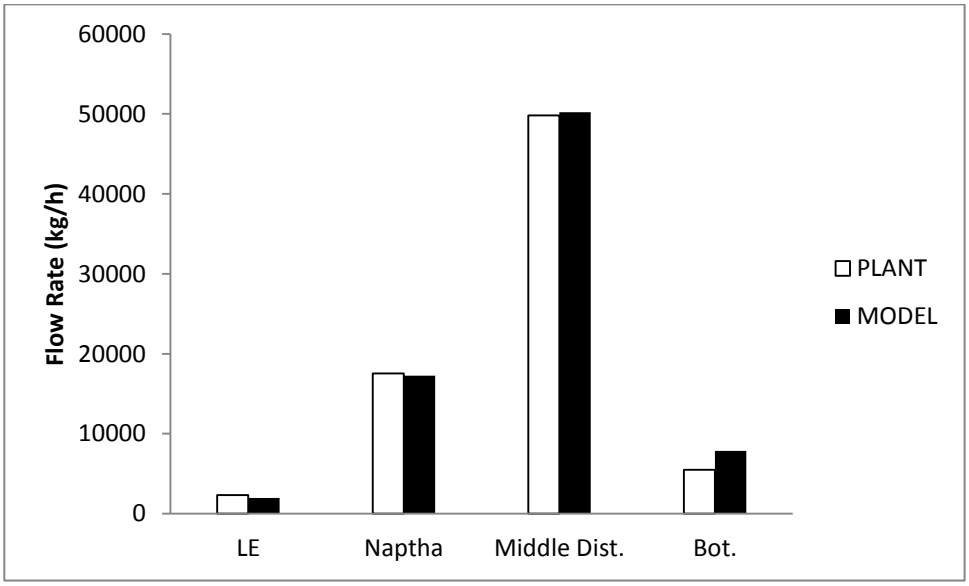

Figure 7.43 Comparison of product flows for Day 8

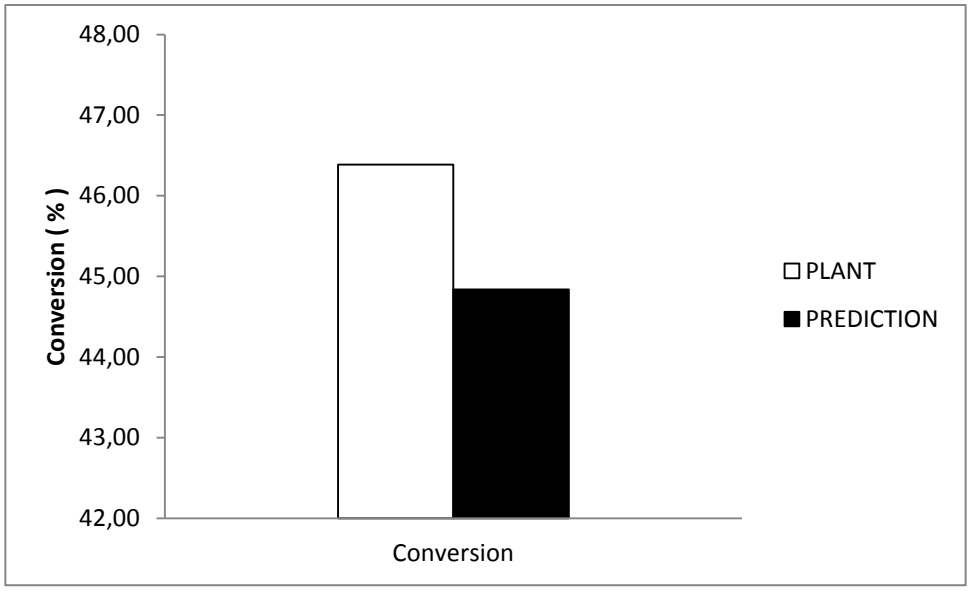

Figure 7.44 Comparison of conversion for Day 8

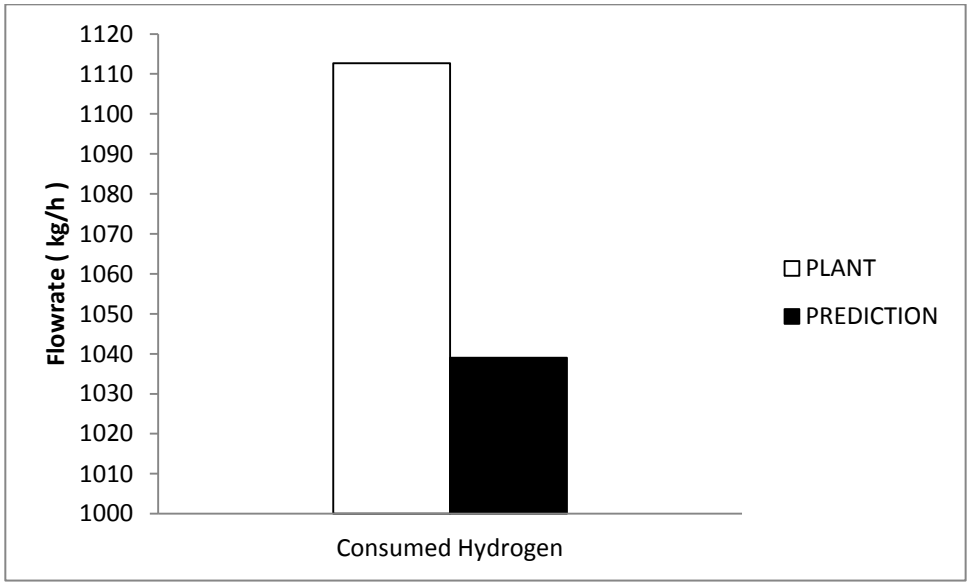

Figure 7.45 Comparison of hydrogen consumption for Day 8

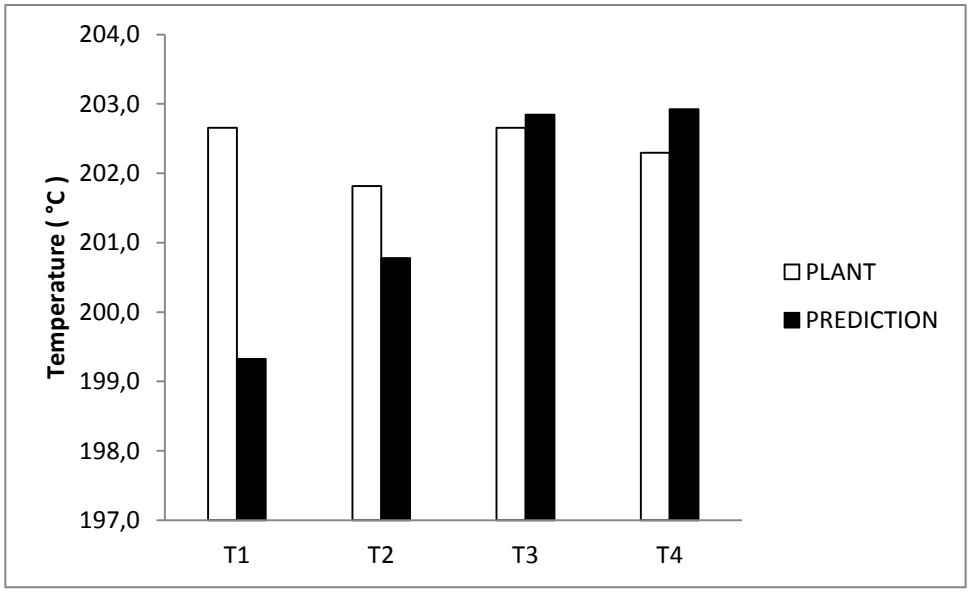

Figure 7.46 Comparison of bed exit temperatures for Day 9

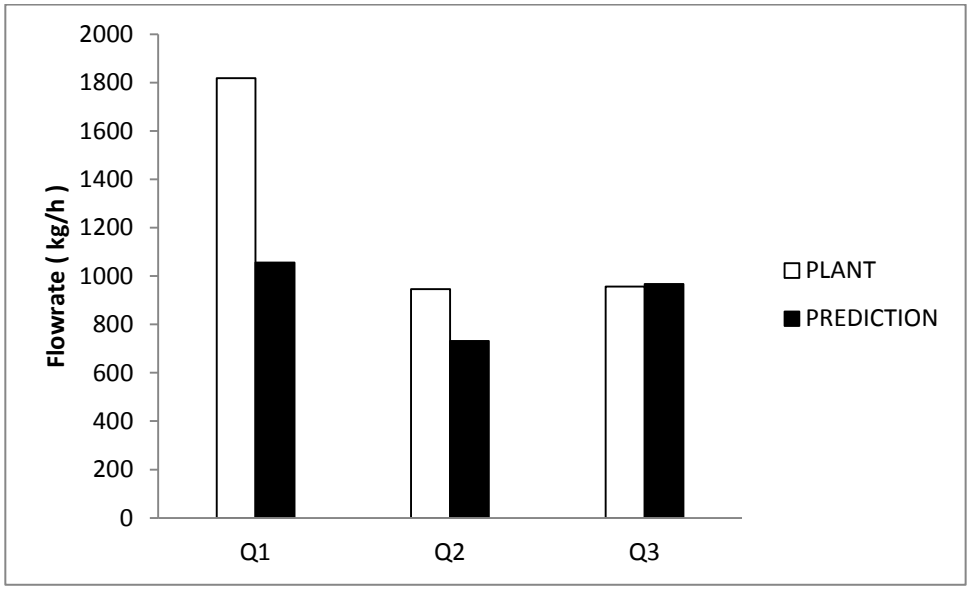

Figure 7.47 Comparison of quench flows for Day 9

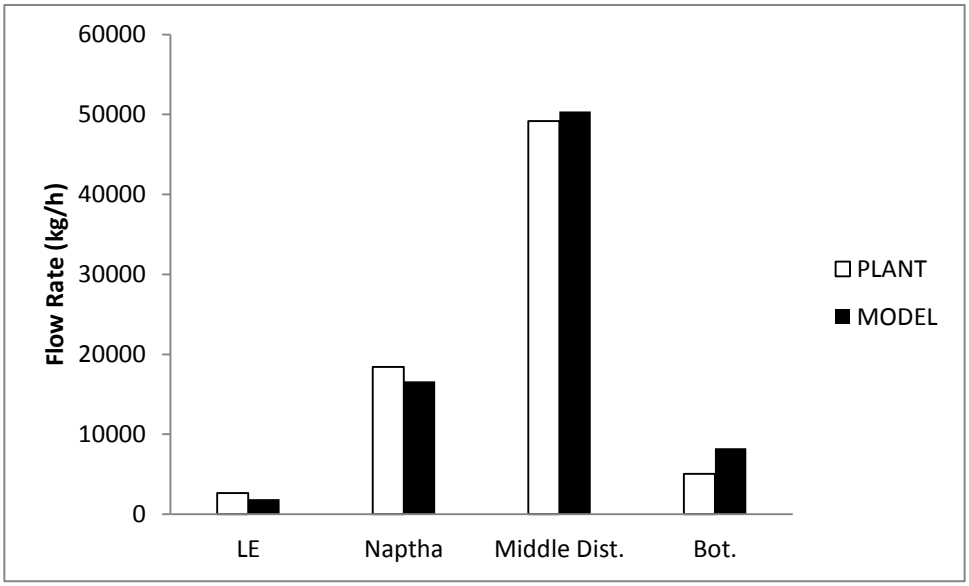

Figure 7.48 Comparison of product flows for Day 9

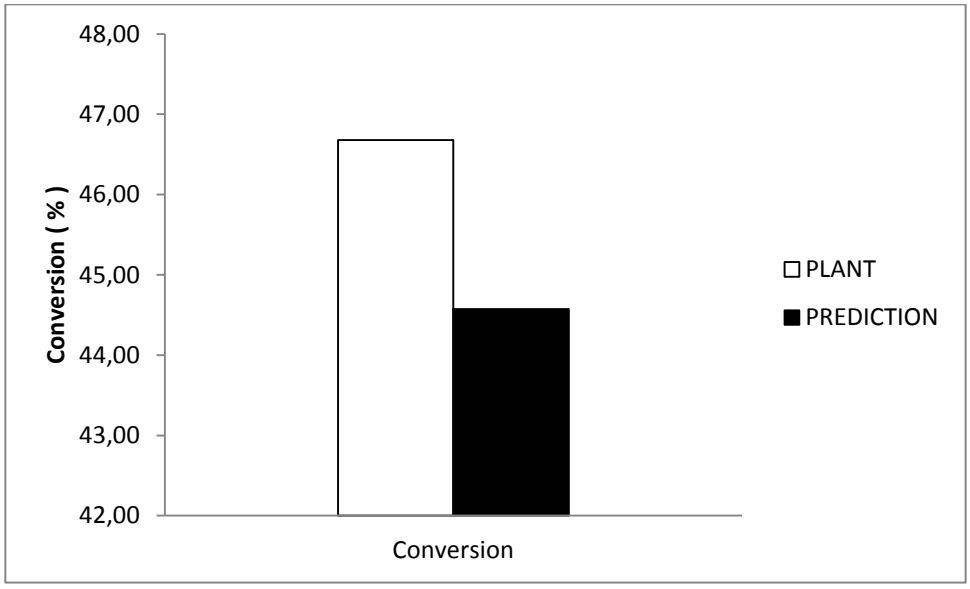

Figure 7.49 Comparison of conversion for Day 9

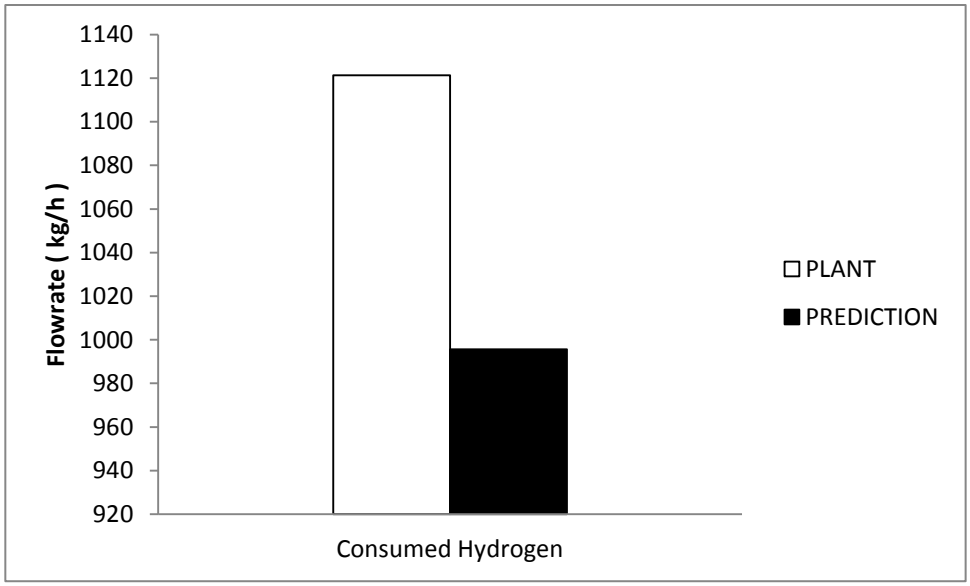

Figure 7.50 Comparison of hydrogen consumption for Day 9

7.3.2. Updated Parameters

As observed in the previous section, the model predictions for Days 7-8-9 are poor. Therefore, a new parameter set was found by using Days 7-8-9 data simultaneously. The comparison of parameter sets are given in the following table.

Table 7.7 Comparison of parameter sets

	1	2	Change %
A1	2066024.0484	1705556.5436	-17.4474
A2	2746550.0936	2011567.9958	-26.76019
A3	2661407.9350	1800273.8678	-32.35633
A4	3330575.6629	2137245.9047	-35.82953
D1	4.2372	3.7844	-10.68605
D2	-0.0393	-0.0301	-23.49595
D3	0.0002	0.0002	-5.342312
D4	-1.73E-07	-1.42E-07	-18.05449
C	0.0006	0.0006	11.40173
W	-0.0060	-0.0058	-3.485083
B1	0.5230	0.5612	7.308198
B2	0.5223	0.5595	7.121235
HR1	-0.3243	-0.3403	4.936386
HR2	-37.7335	-42.9370	13.79019
1: estimated by Day1-2-3 data (2010)			
2: estimated by Day 7-8-9 data (2009)			

C-w-B1 and B2 are product distribution parameters. As can be observed in the above table, the values of these parameters for set 1 and set 2 are very similar. In fact, it is reasonable because same products are produced in the plant.

The distillation data (TBP data) of feeds into the plant are very similar to each other. Since C/H ratio is a function of TBP, feeds for different days have similar C/H ratios. Heat of reaction depends on C/H ratios and would be similar as well. Delta1 and delta2 are parameters used to evaluate heat of reaction and the values of them are close to each other for set 1 and set 2.

Catalyst has a higher activity for set 2. Hence, a higher reaction rate is expected for set 2. The parameters A1-4 and D1-4 are used to calculate reaction rate constant. The evaluated rate constants of pseudocomponents for set 1 and set 2 are given in Table 7.8 and 7.9. The values for set 2 are higher as the catalyst is fresher.

Table 7.8 Comparison of rate constants for parameter set 1 and 2

	BED1		BED2	
	1	**2**	**1**	**2**
14	3547750.30	4120356.13	4716341.00	4859631.63
15	3546330.18	4272361.06	4714453.11	5038909.33
16	3583681.01	4437853.82	4764106.90	5234094.85
17	3664310.96	4654542.62	4871295.48	5489662.02
18	3781313.40	4900285.31	5026837.26	5779495.93
19	3932779.02	5175949.92	5228194.02	6104620.36
20	4117127.09	5481373.53	5473264.36	6464843.17
21	4334057.53	5817875.67	5761649.35	6861720.61
22	4582196.31	6184770.48	6091522.36	7294443.81
23	4856164.42	6575792.39	6455732.62	7755622.98
24	5151873.43	6987004.93	6848844.99	8240615.39
49	14353823.40	20991164.34	19081818.06	24757405.17
50	14549489.70	21547288.26	19341934.73	25413309.00
51	14713368.23	22100270.48	19559793.08	26065507.46
52	14823219.87	22562656.71	19705828.66	26610855.15
53	14912657.27	23086386.14	19824725.78	27228552.28
54	14952296.10	23495903.42	19877421.22	27711545.26
55	14957808.28	23989670.27	19884749.05	28293903.90
56	14919723.92	24402266.20	19834120.11	28780527.91
57	14826595.22	24840040.31	19710315.82	29296847.58
58	14686165.96	25229777.51	19523630.68	29756511.54
59	14502158.80	25577023.81	19279013.55	30166060.88

Table 7.9 Comparison of rate constants for parameter set 1 and 2

	BED3		BED 4	
	1	**2**	**1**	**2**
14	4570135.97	4349178.27	5719222.31	5163249.67
15	4568306.60	4509624.74	5716932.97	5353728.21
16	4616421.13	4684308.06	5777145.12	5561108.45
17	4720286.91	4913030.58	5907126.26	5832642.84
18	4871006.94	5172420.48	6095742.39	6140584.88
19	5066121.71	5463393.99	6339915.59	6486022.29
20	5303594.94	5785779.17	6637097.61	6868750.95
21	5583040.10	6140968.80	6986804.70	7290424.34
22	5902687.15	6528238.96	7386821.81	7750183.03
23	6255607.01	6940976.10	7828477.63	8240175.57
24	6636533.02	7375025.14	8305181.29	8755469.13
49	18490287.91	22156899.32	23139370.00	26304188.03
50	18742341.05	22743907.33	23454797.79	27001071.16
51	18953445.87	23327599.18	23718981.48	27694017.39
52	19094954.39	23815663.82	23896070.03	28273437.10
53	19210165.74	24368478.33	24040249.39	28929726.44
54	19261227.64	24800737.97	24104149.97	29442895.67
55	19268328.30	25321925.94	24113035.98	30061638.67
56	19219268.85	25757435.20	24051641.33	30578665.77
57	19099302.45	26219520.90	23901511.33	31127243.84
58	18918404.48	26630901.98	23675129.51	31615626.50
59	18681370.41	26997432.45	23378497.07	32050763.49

7.4. THE RESPONSES TO INLET REACTOR BED TEMPERATURES

Although economic optimization is not in the scope of this study, the model was still tested whether it can be used in an optimization process or not. It is known that the changes in inlet temperatures will affect the conversion. In order to observe the temperature effect on conversion of the model, simulations were performed by changing bed inlet temperatures by 1 °C. The changes were done one at a time. That is, the first simulation was performed by changing only the first bed inlet temperature. The second one was done by changing only the

second bed inlet temperature and so on. In the following figure, it is observed that temperature change did not make much difference on conversion.

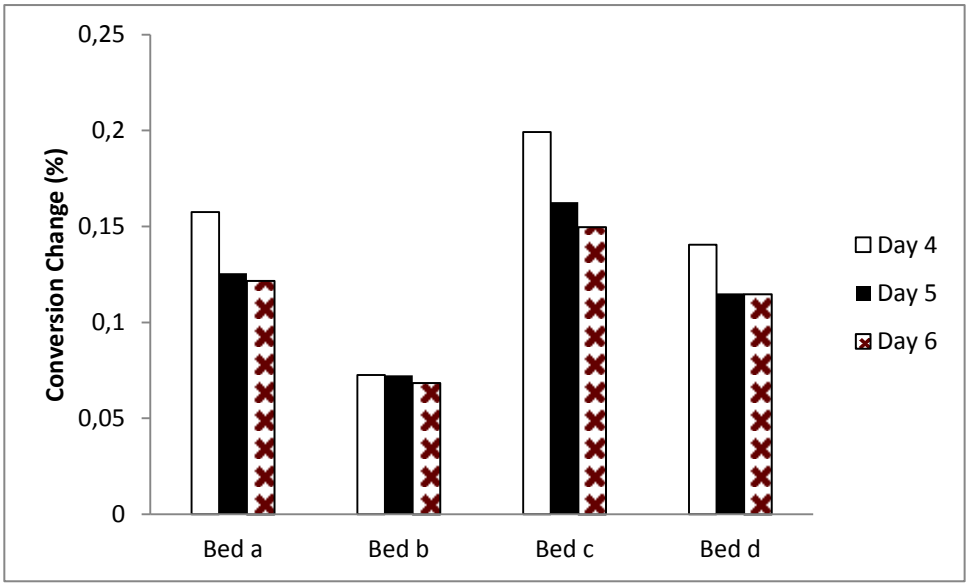

Figure 7.51 Effect of temperature on conversion

The aim of the optimization is to find the optimum inlet temperatures which will provide higher conversion, hence higher profit. According to the results given in Figure 7.51, the developed model is not proper for an optimization process because higher conversions will only be achieved by higher temperatures. When the reasons were investigated, it was noticed that the plant operates at almost a constant conversion under closed loop control as can be seen in the following figure.

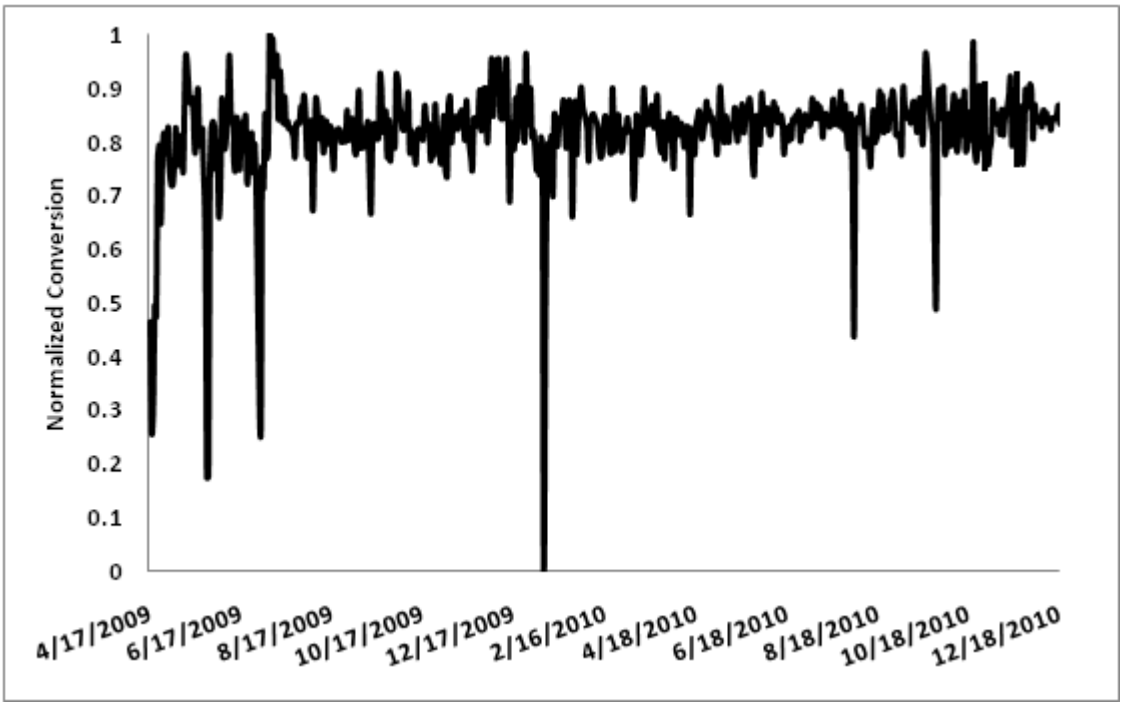

Figure 7.52 The conversion trend of the plant for a long period

Since the available data were generated for constant conversion operation, the trained model is insensitive to temperature. In order to overcome this limitation, the parameter estimation was re-performed by six data sets where the conversion was at two different levels. The available different conversion data is given in the following figure.

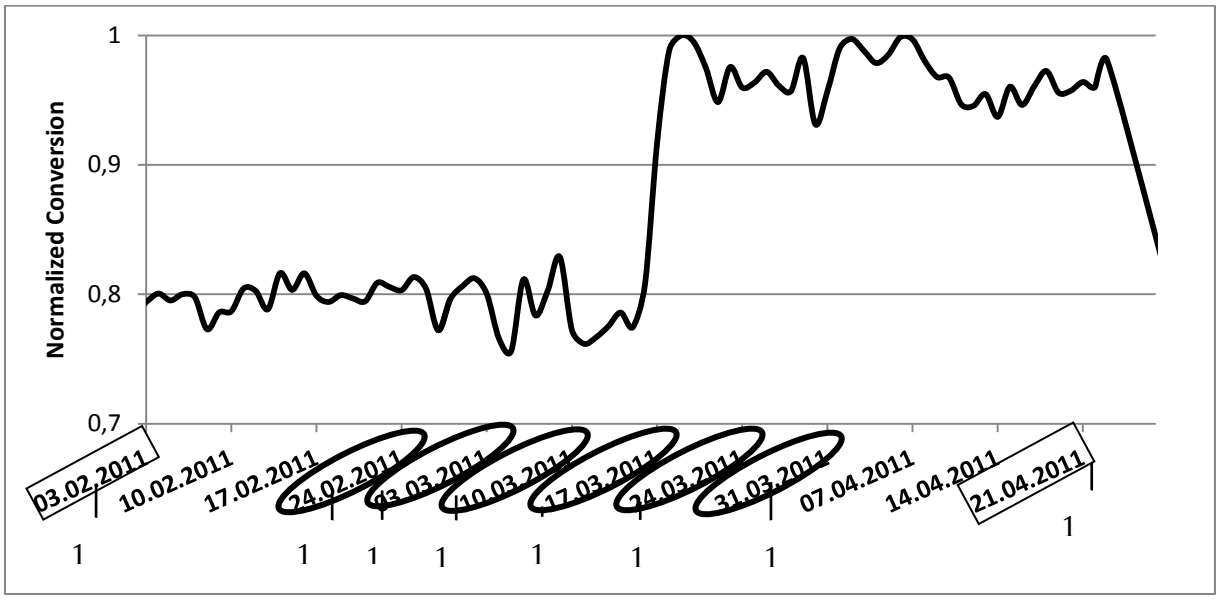

Figure 7.53 The conversion data of the plant for the year 2011

As can be seen from the figure above, plant operates at two different conversions: one is around 0.8 and the other is around 0.95. The new parameter set which was found by using Days 10-15 data simultaneously is given in Table 7.10.

Table 7.10 The parameter set found by using Days 10-15 data having two different conversion levels

Parameter	Value	Description
A1	2227929.6803	Frequency factor of the estimated rate for Bed 1
A2	2900000.6834	Frequency factor of the estimated rate for Bed 2
A3	2842830.5618	Frequency factor of the estimated rate for Bed 3
A4	3545167.0719	Frequency factor of the estimated rate for Bed 4
D1	4.1880	The first constant of relative rate equation
D2	-0.0443	The second constant of relative rate equation
D3	0.0002	The third constant of relative rate equation
D4	-1.97E-07	The fourth constant of relative rate equation
C	0.0015	Product Distribution parameter
w	-0.0044	Product Distribution parameter
B1	0.3855	Product Distribution parameter
B2	0.3847	Product Distribution parameter
HR1	-0.0957	Constant 1 in heat of reaction equation
HR2	-134.7502	Constant 2 in heat of reaction equation

Simulations were performed for Days 12-13 by this new parameter set. As can be observed in Figure 7.54, this new model has temperature sensitivity. That is, the change in inlet temperature affects the conversion. A total 3.1 °C increase in inlet temperatures along the reactor increases the conversion by 0.75 % which is a remarkable value for an HCU.

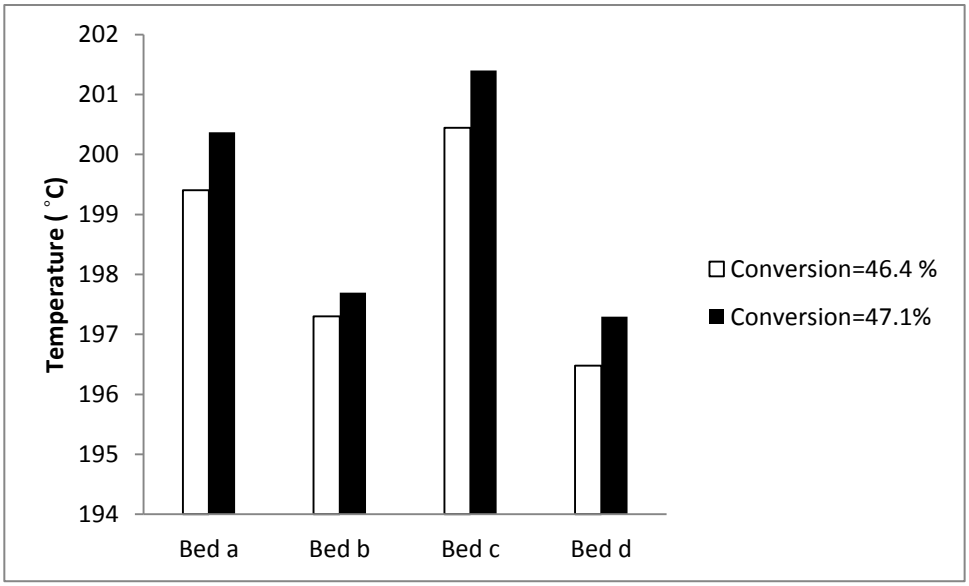

Figure 7.54 Effect of bed inlet temperatures on conversion

Predictions were performed for Days 16-17 having different conversions. Results are given in the following figures.

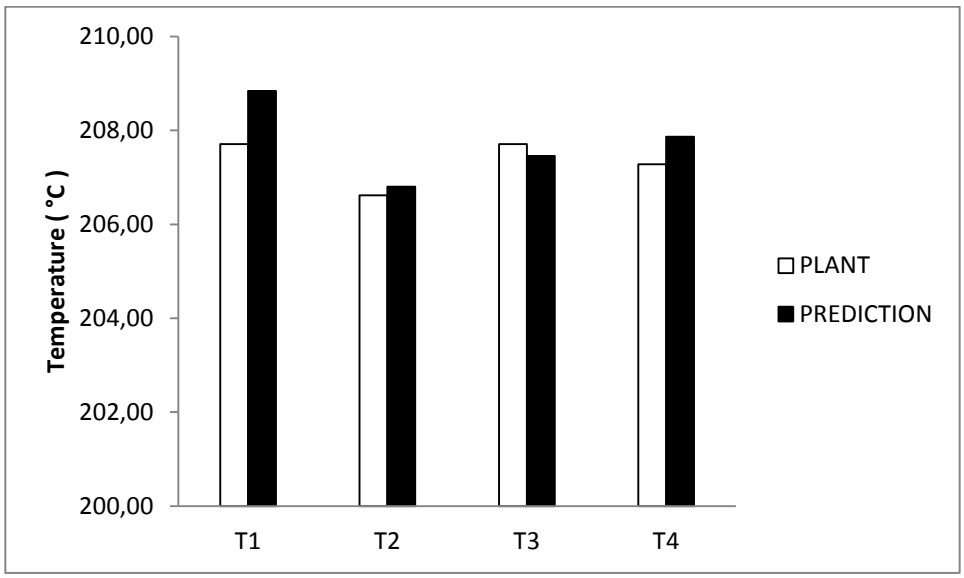

Figure 7.55 Comparison of bed exit temperatures for Day 16

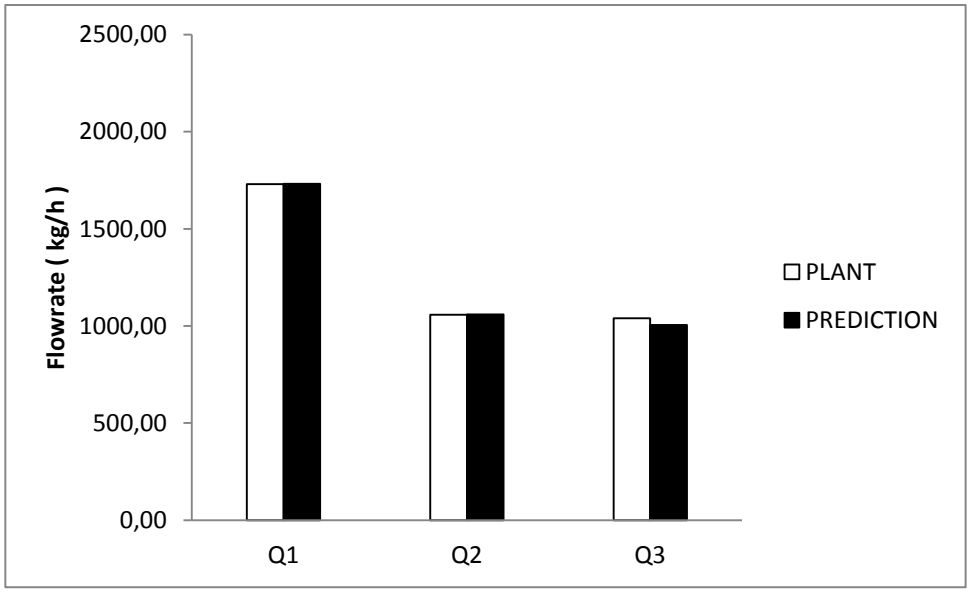

Figure 7.56 Comparison of quench flows for Day 16

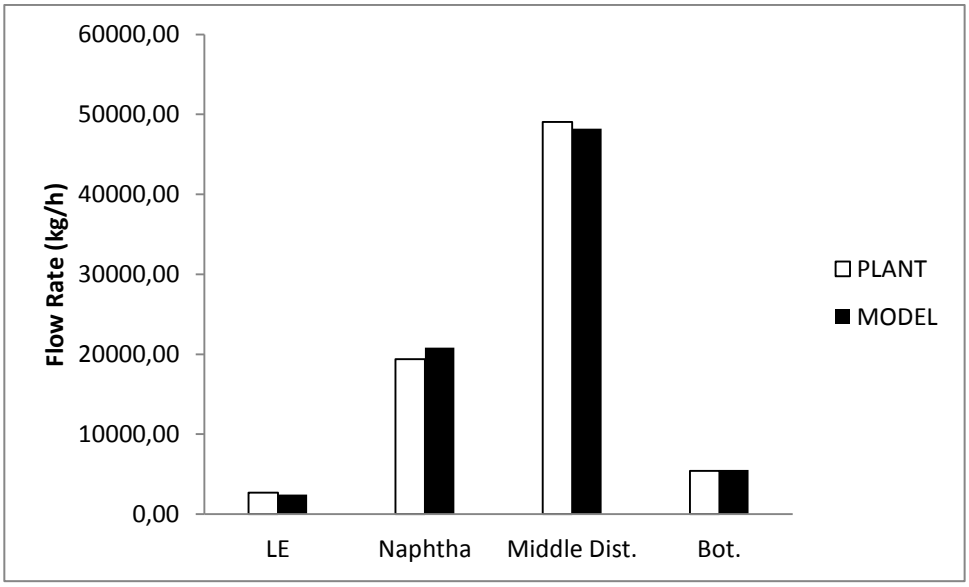

Figure 7.57 Comparison of product flows for Day 16

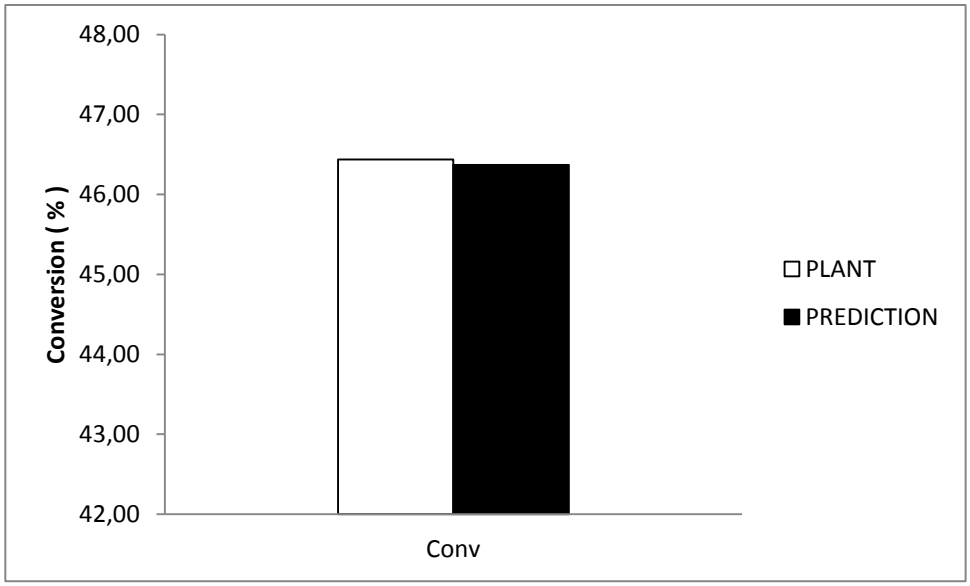

Figure 7.58 Comparison of conversion for Day 16

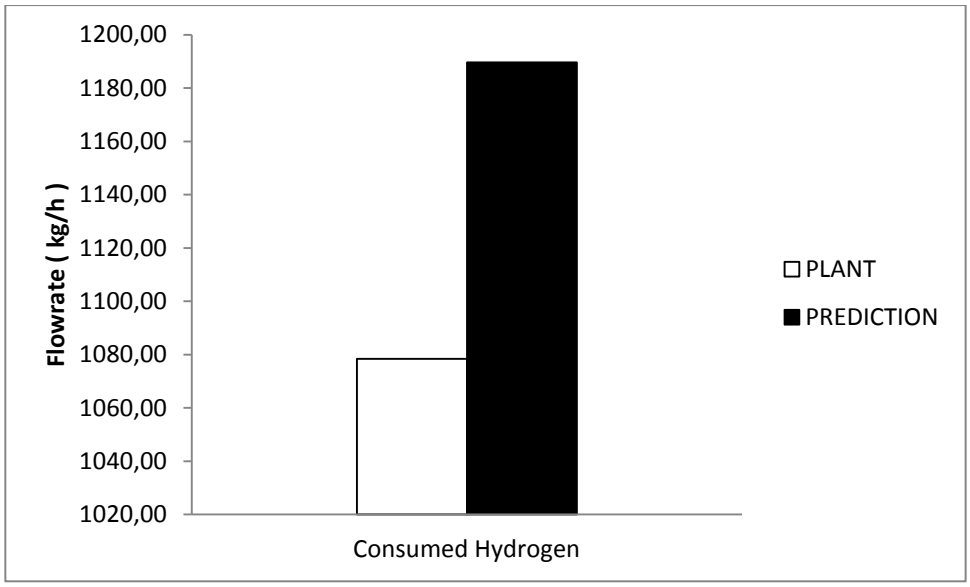

Figure 7.59 Comparison of hydrogen consumption for Day 16

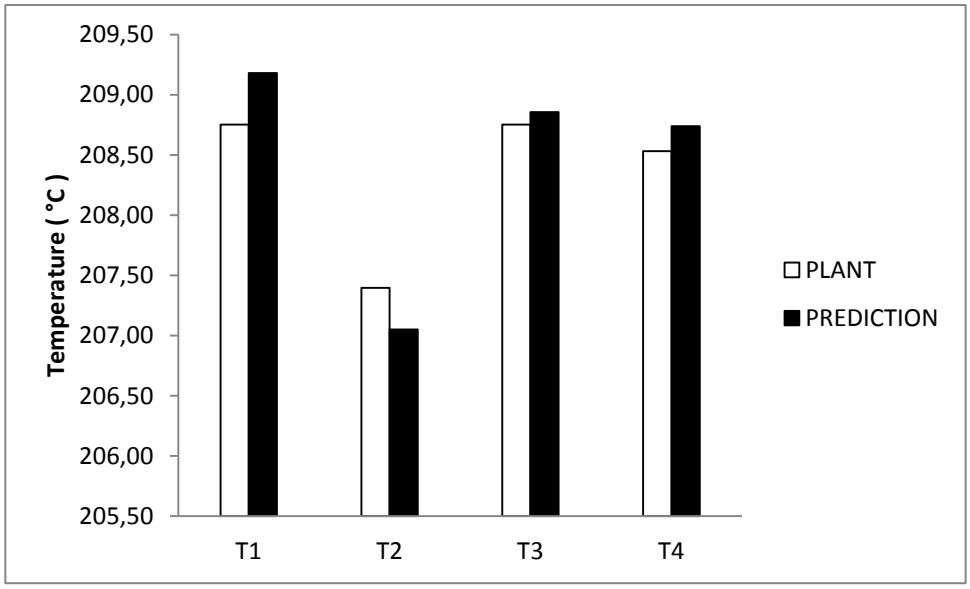

Figure 7.60 Comparison of bed exit temperatures for Day 17

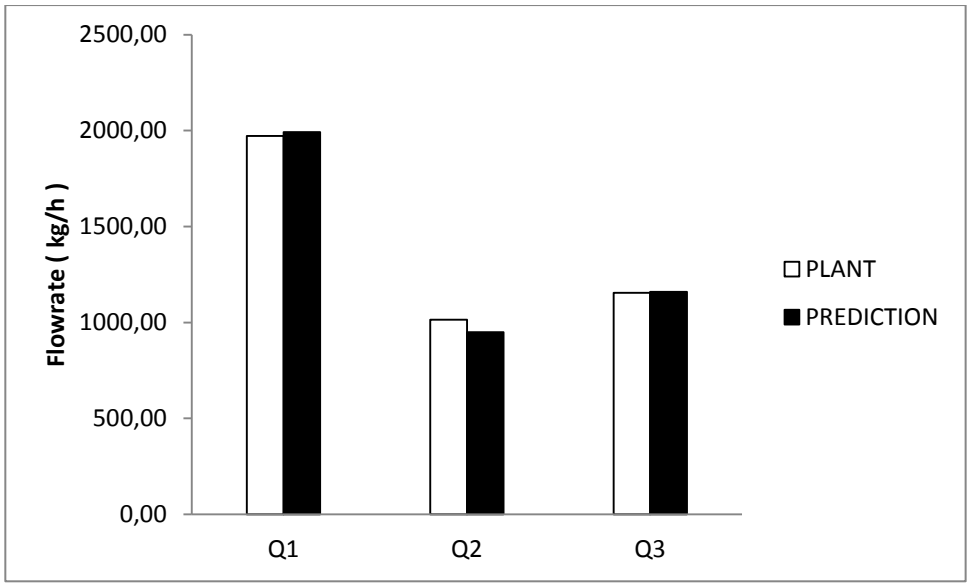

Figure 7.61 Comparison of quench flows for Day 17

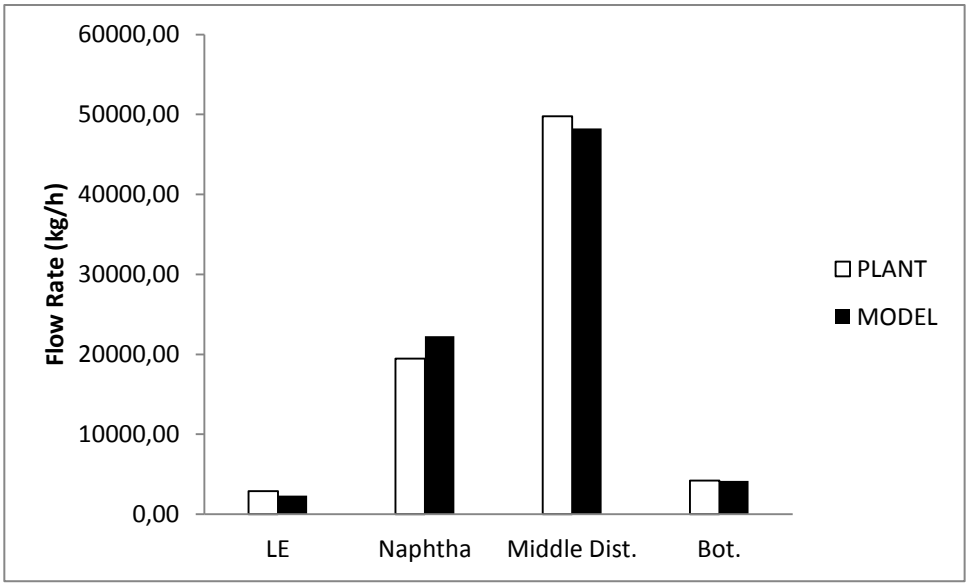

Figure 7.62 Comparison of product flows for Day 17

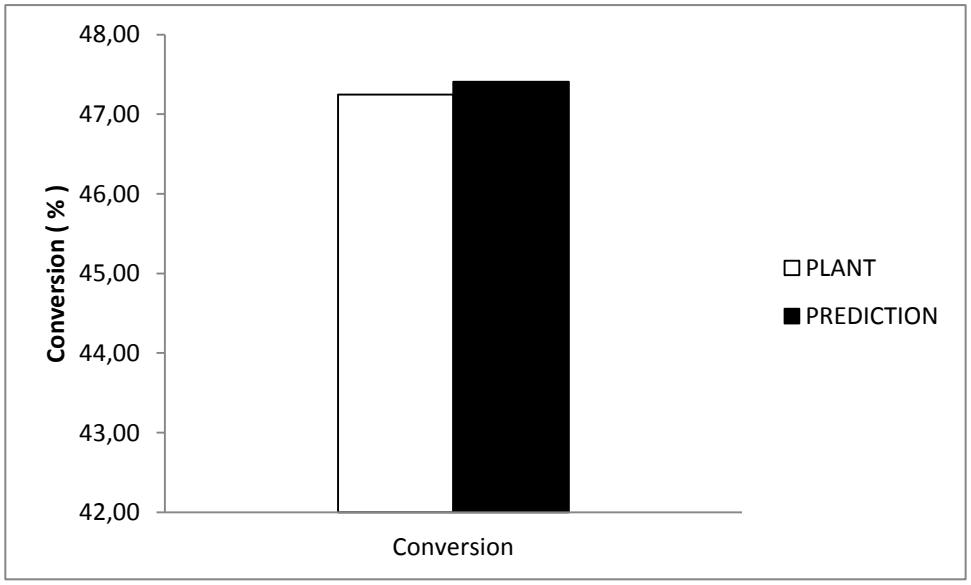

Figure 7.63 Comparison of conversion for Day 17

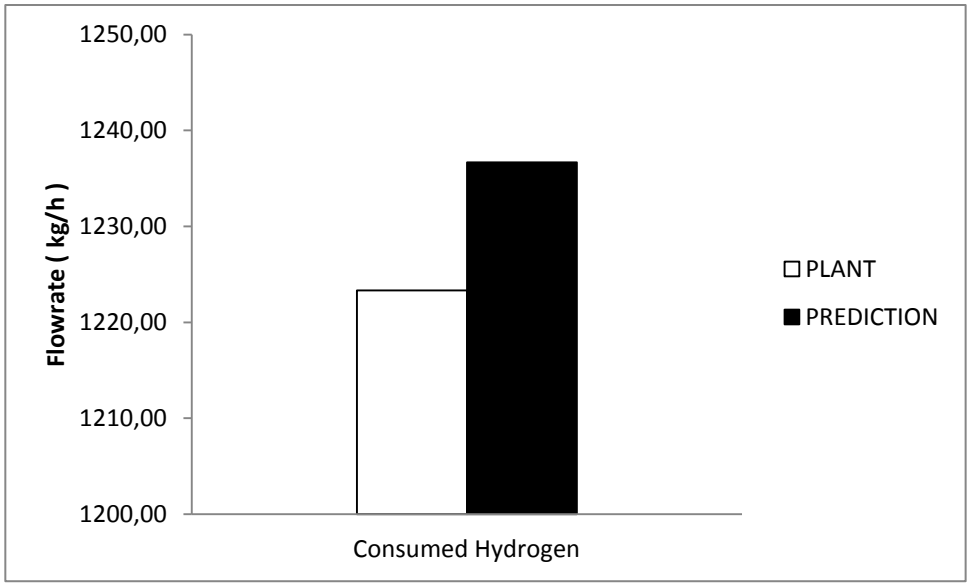

Figure 7.64 Comparison of hydrogen consumption for Day 17

The model has better predictions for Day 17 when compared with Day 16. Therefore, the predictive ability of the model should be questioned. When the available plant data is investigated, it is observed that while the conversion is fixed at some values, the bed inlet temperatures vary.

Table 7.11 Bed inlet temperatures and conversion values for different periods

	Oct-09		Oct-10		Mar-11	
Bed 1	192.05	192.54	194.96	196.14	197.38	197.69
Bed 2	192.89	193.31	195.45	196.31	196.65	197.35
Bed 3	196.45	196.94	198.97	199.80	199.94	200.38
Bed 4	197.47	197.99	199.98	200.82	200.87	201.28
Conv.	0.46	0.46	0.46	0.46	0.47	0.47

In the Table 7.30, an overall increase in inlet temperatures does not change the conversion in plant. However, the model would respond to temperature increase and affect the conversion as stated earlier. Hence, it cannot guarantee to predict the future behavior of the process. In the plant operation, the changes in temperatures are done against disturbances such as feed properties, catalyst deactivation or other operation conditions. Therefore, a disturbance model should be integrated into the developed model in order to predict the operation in the plant.

7.5. MONITORING OF THE MODEL PARAMETERS

The process variables like temperatures, pressures, flow rates and product properties are monitored in a refinery in order to have an efficient and safe plant operation. Apart from process variables, estimation of model parameters is also an important tool for efficient process monitoring. Therefore, parameter estimation was performed for many days of operation over a three months period.

The product of parameters A1-4 and D1-4 gives the reaction rate constant. Hence, the Figures 7.65 and 7.66 should be discussed together. While parameters A1-4 show a decreasing trend, there is not much difference in parameters D1-4, especially the parameters D2-4 remain constant over the period. Therefore, the reaction rate constant decreases along the period which can easily be attributed to catalyst deactivation. When the Figure 7.67 and 7.68 are investigated, the kinks are seen between points 3/10/2011 and 3/24/2011. In fact, it is the region where the conversion is switched to a higher value. Higher conversion means higher cracking. Hence, both the product distribution and heat of reaction will be different from lower conversion period and so the parameters related with those phenomenon.

As a result, it can easily be claimed that parameter estimation is performed successfully as dramatic changes are not observed in the parameters. Moreover they change within an acceptable range.

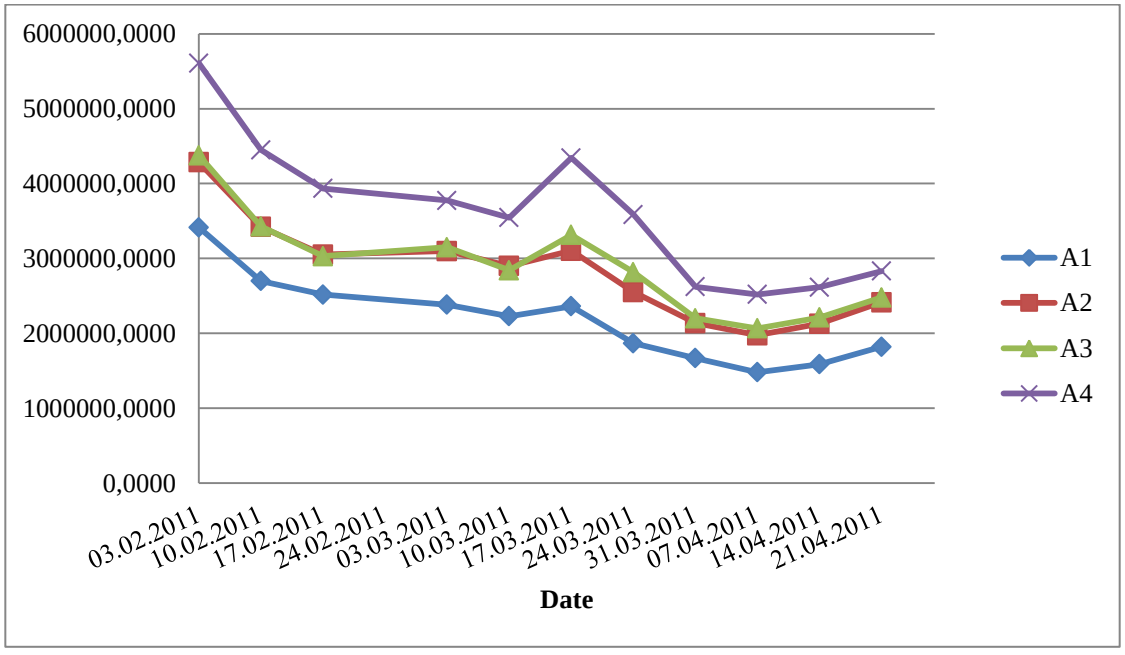

Figure 7.65 Trend of estimated rate constants for a three months period

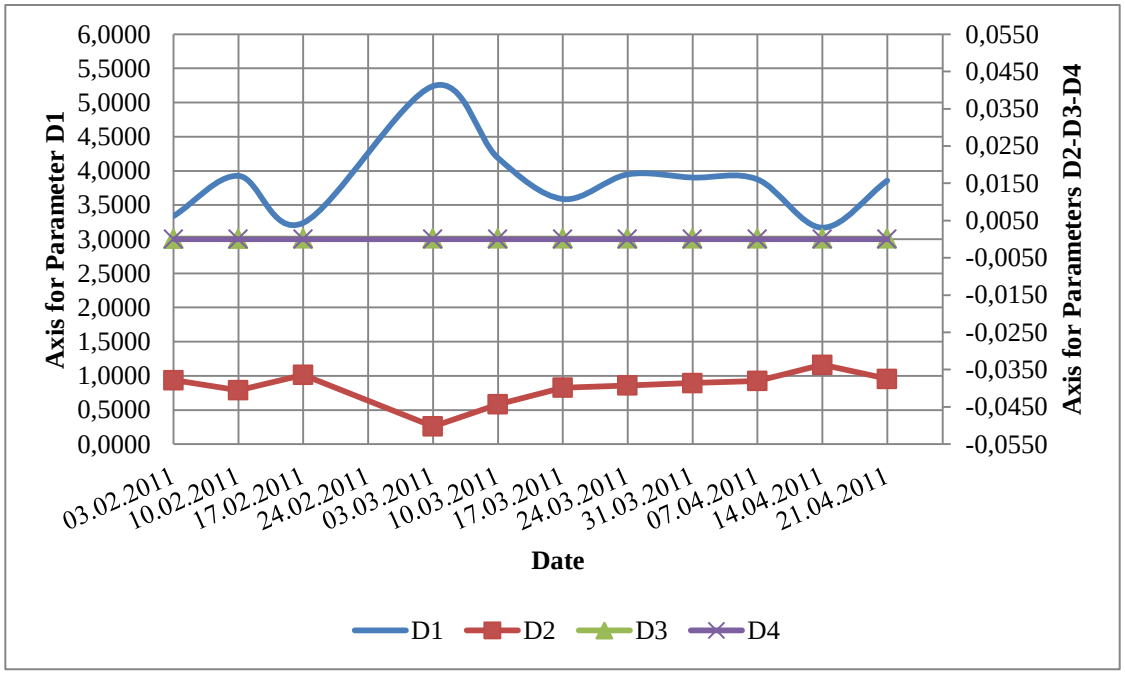

Figure 7.66 Trend of relative rate constants for a three months period

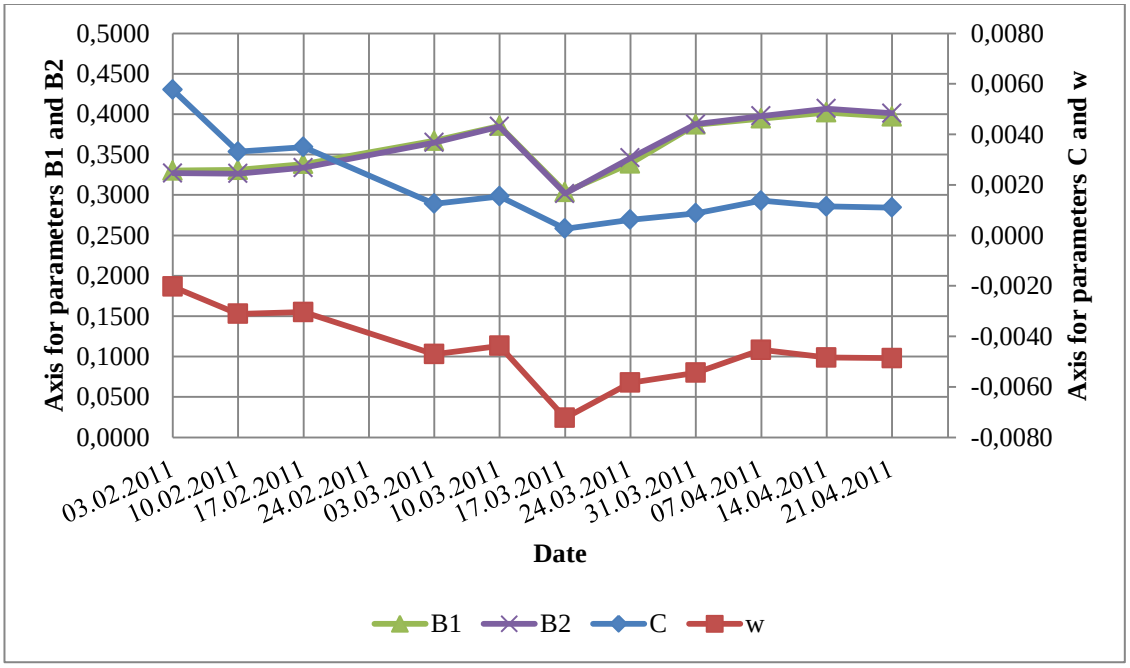

Figure 7.67 Trend of product distribution constants for a three months period

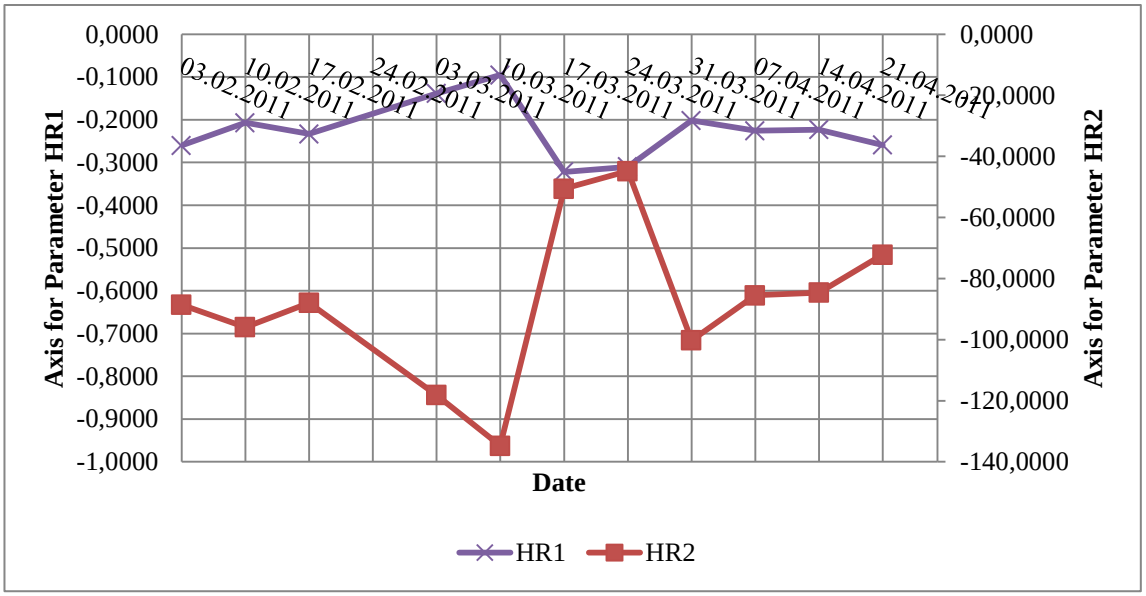

Figure 7.68 Trend of heat of reaction constants for a three months period

Chapter 8

8. CONCLUSIONS

In this study, an industrial hydrocracker reactor model was developed by discreet lumping method and it was shown that under constant conversion operating conditions, model estimates matched the plant data closely. Besides, the effect of catalyst deactivation on model parameters was investigated and it was indicated that rate constant parameters correlated well with catalyst deactivation. Moreover, temperature sensitivity was introduced to the model by estimating the parameters using operating data at two different conversion levels. Simulations revealed that an overall 3.1 °C increase in inlet temperatures along the reactor affected the conversion by 0.75 %. However, for some days of operation, increase in inlet temperatures resulted in the same conversion in the plant. This indicates that inlet temperatures are adjusted by control system against disturbances such as feed properties, catalyst deactivation or other operation conditions. Although the developed model cannot predict such disturbances, its parameters can be updated on-line to match different plant data that includes disturbance effects. For a better solution, a fundamental or empirical disturbance model can be integrated into the developed model in order to predict the behavior of the process under realistic disturbances.

9. BIBLIOGRAPHY

[1] **Bhutani, N., Ray, A.K., Rangaiah, G.P.,** "Modeling, Simulation and Multi-Objective Optimization of An Industrial Hydrocracking Unit," *Ind. Eng. Chem. Res.* 45, pp. 1354-1372 (2006).

[2] "Handbook of Petroleum Processing," available via http://books.google.com/books?id=D6pb1Yn0vYoC&dq=%22processengineers%22&ie=ISO-8859-1&source=gbs_gdata .

[3] **Bhutani, N.,** "Modeling, Simulation and Multi-Objective Optimization of An Industrial Hydrocrackers,"thesis, presented to National University of Singapore, in partial fulfillment of the requirements for the degree of Doctor of the Philosophy (2007).

[4] **Elizalde, I., Rodriguez, M.A., Ancheyta, J.,** "Application of Continuous Kinetic Lumping Modeling to Moderate Hydrocracking of Heavy Oil," *Applied Catalysis* 365, pp. 237-242 (2009).

[5] **Laxminarasimhan, C.S., Verma, R.P., Ramachandran, P.A.,** "Continuous Lumping Model for Simulation of Hydrocracking," *AIChE J.*, 42,9 (1996).

[6] **Basak, K., Sau, M., Manna, U., Verma, R.P.,** "Industrial Hydrocracker Model Based on Novel Continuum Lumping Approach for Optimization in Petroleum Refinery," *Catalysis Today* 98, pp. 253-264 (2004).

[7] "Fundamentals of Petroleum Refining" available via http://books.google.com/books/about/Fundamentals_of_Petroleum_Refining.html?id=UcFsv1mMFHIC.

[8] **Billon, A., Bigeard, P.H.,** "Petroleum Refining Conversion Processes" *Institut Fracais du Pétrole Publications,* Technip editions, Paris, pp. 333-364 (2001).

[9] "Refining Processes Handbook," available via http://books.google.com/books?id=noMPVq7V4IAC&source=gbs_similarbooks_r&cad=2.

[10] **Quader, S.A., Hill, G.R.,** " Hydrocracking of gas oils," *Ind. Eng. Chem. Pro. Des. Dev.*, 8(1), pp. 98-105 (1969).

[11] **Weekman, V. W., Jr., Nace, D.M.,** "Kinetics of Catalytic Cracking Selectivity in Fixed, Moving and Fluid Bed Reactors," *AZChE J.*, 16, 397 (1970).

[12] **Orochko, D. I., et al.,** *Khim. Technol. Topl. Masel.*, 15(8), 2 (1970).

[13] **Zhorov, Y.M., Panchenkov, G.M., Tatarintseva, G.M., Kuzmin, S.T., Zenkovskii, S.M.,** "Chemical Scheme and Structure of Mathematical Description of Hydrocracking," *Znt. Chem. Eng.*, 11(2), 256 (1971).

[14] **Usami, H.,** "Computer Checks Stream Cracker," *Hydrocarbon Process.*, 103 (1972).

[15] **Stangeland, B. E.,** "Kinetic Model for Prediction of Hydrocracker Yields," *Znd. Eng. Chem. Proc. Des. Deu.,* 13(1), 72 (1974).

[16] **Pacheco, M.A., Dassori, C.G.,** "Hydrocracking: An improved Kinetic Model and Reactor Modeling," *Chemical Engineering Communications,* 189: 12, 1684 -1704 (2002).

[17] **Mohanty, S., Saraf, S.N., Kunzru, D.,** "Modeling of a Hydrocracking Reactor," *Fuel Processing Technology*, 29, pp. 1-17 (1991).

[18] **Ancheyta, J., Sanchez, S., Rodriguez, M.,** "Kinetic Modeling of Heavy Oil Fractions: A Review," *Catalysis Today,* 109, pp. 76-92 (2005).

[19] **Krishna, R., Saxena, A.K.,** "Use of an Axial-dispersion Model for Kinetic Description of Hydrocracking," *Chem. Eng. Sci.* 44, pp. 703-712 (1989).

[20] **Mosby, F., Buttke, R.D., Cox, J.A., Nikolaides, C.,** "Process Characterization of Expanded-Reactors in Series*," Chem. Eng. Sci.* 41, pp. 989-995 (1986)

[21] **DeDonder, T.,** L'Affinite, Chapter 3, 2nd edition, Gauthier-Villars, Paris (1931)

[22] **Aris, R., Gavalas, G.R.,** "On The Theory of Reactions in Continuous Mixtures," *Phil. Trans. Roy. Soc. Lond.,* Ser. A, 260, pp. 351-393 (1966).

[23] **Chou, M.Y., Ho, T.C.,** "Continuum Theory for Lumping Nonlinear Reactions," *AIChE J.*, 34 (9), pp. 1519–1527 (1988).

[24] **McCoy, B.J., Wang, M.,** "Continuous-Mixture Fragmentation Kinetics: Particle Size Reduction and Molecular Cracking," *Chem. Eng. Sci.*, 49, pp. 3773-3785 (1994).

[25] **Browarzik, D., Kehlen, H.,** "Hydrocracking Process of n-Alkanes by Continuous Kinetics," *Chem. Eng. Sci.*, 49(6), pp. 923-926 (1994).

[26] **Peixoto, F.C., deMedeiros, J.L.,** "Modeling and Parameter Estimation in Reactive Continuous Mixtures: the Catalytic Cracking of Alkanes-PartI," *Brazil J. Chem. Eng.,* 16, pp.65-81 (1999).

[27] **Khorasheh, F., Zainali, H., Chan, E.C., Gray, M.R.,** "Kinetic Modeling of Bitumen Hydrocracking Reactions," *Petroleum Coal,* 43, pp. 208-218 (2001).

[28] **Khorasheh, F., Chan, E.C., Gray, M.R.,** "Development of a Continuous Kinetic Model for Catalytic Hydrodesulfurization of Bitumen," *Petroleum&Coal,* 47(1), pp. 40-48 (2005).

[29] **Khorasheh, F., Ashuri, E., Gray, M.R.,** "Development of a Continuous Kinetic Model for Catalytic Hydrodenitrogenation of Bitumen," *Scientia Iranica*, 14, pp.152-160 (2007).

[30] **Liguras, D. K., Allen, D.T.,** "Structural Models for Catalytic Cracking: 1. Model Compounds Reactions," *Ind. Eng. Chem. Res.,* 28, 665 (1989a).

[31] **Liguras, D. K., Allen, D.T.,** "Structural Models for Catalytic Cracking: 2. Reactions of Simulated Oil Mixtures," *Ind. Eng. Chem. Res.*, 28, 674 (1989b).

[32] **Quann, R. J., and S. B. Jaffe,** "Structure-Oriented Lumping: Describing the Chemistry of Complec Hydrocarbon Mixtures,'' *Ind. Eng.* Chem. *Res.*, 31, 2483 (1992).

[33] **Quann, R. J., and S. B. Jaffe,** "Building Useful Models of Complex Reaction Systems in Petroleum Refining," Chem. *Eng.* Sci.. 51, 1615 (1996).

[34] **Froment, G.F., M.A, Baltanas, K. K. Van Raemdonck, G. F. and S. R. Mohedas,** "Fundamental Kinetic Modeling of Hydroisomerization and Hydrocracking on Noble-Metal-Loaded Faujasites: 1. Rate Parameters for Hydroisomerization," *Ind.* Eng. Chem. Res., 28,899 (1989).

[35] **Froment, G.F., and E. Vynckier,** "Modeling of the Kinetics of Complex Processes Based upon Elementary Steps," *Kinetic and Thermodynamic Lumping of Multicomponent Mixtures,* G. Asarita and S.**1.** Sandler, eds.. *Elsevier Science Publishers,* Amsterdam, p. 131 (1991).

[36] **Pushpavanam, S., and P. Balasubramannian,** "Model Discrimination in Hydrocracking of Vacuum Gas Oil using Discreet Lumped Kinetics," *Fuel,* 87, pp.1660-1672 (2008).

[37] **Martens, G.G., and G.B. Marin,** "Kinetics for Hydrocracking Based on Structural Classes:Model Development and Application," *AIChE J.,* 47(7), pp.1607-1622 (2001).

[38] **Ferreira da Silva, R.M.C., J.L. de Medeiros, O.Q.F. Araujo,** "A Network of Chemical Reactions for Modeling Hydrocracking Reactions," *European Congress of Chemical Engineering (6),* Copenhagen (Sept. 2007).

[39] ASPEN HYSYS Refining Manuel, version 7.1

[40] **No, M.H., E. Kim, J.S. Lee, H. Jung,** "Hydrocarbon Compound Type Analysis of Lube Base Oil by GC-MSD: Advantages on Replacements of the GHIS Magnetic Sector Type Mass Spectrometer," *Energy Fuels*, 21(6), pp. 3341-3345 (2007).

[41] "Liquid Hydrocarbon Based Fuels for Fuel Cell on-board Reformers," available via http://osdir.com/patents/Chemistry-current/Liquid-hydrocarbon-based-fuels-fuel-cell-board-reformers-06884531.html.

[42] API Technical Data Book, 6th edition, API Publishing Services, Washington D.C. (1997)

[43] **Lee, B. I., M. G. Kesler,** "Improve Prediction of Enthalpy of Fractions," *Hydrocarbon Processing,* pp. 153-158, (1976)

[44] **Hibbert, D.B.,** "Genetic algorithms in chemistry," *Chemometrics and Intelligent Laboratory Systems,* 19 (3), pp. 277- 293 (1993).

[45] **Schwaab, M., E.C. Biscaia, J.L. Monterio, J.C. Pinto,** "Nonlinear Parameter Estimation through Particle Swarm Optimization," *Chemical Engineering Science,* 63, pp. 1542-1552 (2008).

[46] **Bard, Y.,** "Nonlinear Parameter Estimation," Academic Press, New York (1974).

[47] **Bard, Y.,** "Comparison of gradient methods for the solution of nonlinear parameter estimation problems," *SIAM Journal on Numerical Analysis*, 7(1), pp. 157-186 (1970).

[48] **Edgar, T.F., Himmelblau, D.M.,** "Optimization of Chemical Processes," McGraw-Hill, New York (1988).

[49] **Holland, J.H.**, "Adaptation in natural and artificial systems: An introductory analysis with applications to biology, control and artificial intelligence," University of Michigan Press, Ann Arbor (1975).

[50] **Goldberg, D.E.,** "Genetic Algorithms in Search, Optimization and Machine Learning," Addison Wesley Longman Inc., Boston (1989).

[51] **Deb, K.,** "Multi-objective optimization using evolutionary algorithms," Wiley, Chichester, UK, (2001).

[52] **Balasubramanian, P., S.J. Bettina, S. Pushpavanam, K.S. Balaraman,** "Kinetic parameter estimation in hydrocracking using a combination of genetic algorithm and sequential quadratic programming," *Ind. Eng. Chem. Res.*, 42(20), pp. 4723- 4731 (2003).

[53] **Kasat, R.B., S.K. Gupta,** "Multi-objective optimization of an industrial fluidizedbed catalytic cracking unit (FCCU) using genetic algorithm (GA) with the jumping genes operator," *Comp. and Chem. Eng.,* 27, pp. 1785 (2003).

[54] **Mitra, K., K. Deb and S.K. Gupta,** "Multiobjective optimization of an industrial nylon-6 semibatch reactor using genetic algorithm," *Journal of Applied Polymer Science,* 69, pp. 69- 87 (1998).

[55] **Nandi, S., Y. Badhe, J. Lonari, U. Sridevi, B.S. Rao, S.S. Tambe and B.D. Kulkarni,** "Hybrid process modeling and optimization strategies integrating neural 210 networks/support vector regression and genetic algorithms: study of benzene isopropylation on Hbeta catalyst," *Chem. Eng. J.*, 97, pp. 115-129 (2004).

[56] **Pina, J.M. and P.U. Lima,** "A glass furnace operation system using fuzzy modeling and genetic algorithms for performance optimization," *Engineering Applications of Artificial Intelligence*, 16, pp. 681- 690 (2003).

[57] **Rajesh J.K., S.K. Gupta, G.P. Rangaiah, and A.K. Ray,** "Multi-objective Optimization of Steam Reformer Performance Genetic Algorithm," *Ind. Eng. Chem. Res.*, 39, pp. 706- 717 (2000).

[58] **Sarkar, D. and J.M. Modak,** "Optimization of fed-batch bioreactors using genetic algorithm: multiple control variables," *Comp. and Chem. Eng.*, 28, pp. 789-798 (2004).

[59] **Tarafder, A., B.C.S. Lee, A.K. Ray and G.P. Rangaiah,** "Multi-objective optimization of an industrial ethylene reactor using a non-dominated sorting genetic algorithm," *Ind. Eng. Chem. Res.*, 44, pp. 124-141 (2004).

[60] **Kennedy, J., Eberhart, R.,** "Particle swarm optimization," presented at Proceedings of the IEEE International Conference on Neural Networks, Perth, Australia, vol. 4, pp. 1942-1948 (1995).

[61] **Costa Jr., E.F., Lage, P.L.C., Biscaia Jr., E.C.,** "On the numerical solution and optimization of styrene polymerization in tubular reactors," *Computers and Chemical Engineering*, 27 (11), pp. 1591- 1604 (2003).

[62] **Parsopoulos, K.E., Vrahatis, M.N.,** "Recent approaches to global optimization problems through particle swarm optimization," *Natural Computing* ,1(2-3), pp. 235-306 (2002).

[63] **Beale, E.M.L.,** "Confidence-regions in non-linear estimation," *Journal of the Royal Statistical Society B-Statistical Methodology*, 22 (1), pp.41- 88 (1960).

[64] **Williams, E.J.,** "Exact fiducial limits in non-linear estimation," *Journal of the Royal Statistical Society B-Statistical Methodology*, 24 (1), pp.125-139 (1962).

[65] **Halperin, M.,** "Confidence interval estimation in non-linear regression," *Journal of the Royal Statistical Society B-Statistical Methodology*, 25 (2), pp.330-333 (1963).

[66] **Hartley, H.O., "**Exact confidence regions for the parameters in non-linear regression laws," *Biometrika*, 51 (3-4), pp.347-353 (1964).

[67] **Watts, D.G.,** "Estimating parameters in nonlinear rate equations," *Canadian Journal of Chemical Engineering*, 72 (4), pp.701-710 (1994).

[68] **Englezos, P., N., Kalogerakis,** "Applied Parameter Estimation for Chemical Engineers," Marcel-Deccer, New York (2001).

[69] **Ooi, H.B.,** "Global Sensitivity Analysis of Fault Location Algorithms," thesis, presented to University of Adelaide, in partial fulfillment of the retirements for the degree of Master of Engineering Science (2008)

[70] **Cukier, R. I., Fortuin, C. M., Shuler, K. E., Petschek, A. G., Schaibly, J. H.,** "Study Of Sensitivity Of Coupled Reaction Systems To Uncertainties In Rate Coefficients 1," *Theory Journal Of Chemical Physics,* 59, pp. 3873-3878 (1973).

[71] **Schaibly, J. H., Shuler, K. E.,** "Study Of Sensitivity Of Coupled Reaction Systems To Uncertainties In Rate Coefficients 2," *Applications Journal Of Chemical Physics,* 59, pp. 3879-3888 (1973).

[72] **Cukier, R. I., Schaibly, J. H., Shuler, K. E.,** "Study Of Sensitivity Of Coupled Reaction Systems To Uncertainties In Rate Coefficients 3; Analysis Of Approximations," *Journal Of Chemical Physics,* 63, pp. 1140-1149 (1975).

[73] **Cukier, R. I., Levine, H. B., Shuler, K. E.,** "Non-Linear Sensitivity Analysis Of Multi-Parameter Model Systems," *Journal Of Computational Physics,* 26, pp. 1-42 (1978).

[74] **Sobol, I.M.,** "Sensitivity Estimates for Nonlinear Mathematical Models," *Mathematical Modeling and Computational Experiment,*1, pp.407-414 (1993).

[75] **Saltelli, A., M. Ratto, S. Tarantola, F. Campolongo,** "Sensitivity Analysis for Chemical Models," *Chemical Reviews,* 105(7), pp. 2811 -2828 (2005).

[76] **Rapaport, I.B.,** "Chemistry and Technology of Synthetic Liquid Fuels," 2nd ed., Israel Program for Scientific Translations, Jerusalem (1962).

[77] **Weir, H.M., Eaton, G.L.,** "Heat Content of Petroleum-Oil Fractions at Elevated Temperatures," *Ind. Eng. Chem.,* 24, pp.211-218 (1932).

[78] **Kurganov, V.M., Gorshtein, A.B., Starodubskaya, G. Ya.,** "Calculation of Heats of Reaction in Hydrocracking," *Khim. Technol. Topl. Masel,* 9, pp.46-48 (1980)

[79] "How to Predict Fluid Coker Performance," available via http://www.etxsystems.com/Publications/Papers/HP_Dec_2007.pdf.

[80] **Tushar, V.C., Meier, P.F.,** "Characterization of Heavy Petroleum Feedstocks," *Fuel Process. Tech.,* 89, pp.697-703 (2008)

[81] **Walas, S.H.,** "Phase Equilibria in Chemical Engineering," Butterworth, Boston (1985).

10. VITA

Ümmühan CANAN was born in 1982, Çanakkale, Turkey. She recevied her B.Sc. degree in Chemical Engineering from Middle East Technical University (METU), Ankara, Turkey, in June 2005. After having four years work experience, she attended Chemical and Biological Engineering M.Sc. program of Koc University, Istanbul, Turkey, in October 2009. During her graduate studies, she had worked as a research and teaching assistant at the same university.